APPENDIX A – HYDROLOGY

January 2, 2024

Attn: **Mr. Hendrick Amo**
Manager, Information Services and Technology
Nottawasaga Valley Conservation Authority
John Hix Conservation Administration Centre
8195 8th Line, Utopia, ON L0M 1T0

Re: Upper Mad River Hydrologic Modelling Update – Technical Memorandum

Aquafor Beech Limited (Aquafor) is pleased to provide an updated version of the hydrologic model for the Upper Mad River watershed, along with an overview of the modelling approach and results. Updates to the model were primarily undertaken to address deficiencies that were noted in our Technical Review of the existing hydrologic model and accompanying report, and to ensure compliance with the funding requirements for the Flood Hazard Identification and Mapping Program (FHIMP). Hydrographs produced by this updated hydrologic model will subsequently be used as inputs to the hydraulic model for floodplain mapping purposes. The previous report that was prepared in 2023 by the Oak Ridges Moraine Groundwater Program (ORMGP) outlining their hydrologic modelling approach and results for the Upper Mad River watershed is included in Appendix E as a point of reference.

Upon your review, should you have any questions or comments, please do not hesitate to contact Rob Amos at 416.705.2367 or by email at amos.r@aquaforbeech.com.

Sincerely,

Robert Amos, MASc., P.Eng.
Project Manager
Aquafor Beech Limited

Tim Koen, P.Eng.
Senior Project Advisor & QA/QC Engineer
Aquafor Beech Limited

Gabriel Dubé, MSc., EIT
Hydrologic Modelling Technologist
Aquafor Beech Limited

Table of Contents

List of Figures

List of Tables

1 DESCRIPTION OF THE WATERSHED

1.1 Drainage Network

The Upper Mad River drains a watershed area that is approximately 270 km^2 in size. The watershed drainage network (**Figure 1-1**) comprises two main branches that flow in a northeastern direction, descending the escarpment before merging near County Road 9, approximately 2.7 km upstream of the Village of Creemore.

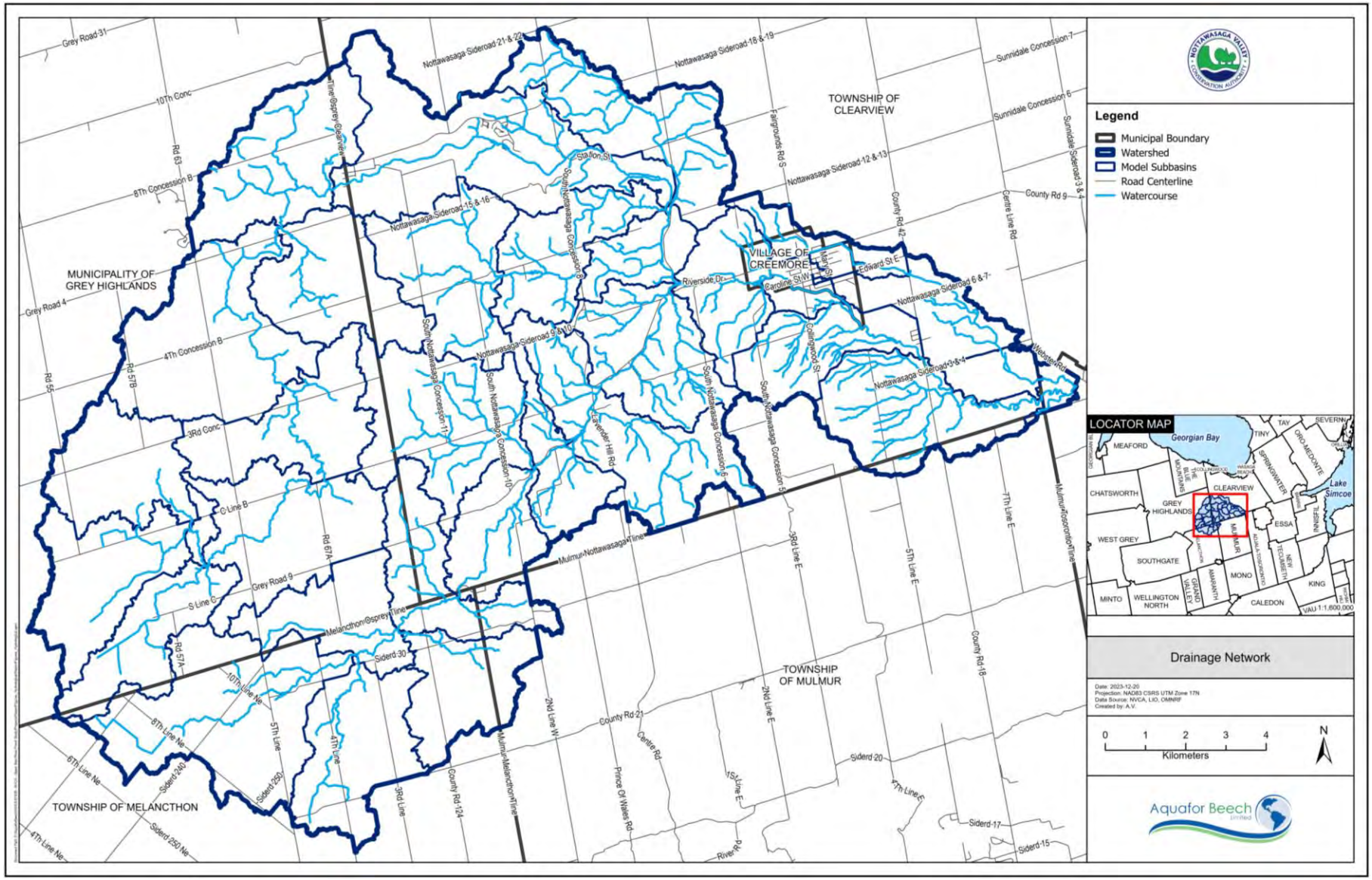

Figure 1-1: Study Area Drainage Network

1.2 Land Use

The Southern Ontario Land Resource Information System (SOLRIS, ver. 3.0) was used as a basis for determining land use within the study area. Aquafor modified the database to identify large commercial impervious areas, so as to improve runoff estimates in the hydrologic model.

As shown in **Figure 1-2**, the study area catchment is predominantly rural, with development mostly concentrated within the Village of Creemore. Agricultural and undifferentiated land (which mainly corresponds to agricultural land and undeveloped land) account for 60.6% of the watershed area. Other significant land uses include: wetlands (19.5%); forests and tree plantations (16.8%); transportation (2.3%); and built-up impervious and commercial areas (0.5%). Wetlands are mostly concentrated in the upstream extents of the watershed and play a vital role in attenuation of runoff flow rates, as described in **Section 2.10**.

The application of land use for calculating initial abstraction, imperviousness, and 'C' runoff coefficients is described in **Section 2.9**. The areas occupied by wetlands and open water were also used to estimate subbasin storage coefficients, as described in **Sections 2.7** and **2.10**.

1.3 Soils

Hydrologic soil group data was retrieved from the Soil Survey Complex (OMAFRA) layer, rather than deriving this data from OGS Surficial Geology layer, which was used by ORMGP for building the previous hydrologic model. A key difference between these two sources is that the OMAFRA layer directly classifies hydrologic soil group based on overall drainage characteristics (i.e., poorly drained vs. well drained), whereas the OGS layer only describes the permeability component of soil drainage. The hydrologic soil group data contained within the OMAFRA layer is more suitable for predicting the amount of precipitation that becomes runoff. For example, peaty areas with swamps have a high permeability but tend to be poorly drained because they are often at or near saturation, such that the majority of precipitation becomes runoff rather than infiltrating. The OMAFRA layer was therefore preferred for developing the updated hydrologic model.

Areas where hydrologic soil groups were not described, generally located within urban areas and watercourse valleys, were manually assigned a soil group based on nearby soil properties. The resulting distribution of hydrologic soil groups is shown in **Figure 1-3**. The majority of soils within the Upper Mad River watershed are well drained, though areas of lower infiltration capacity (Hydrologic Soil Groups C and D) exist in upstream subbasins, primarily within wetlands. Group B occupies 56.4% of the total area, followed by Groups C (16.7%), A (16.7%), and D (10.1%).

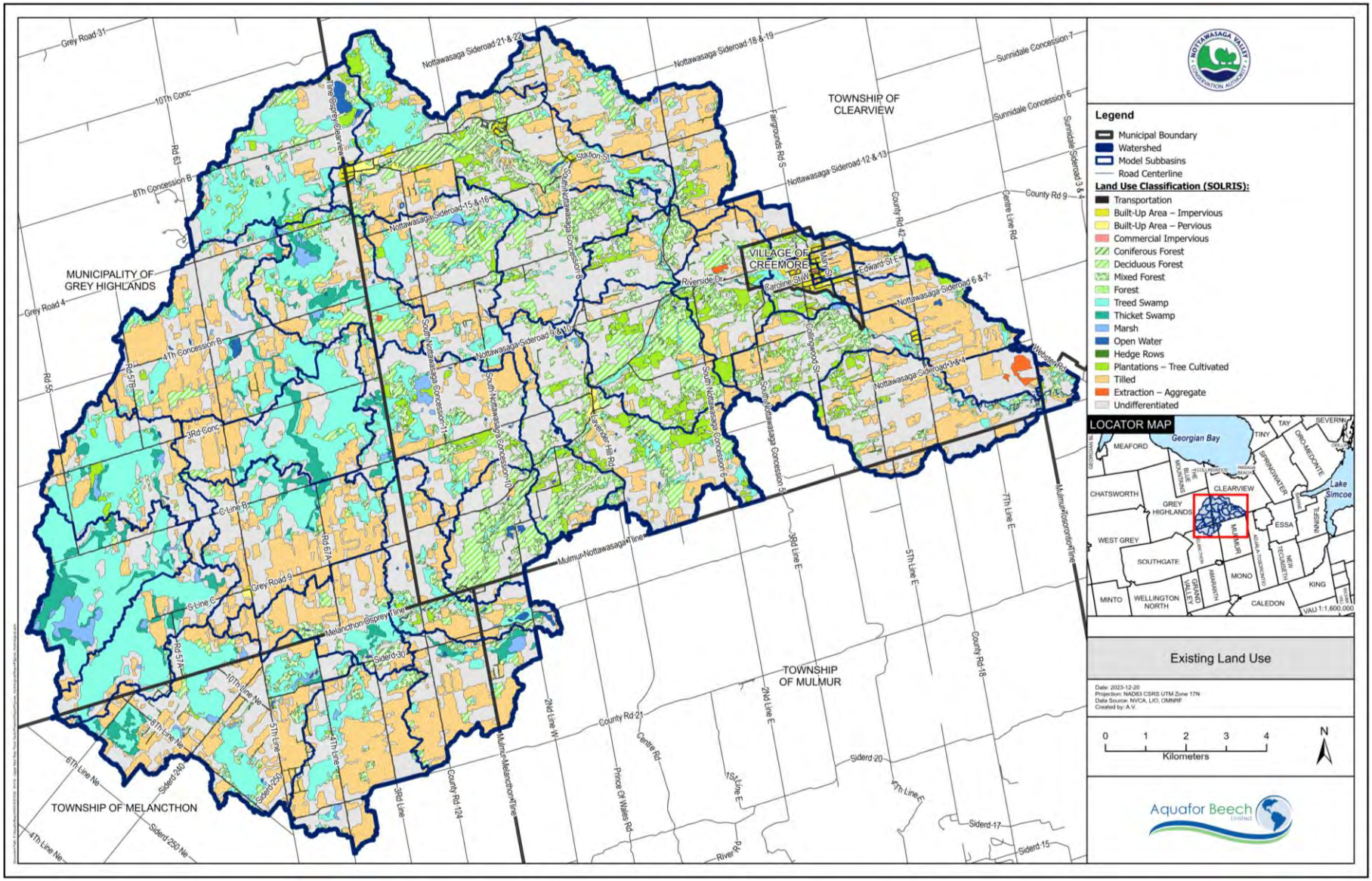

Figure 1-2: Land Use within the Study Area Watershed

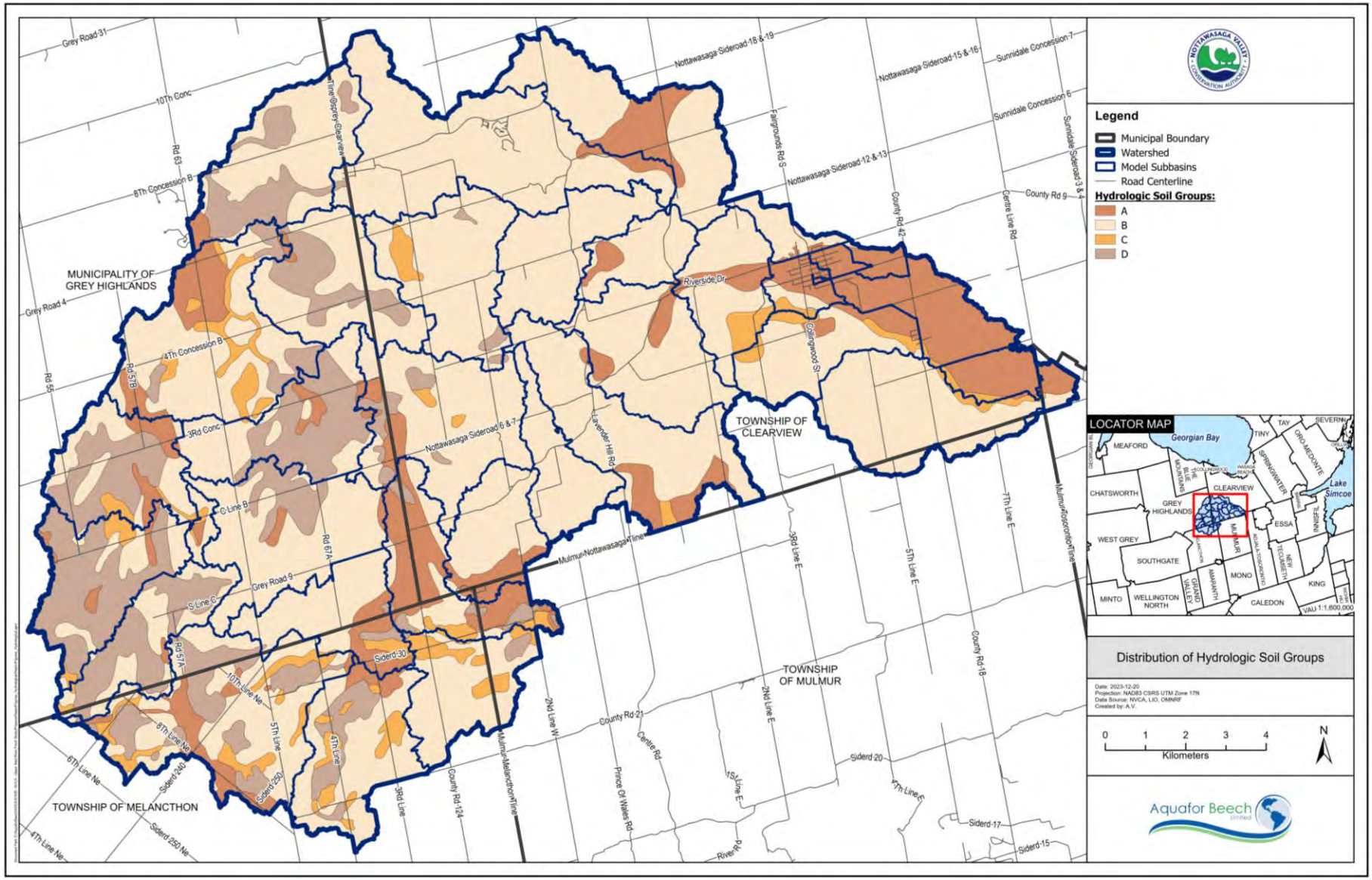

Figure 1-3: Distribution of Hydrologic Soil Groups within the Study Area Watershed

2 HYDROLOGICAL MODEL DEVELOPMENT, RESULTS, AND ANALYSIS

2.1 Model Selection and Setup

The hydrologic model was created using the US Army Corps of Engineers HEC-HMS software (Ver. 4.10). HEC-HMS was selected because it is publicly available and is widely used for floodplain mapping studies, incorporating a variety of loss, transform, and routing methods.

The model was set up using the NAD83 (CSRS) UTM Zone 17N horizontal coordinate system and the CGVD2013 vertical datum. All associated GIS files used the same projection and vertical datum.

2.2 Digital Terrain Model

A LiDAR-derived digital terrain model (DTM) was used in the hydrological study for discretizing the watershed into smaller subbasins, tracing longest flowpaths, determining reach and longest flowpath slopes, and extracting cross-section elevations used for flow routing. The DTM was produced by Natural Resources Canada (NRCan) based on LiDAR data, most of which was collected in 2022, though a small portion of the data was collected between 2016-2018 in the southwest quadrant of the watershed. The DTM is has a 0.5 m horizontal resolution and is referenced to the NAD83(CSRS) UTM Zone 17N horizontal coordinate system and the CGVD2013 vertical datum, which is consistent with the coordinate system and datum used in the updated hydrologic model. The DTM is the most recent, detailed, and accurate elevation product available for the study area, and it constitutes an improvement over the imagery-derived DTMs (SWOOP and SCOOP) that were used in older ORMGP hydrologic model, which was developed prior to release of the LiDAR-derived DTM.

2.3 Available Hydrological and Meteorological Data

As shown in **Figure 2-1**, there is 1 flow gauge (ID #02ED015) managed by the Water Survey of Canada (WSC) that is located along the main branch of the Upper Mad River at Avening, immediately upstream of County Road 42. A rainfall gauge is also located at this monitoring station, though no useable rainfall data was available.

The existing ORMGP model was calibrated using 6-hour CaPA-RDPA grid data, which has a spatial resolution of ~10 km^2 and was interpolated to define rainfall that occurred within each subbasin. Aquafor used the ORMGP model to retrieve 6-hour rainfall data for 6 of the ORMGP subbasins. This produced 6 sets of rainfall data that were each assigned to an artificial rainfall gauge placed at the centroids of the subbasins from which the data was retrieved.

The 6-hour data was used to scale rainfall volumes throughout the watershed. However, the temporal resolution of this data was deemed to be too coarse since it does not adequately capture high-intensity rainfall that is typically responsible for large amounts of runoff and high peak flows during storm events. In fact, by discretizing the rainfall data in 6-hour increments, the average rainfall intensity over these intervals can be much lower than the actual maximum storm intensities that occur during storms, which can far exceed the infiltration capacity of the soil and create large amounts of runoff within a short period of time.

In order to obtain a higher temporal resolution of rainfall, hourly data was retrieved from the Mount Forest (ID #6145504) and Collingwood (ID # 6111792) rainfall gauges, which are managed by the Meteorological Service of Canada (MSC). The hourly data from each MSC gauge was scaled using the 6-hour CaPA-RDPA data at each of the 6 artificial rainfall gauges. This produced two larger rainfall datasets, each comprising scaled hourly data from 6 gauges: one dataset that was derived from the Mount Forest records, and a second dataset that was derived from the Collingwood records. After carefully reviewing the rainfall data from the two MSC gauges, reviewing historical radar imagery, and conducting preliminary model simulations using the two datasets, it was decided that the Collingwood gauge would be used as a basis for determining the temporal distribution of rainfall within the watershed. Model calibration was thus performed using scaled rainfall data derived from this gauge.

2.4 Timestep

The model computation time step should be less than 1/5 of the smallest subbasin time to peak (lag time). The smallest subbasin lag time was approximately 77 minutes, and a timestep of 10 minutes was selected accordingly for the model's control specifications.

The time interval for Muskingum-Cunge routing is dependent on reach index flow, which was selected as the average between baseflow (assumed to be negligeable for the study areas) and peak flow within each reach, as per the HEC-HMS Technical Reference Manual (US Army Corps of Engineers, 2000).

2.5 Subbasin Discretization

The Upper Mad River watershed was subdivided into 34 subbasins (**Figure 2-2**), each having relatively uniform land use, topography, and soil texture. Discretization was performed by using the DTM and by manually burning watercourse connections into the terrain surface, as needed. Manual burning was necessary since the watercourse polyline layer did not accurately follow the watercourse centrelines and because many smaller watercourses (e.g., small streams and ditches) were not included in the layer. Manual correction and delineation of subbasin boundaries was also performed, mainly in areas where the accuracy of the DTM was reduced and/or where stream channels are not clearly defined.

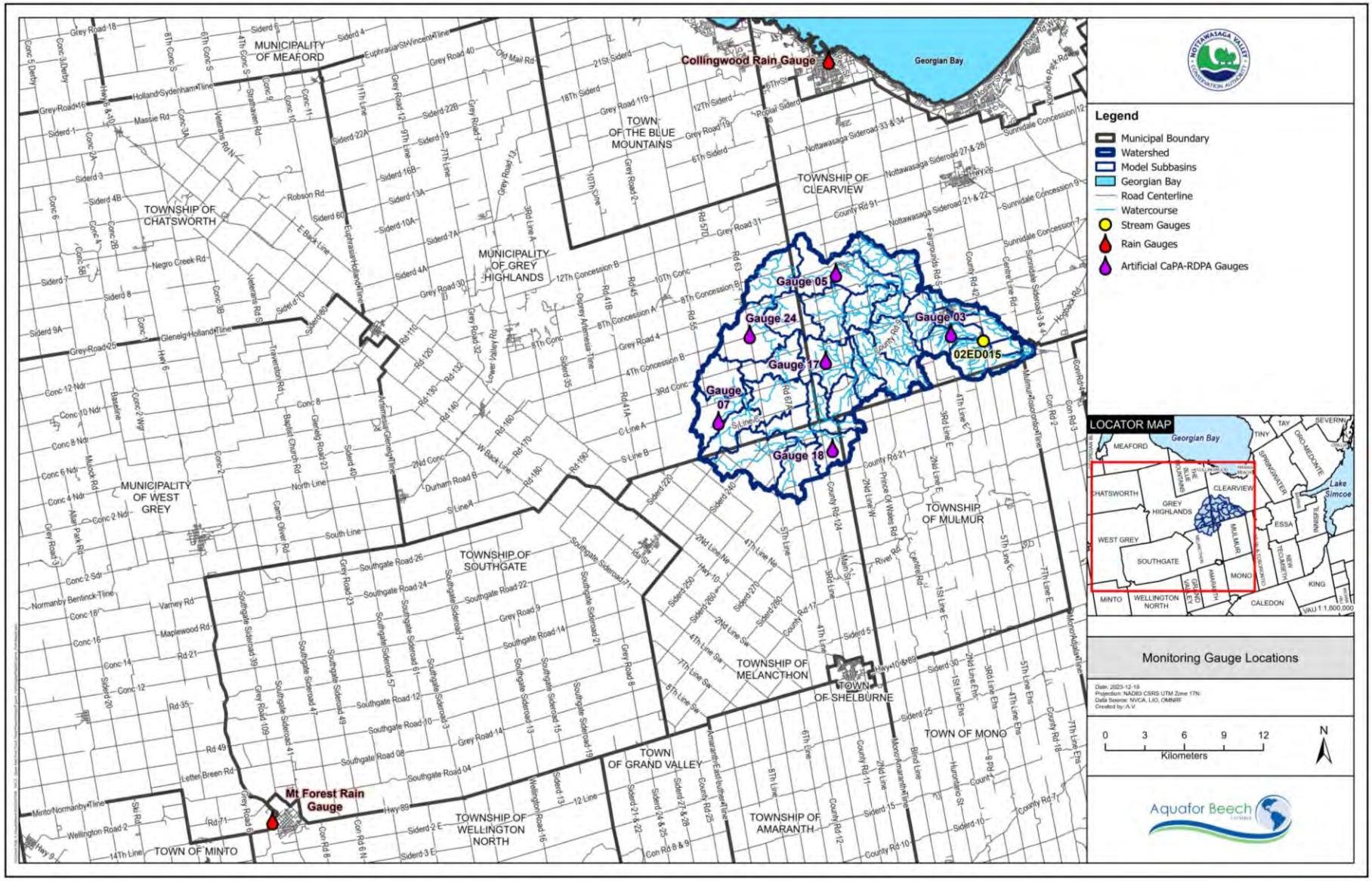

Figure 2-1: Monitoring Gauge Locations

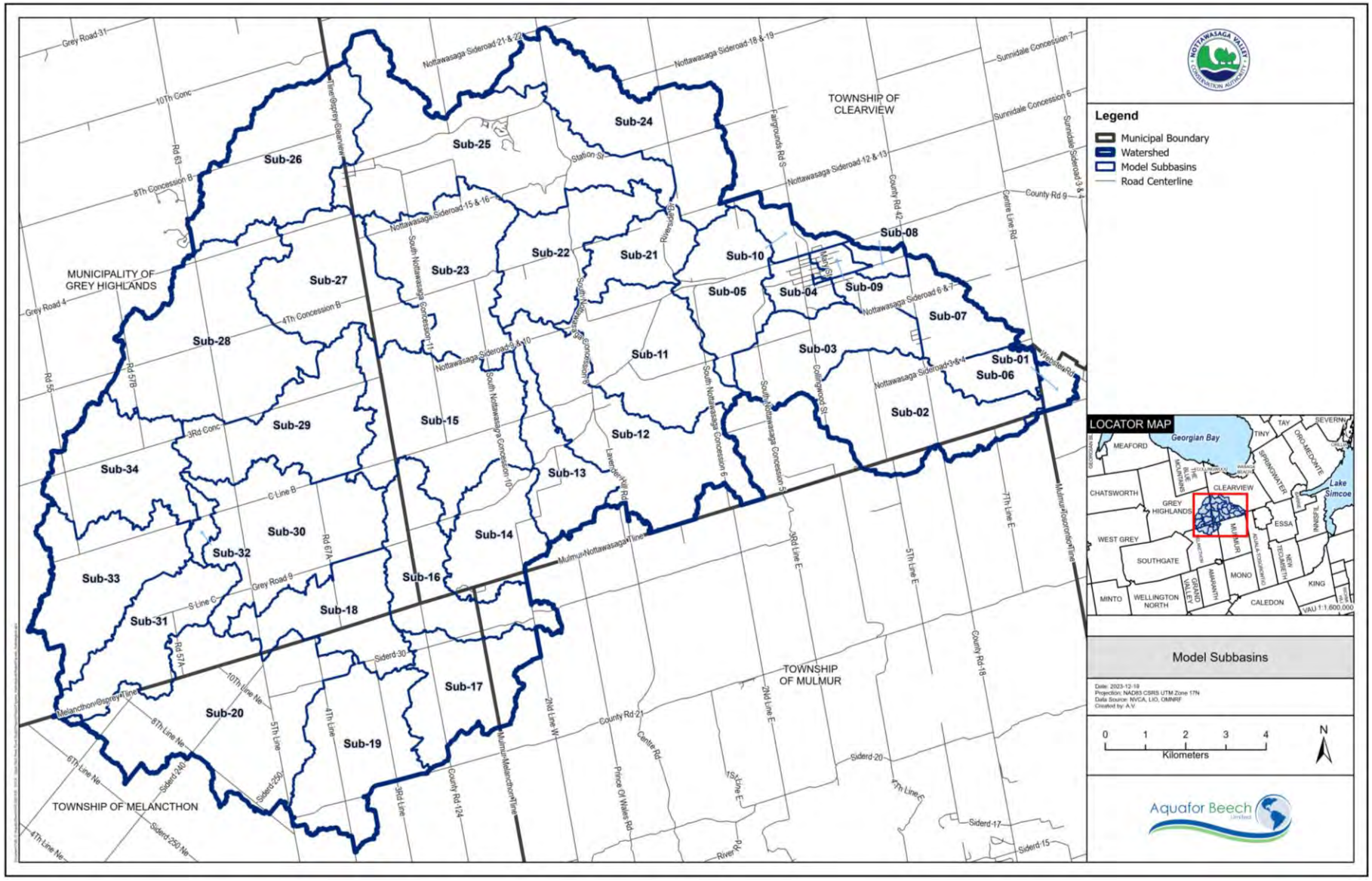

Figure 2-2: Delineated Subbasins in the HEC-HMS Model

2.6 Reach Routing

Reaches were defined using the prepared terrain surface (with burned-in stream connections), and slopes and cross-sectional geometry were determined using the LiDAR-derived DTM. A review of the DTM revealed that some reaches are characterized by wide floodplains. In addition, some of the reaches are characterized by low slopes (≤0.002 m/m). Based on these characteristics, the Muskingum-Cunge routing method was selected, since it is appropriate for use in reaches with low slopes and has the ability to account for flow within floodplains using 8-point cross-sections (US Army Corps of Engineers, 2000, 2022). For most reaches, representative 8-point cross-sections were used to represent the cross-sectional geometry, though trapezoidal, triangular, and rectangular geometries were used for shallow streams and ditches. Standard values of Manning's n for natural channels and overbanks were applied to the reaches (**Table 2-1**).

The locations of the reaches and the junctions connecting them are shown in **Figure 2-3**. A summary of reach parameters is provided in **Appendix A**.

Table 2-1: Standard Manning Roughness Coefficients for Open Channels (TRCA et al., 2017)

Land Cover	Standard 'n' Value
Natural Channel	0.035
Concrete Channel	0.013
Woods (Overbank)	0.08
Meadows (Overbank)	0.055
Marshes (Overbank)*	0.055
Lawns (Overbank)	0.045

*Defined by Aquafor to be equivalent to overbank meadows

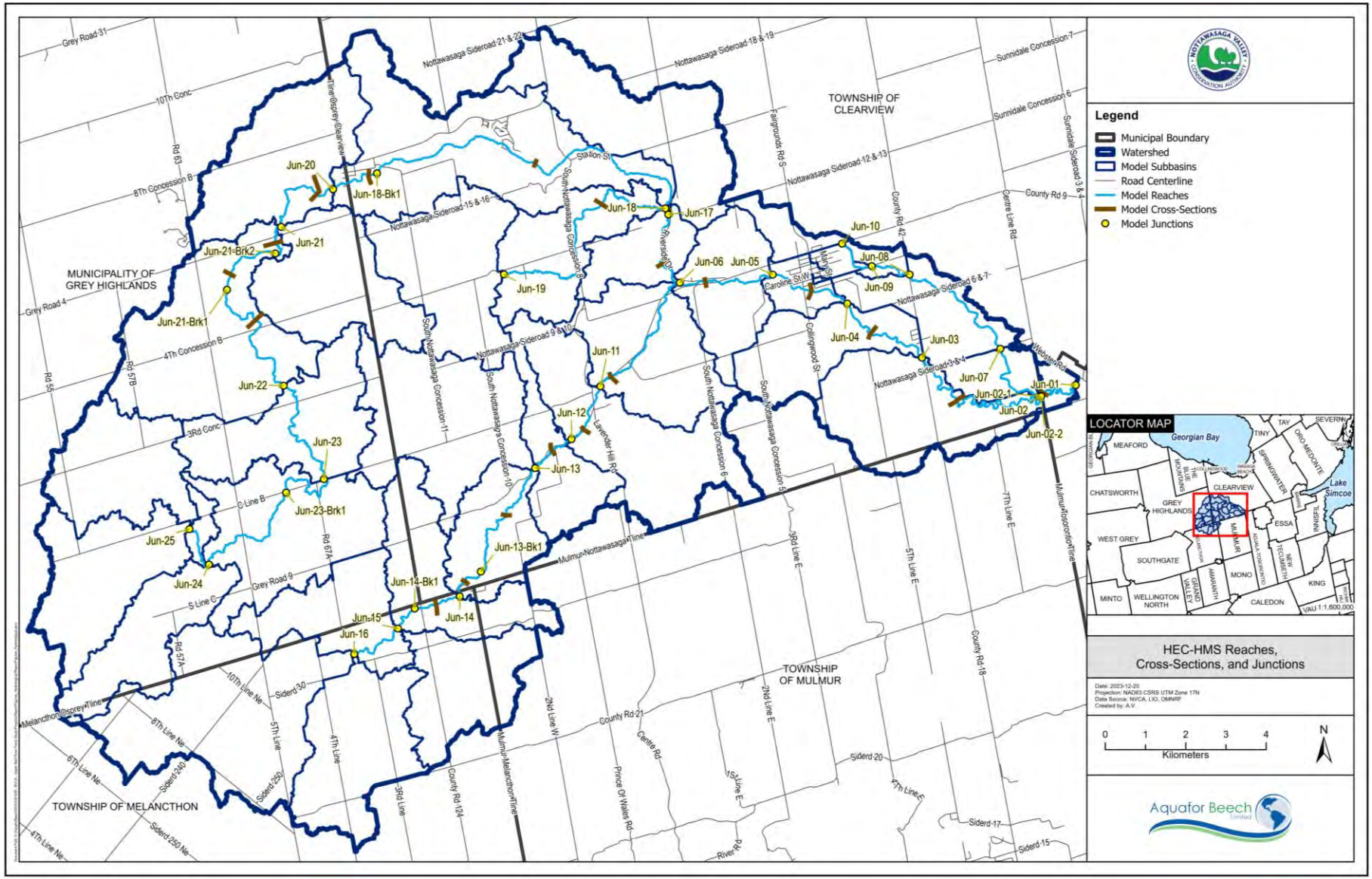

Figure 2-3: HEC-HMS Reaches, Cross-Sections, and Junctions

2.7 Transform Method

The Clark Unit Hydrograph transform method was used in the updated model, rather than the Snyder method, which was used in ORMGP's model. In the HEC-HMS modelling platform, the Snyder hydrograph is defined by determining peak flow based on the standard lag and the peaking coefficient, with the remaining ordinates of the hydrograph defined by creating a Clark Hydrograph such that the timing and flowrate of the hydrograph peak are maintained. In this regard, the two transform methods are similar. However, the Clark method allows the user to explicitly define subbasin storage, which is particularly advantageous for the Upper Mad River watershed, where large amounts of storage are provided by wetlands and waterbodies.

Time of concentration was calculated using 'C' runoff coefficients, which were defined for each land use based on either standard values (for homogeneous land use types) or sampled values (for residential areas and transportation corridors), as described in **Section 2.9** below. For subbasins having a composite 'C' value greater than 0.4, the Bransby-Williams equation was used to calculate time of concentration:

$$t_c = 0.057 \cdot L \cdot {S_w}^{-0.2} \cdot A^{-0.1}$$

where L [m] is length of the watershed's longest flowpath, S_w [%] is slope of the watershed's longest flowpath, and A [ha] is watershed area.

For subbasins having a composite 'C' value less than 0.4, the Airport equation was used to calculate time of concentration:

$$t_c = 3.26 \cdot (1.1 - C) \cdot L^{0.5} \cdot {S_w}^{-0.33}$$

Subbasin storage coefficients were defined based on time of concentration and area occupied by wetlands and open water. Further details regarding the derivation of these coefficients are provided in **Section 2.10**.

2.8 Infiltration Loss

The SCS curve number (CN) method for infiltration loss was adopted for estimating runoff, from which precipitation excess (equivalent to runoff in this case) can be calculated. HEC-HMS calculates precipitation excess, P_e [mm], as follows:

$$P_e = \frac{(P - I_a)^2}{P - I_a + \frac{(25400 - 254\,CN)}{CN}}$$

where *P* [mm] is precipitation and I_a [mm] is initial abstraction. Values of CN under average antecedent moisture conditions (AMC II) and initial abstraction corresponding to each land use type are shown in **Table 2-2** in **Section 2.9** below.

2.9 Land Use Parameters

Standard values of initial abstraction, directly connected imperviousness, and 'C' runoff coefficients are defined for homogeneous land use types. However, parameters for land uses containing a mix of impervious and pervious surfaces – namely, residential areas and transportation corridors – should be defined locally for the study area

to increase model accuracy. Representative samples were therefore collected to estimate impervious fractions for residential areas (n=15) and transportation corridors (n=5). The area occupied by directly and indirectly connected impervious surfaces was measured for each sample using areal imagery and building polygons obtained from Google Earth.

Average values of initial abstraction, directly connected imperviousness, and 'C' runoff coefficients were then calculated based on the sampled values. Standard parameter values for all land use types are recorded in **Table 2-2**. These values were subsequently used to calculated composite (weighted average) values for each subbasin.

Table 2-2: Standard Land Use Hydrological Parameters (based on TRCA et al., 2017)

Land use	CN under AMC II				I_a (mm)	'C' Coefficient	% Connected Impervious
	Hydrologic Soil Group						
	A	B	C	D			
Woods	32	60	73	79	10	0.3	0
Meadows	38	65	76	81	8	0.35	0
Cultivated	62	74	82	86	7	0.45	0
Lawns	49	69	79	84	5	0.15	0
Commercial Impervious	–	–	–	–	2	0.95	100
Open Water	100	100	100	100	0	0.95	0
Gravel	76[(1)]	85[(1)]	89[(1)]	91[(1)]	4[(2)]	0.5[(3)]	0
Swamps	98[(2)]	98[(2)]	98[(2)]	98[(2)]	15	0.05	0
Marshes	98[(2)]	98[(2)]	98[(2)]	98[(2)]	15	0.05	0
Built Up – Impervious[(4)]	49.7	69.4	79.3	84.2	4.18	0.37	25.29
Built Up – Pervious (Lawns)	49	69	79	84	5	0.15	0
Transportation[(4)]	49	69	79	84	3.45	0.56	51.8

[(1)] From TR-55 Report (USDA, 1986)
[(2)] Assumed
[(3)] From the MTO Drainage Manual (MTO, 1997)
[(4)] Determined from sampling

2.10 Calibration

Three rainfall events were selected for model calibration, occurring in June 2014, June-July 2015, and June 2017. Rainfall data from the network of rainfall gauges was interpolated throughout the watershed using the inverse distance method. Subbasin storage was first modified to account for attenuation of hydrographs peaks, particularly from wetlands and ponds (open water). Through trial and error, the following empirical equation was found to be most appropriate for determining subbasin storage:

$$S_i = a_1 * TOC_i + a_2 * A_{w,i}$$

where S_i [hrs] is the storage coefficient for Subbasin i, TOC_i [hrs] is time of concentration, $A_{w,i}$ [ha] is the area occupied by wetlands and open water, and a_1 and a_2 are coefficients. The calibrated values of a_1 and a_2 were estimated to be 0.6 and 0.1, respectively.

CN and initial abstraction values were subsequently calibrated to improve estimates of peak flow magnitude and runoff volumes. For this step, it was necessary to account for the soil's antecedent moisture condition (AMC), as this has a large impact on CN values and, in turn, on runoff rates. The CN values for dry (AMC I) and wet (AMC III) conditions can be calculated from CN under average conditions (AMC II) using the empirical equations put forth by Chow (1988):

$$CN(I) = \frac{4.2\ CN(II)}{10 - 0.058\ CN(II)}$$

and

$$CN(III) = \frac{23\ CN(II)}{10 + 0.13\ CN(II)}$$

Soil moisture conditions for the June 2014 and June-July 2015 events were considered to be AMC II, given that there were moderate amounts of rainfall and baseflow prior to the two events. The June 2017 event was simulated using CN values under AMC III since baseflow was higher prior to the onset of the event and because the watershed was more sensitive to rainfall for this storm. Ultimately, CN and I_a values under AMC II were lowered for most land uses types through the calibration process (**Table 2-3**). No changes were made to time of concentration and imperviousness estimates. Calibrated values for all subbasins parameters are recorded in **Appendix A**.

Table 2-3: Calibrated Hydrological Parameters (based on TRCA et al., 2017)

Land use	CN under AMC II				I_a (mm)
	Hydrologic Soil Group				
	A	B	C	D	
Woods	16.5	38.7	53.2	61.2	8
Meadows	20.5	43.8	57.1	64.2	6
Cultivated	40.7	54.4	65.7	72.1	4
Lawns	28.8	48.3	61.2	68.8	3
Commercial Impervious	–	–	–	–	1
Open Water	100	100	100	100	0
Gravel	57.1	70.4	77.3	80.9	4
Swamps	98(2)	98(2)	98(2)	98(2)	8
Marshes	98(2)	98(2)	98(2)	98(2)	6
Built Up – Impervious	29.8	49	61.7	69.2	2.45
Built Up – Pervious (Lawns)	28.8	48.3	61.2	68.8	3
Transportation	28.8	48.3	61.2	68.8	1.96

A comparison between modelled and measured hydrographs at the Avening gauge are shown in **Figure 2-4 to Figure 2-6** for the three storm events. Overall, the model performed very well for these events, though the modelled peak flow was 6.9 m^3/s lower than the measured peak flow for the June 2014 event. This is likely a result of high intensity rainfall not being fully captured by the Collingwood gauge, either because the rainfall distribution recorded at this gauge (located outside of the watershed) was different than the distribution of

rainfall within the watershed, or because a short period of very high intensity rainfall (e.g., 15 mins long) was responsible for the high peak flow but was not reflected in the 1-hour data available for the Collingwood gauge.

The calibration process confirmed that large wetland complexes, which are mostly concentrated within the upstream extents of the watershed, play an important role in the watershed hydrology. Wetlands were shown to greatly reduce peak flows by detaining runoff and slowly releasing stored water over an extended period of time (up to several days), despite high proportions of runoff associated with saturated or near-saturated conditions within these areas. These processes can be seen in the hydrograph for Subbasin 34 in response to the July 2017 event (**Figure 2-7**). In contrast, subbasins located further downstream are often much flashier, since there is much less storage capacity within these areas and because slopes are much higher; an example of this is shown for Subbasin 11 in response to the July 2017 event (**Figure 2-8**). These flashier subbasins were found to be primarily responsible for peak flows, while subbasins having high wetland coverage were found to be responsible for the prolonged falling limbs of the river hydrographs.

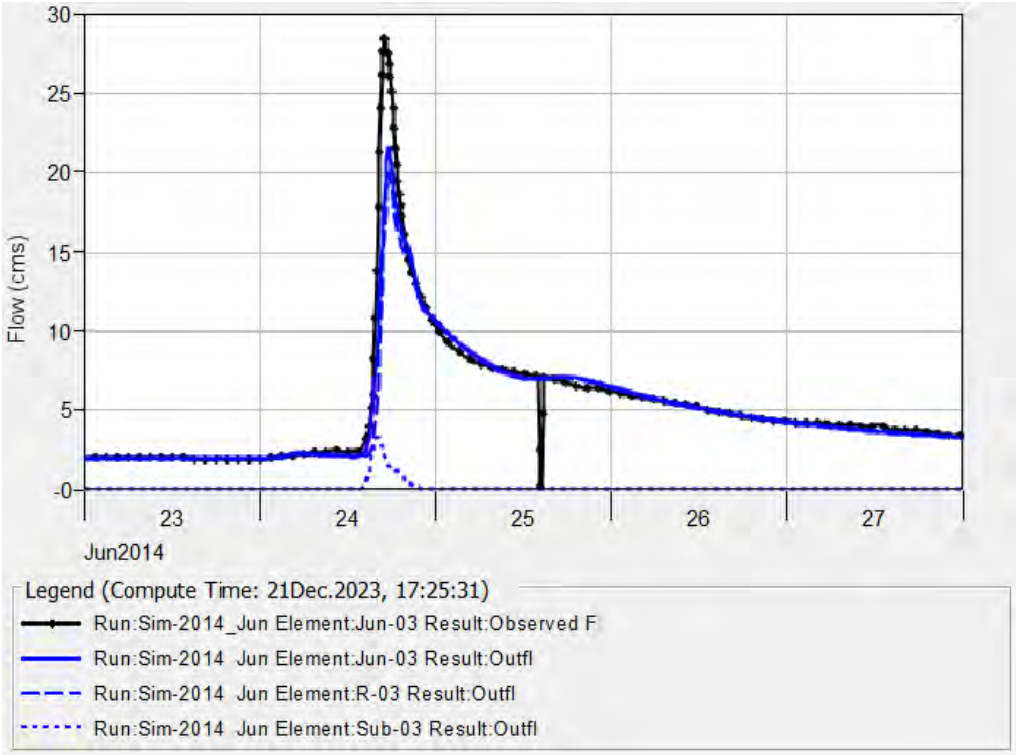

Figure 2-4: Comparison of Measured and Simulated Hydrographs at the Avening Gauge for the Storm Event Occurring in June of 2014 (AMC II)

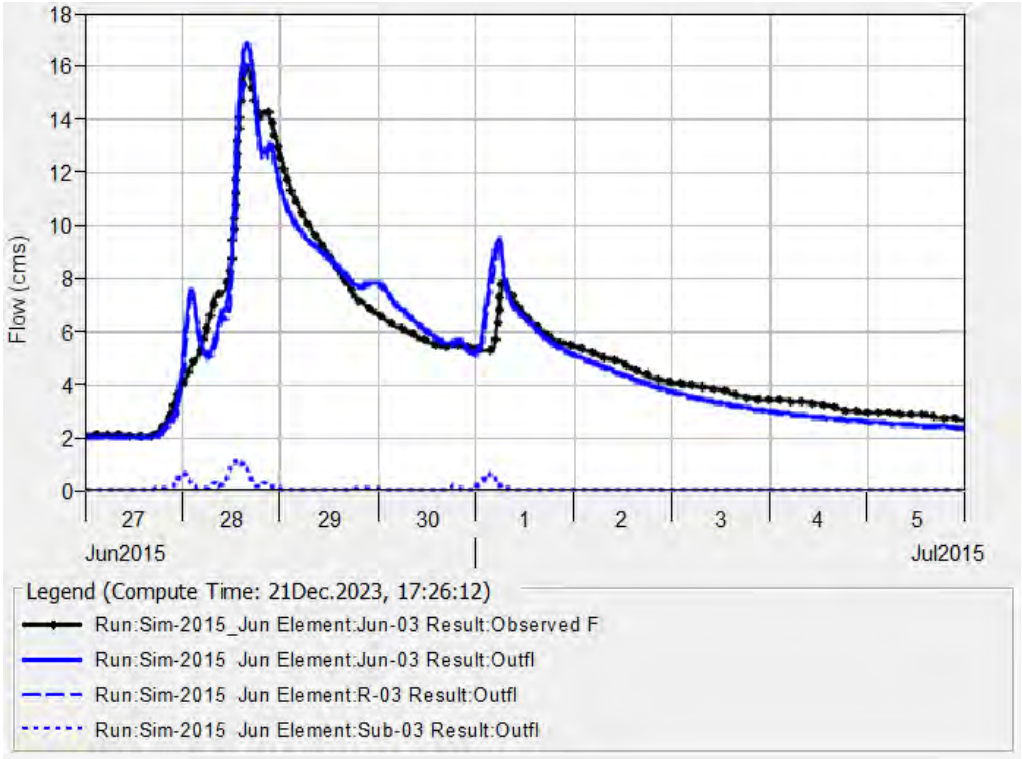

Figure 2-5: Comparison of Measured and Simulated Hydrographs at the Avening Gauge for the Storm Event Occurring in June-July of 2015 (AMC II)

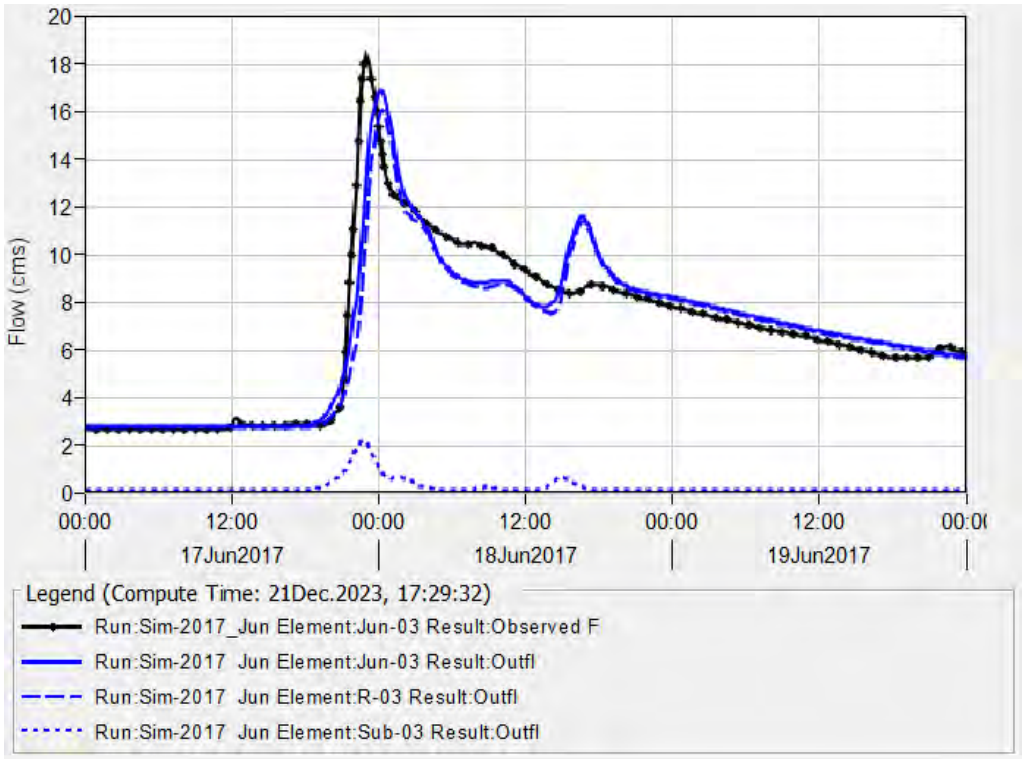

Figure 2-6: Comparison of Measured and Simulated Hydrographs at the Avening Gauge for the Storm Event Occurring in June of 2017 (AMC III)

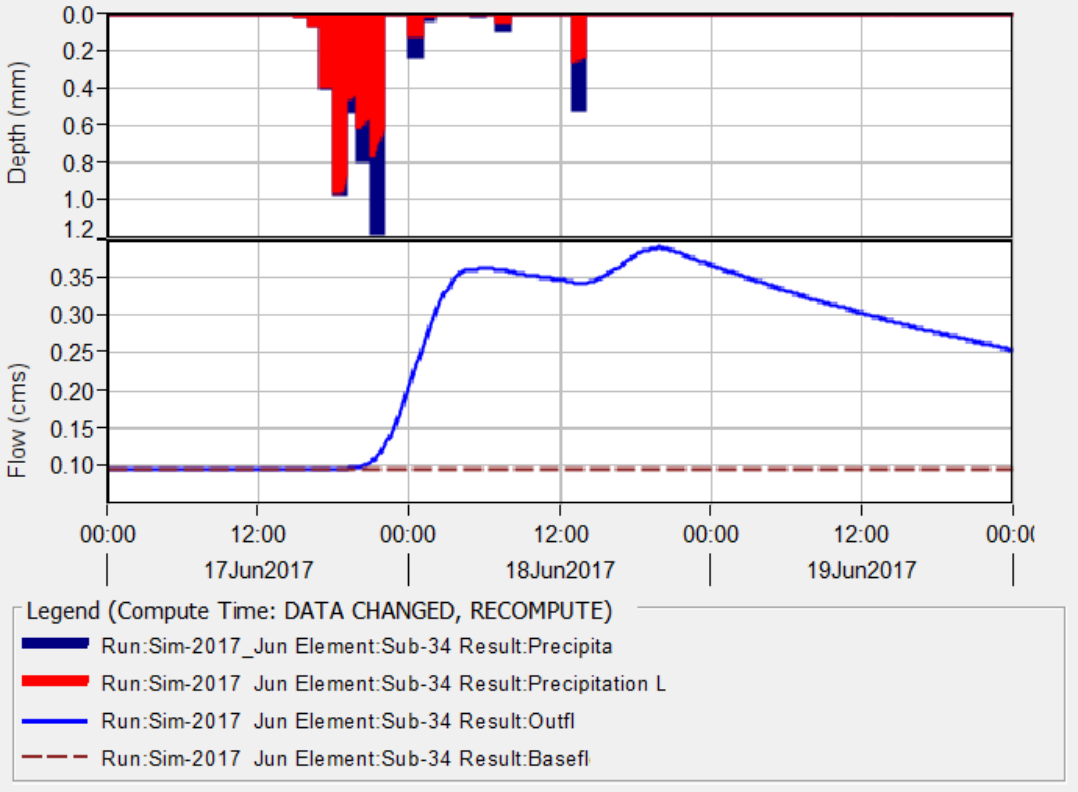

Figure 2-7: Simulated Hydrograph for Subbasin 34 in Response to the June 2017 Storm Event

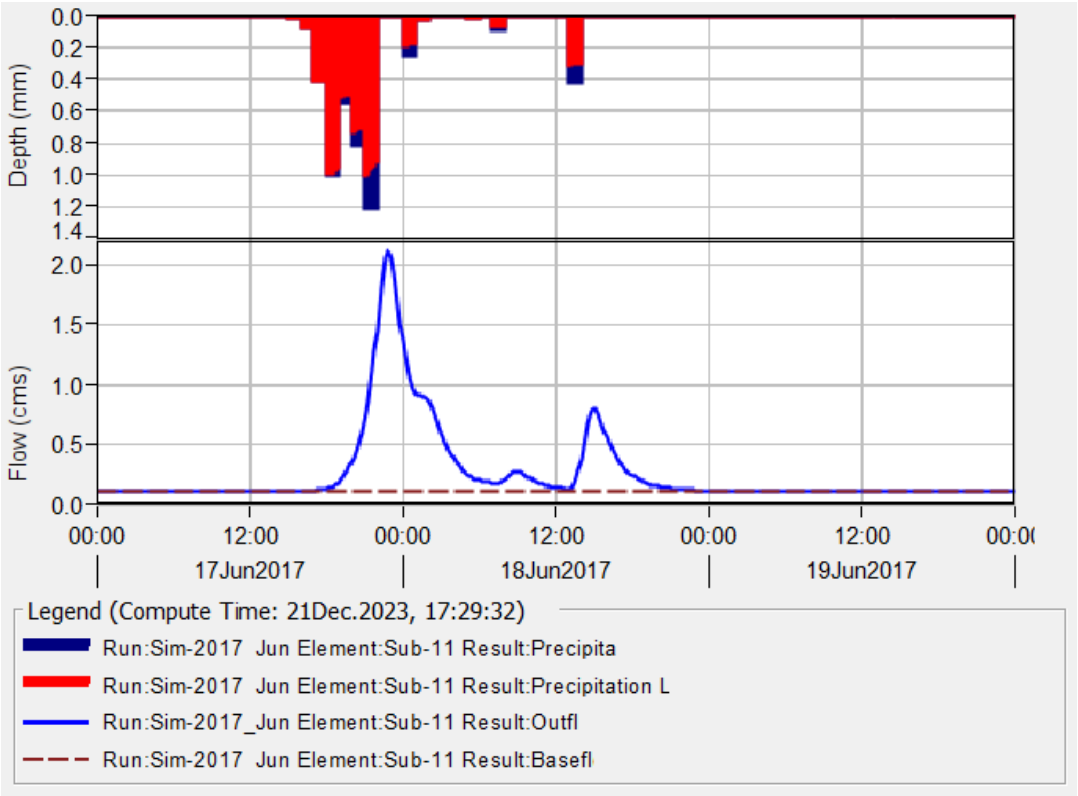

Figure 2-8: Simulated Hydrograph for Subbasin 11 in Response to the June 2017 Storm Event

2.11 Design Storms

2.11.1 *2-year to 100-year Events*

Storm rainfall depths were derived for the 2-year, 5-year, 10-year, 25-year, 50-year, and 100-year return periods using intensity-duration-frequency (IDF) curves. Since no IDF curves were available for the study areas, a set of IDF curves was defined by taking the average of the IDF curve data for the Egbert, Collingwood, and Barrie WPCC stations, which are managed by the Meteorological Service of Canada.

The model was initially run for the 2-year and 100-year return periods using the SCS 6-hour, 12-hour, and 24-hour distributions, as well as the AES 12-hour storm distribution. The peak flow results are shown in **Table 2-4** at the location of the Avening gauge (Jun-03), and were found to be fairly consistent with the flood frequency analysis estimates of summer flood flows at the Avening gauge for the 2-year and 100-year return periods (ORMGP, 2023). For this preliminary analysis, areal reduction factors (ARFs) were applied based on the circular area calculated from the distance between Jun-05 and the farthest upstream watershed boundary; additional details regarding the derivation of ARFs are provided in **Section 2.13**.

Table 2-4: Estimated 2-year and 100-year Peak Flows at the Avening Gauge for Various Storm Distributions and Durations with ARFs

Return Period	SCS 6-hr (m^3/s) with ARF of 0.872	SCS 12-hr (m^3/s) with ARF of 0.893	AES 12-hr (m^3/s) with ARF of 0.893	SCS 24-hr (m^3/s) with ARF of 0.919	Approx. Flood Frequency Analysis Estimates for Summer Flows (m^3/s)
2-year	14.56	16.60	15.08	19.90	11
100-year	83.32	84.54	75.74	100.67	97

However, as described in **Section 2.13**, nearly all annual peak flows recorded at the Avening gauge occurred between November and early June, with the exception of the 2013 flood event. This indicates that snowmelt, wet conditions during the spring freshet, and/or frozen ground conditions were responsible for the majority of recorded annual peak flows. The model was therefore run using a 10-day rain-on-snowmelt events for the 2-year to 100-year events under AMC III, which were found to produce peak flows that were more similar to estimates from the site frequency analysis. As such, it was decided that all subsequent hydrologic modelling and hydraulic modelling would be conducted using the rain-on-snowmelt events for the 2-year to 100-year return periods.

The rain-on-snowmelt distributions were developed using a method that has previously been used by the Upper Thames River Conservation Authority (UTRCA, 2004). First, rain-on-snowmelt IDF curves for 1- to 10-day durations at the Barrie WPCC station were retrieved from Environment Canada's database. The IDF curves were derived using Snowmelt Model 4 (Southern Ontario model). Equivalent precipitation depths are recorded in **Table 2-5**.

Next, precipitation depth for the 10-day duration was broken down into 1-day increments, starting with the precipitation depth for the 1-day duration and then calculating incremental increases in depth for the 2-day to 10-day durations. The resulting precipitation incremental depths were subsequently assigned ranks from 1 to 10,

with Rank 1 representing the peak day (i.e., the day with the highest precipitation) and Rank 10 representing the day when the smallest amount of precipitation occurred. An example of this process is shown in **Table B.1** (**Appendix B**) for the 100-year event. Daily precipitation was then ordered based on rank, per **Table B.2**.

For the peak day, precipitation was defined in 2-hour increments based on the winter rainfall distribution published by Brater, Sangal and Sherrill (1974), which is shown in **Table B.3**. For each of the remaining days constituting the 10-day event, precipitation was defined in 2-hour depth increments based on a modified sinusoidal distribution representing the distribution of precipitation intensity. Modifications to this function consisted of added a value of 1 to the sine function and shifting it right by 6 hours, such that the value of the final function value was 0 at the beginning and end of each day (i.e., at t = 00:00). The fraction of precipitation occurring over each 2-hour interval was determined by calculating the integral over the period and dividing the result by the integral over an entire day (**Table B.4**). For each day, precipitation depth over each time interval could then be calculated by multiplying the fraction of precipitation by total daily precipitation (**Table B.5**).

Table 2-5: Equivalent Rain-on-Snowmelt Precipitation Depths for the 1-day to 10-day Durations

Return Period	Storm Duration									
	1-day	2-day	3-day	4-day	5-day	6-day	7-day	8-day	9-day	10-day
Barrie WPCC Station (mm)										
2-yr	25.7	37.3	44.3	51.1	57.2	62.8	68.4	73.8	79.7	84.8
5-yr	33.0	48.7	58.1	68.5	77.6	87.0	96.0	104.6	113.3	121.4
10-yr	37.7	56.3	67.3	80.0	91.0	103.0	114.2	125.1	135.5	145.6
25-yr	43.8	65.9	78.9	94.5	108.0	123.1	137.2	150.9	163.6	176.2
50-yr	48.2	73.0	87.5	105.3	120.6	138.1	154.3	170.1	184.5	198.9
100-yr	52.7	80.1	96.1	116.0	133.2	153.0	171.2	189.2	205.1	221.4

2.11.2 *Regulatory (Timmins) Event and Climate Change*

The Timmins (Regional) storm is considered to be the regulatory event for the Upper Mad River watershed. Rainfall depths for the Timmins storm event, as defined by the MNRF, are recorded in **Table 2-6**.

The Timmins storm under the effects of climate change was also modelled, in accordance with MRNF guidelines. Using CMIP 5, the 50th percentile of the mean long-term (30-year) mean annual temperature change at Creemore was obtained for the RCP 4.5 (moderate warming) scenario and for the 2050 time horizon. The future estimated rainfall intensity, R_p [mm], was then calculated using the equation:

$$R_p = R_c \times 1.07^{\Delta T}$$

where R_c [mm] is historic rainfall intensity and ΔT [°C] is long-term (30-year mean) annual mean temperature change. For Creemore, ΔT was predicted to be 2.9°C. The calculated rainfall for the Timmins storm at this location under climate change is recorded in **Table 2-6**.

Table 2-6: Timmins Storm Rainfall with and without Climate Change

Time (hrs)	Historic Rainfall (mm)	Rainfall under Climate Change (mm)
1	15	18.25
2	20	24.34
3	10	12.17
4	3	3.65
5	5	6.08
6	20	24.34
7	43	52.32
8	20	24.34
9	23	27.99
10	13	15.82
11	13	15.82
12	8	9.73

2.12 Baseflow

The Constant Monthly baseflow method was used to improve calibration results and design flow estimates. Baseflow measured at the WSC flow gauge at Avening prior to each calibration event was used to calculate baseflow rate per square kilometer, from which baseflow contributions from each subbasin were determined according to their respective areas. Total baseflow at the WSC flow gauge at Avening, as well as baseflow rates per square kilometre, are shown in **Table 2-7** below for each storm event. For the rain-on-snowmelt design storms, a higher baseflow rate contribution of 0.01581 $m^3/s/km^2$ was used to account for very wet conditions. This was derived from the baseflow rate of 3.9 m^3/s measured at the Avening gauge prior to the June 2011 event that was simulated by ORMGP, which was the highest baseflow rate measured at this gauge for all calibration and validation events that were presented in the ORMGP report.

Table 2-7: Total Baseflow Rates and Baseflow Contributions by Area used in Each Simulated Event

Storm Event	Total Baseflow Rate at the Avening Gauge (m^3/s)	Baseflow Contributions by Area ($m^3/s/km^2$)
June 2014 – Calibration Event	2.015	0.00817
June-July 2015 – Calibration Event	2.015	0.00817
June 2017 – Calibration Event	2.81	0.01139
Summer Design Storms, including the Timmins Storm	2.015	0.00817
Rain-on-Snowmelt Events	3.9	0.01581

2.13 Areal Reduction Factors

In order to avoid overestimating the amount of rainfall that occurs throughout the watershed, an areal reduction factor (ARF) was determined using the circular area method. The primary point of interest was selected to be Jun-05, located immediately upstream of Creemore. The distance between this point and the farthest upstream watershed boundary was determined to be 21.01 km, which corresponds to a circular area of 346.69 km^2.

The ARF was then determined to be 0.919 for 24-hour storm distributions, based on relationships developed by the World Meteorological Organization (WMO, **Figure 2-9**). This ARF was applied to the rain-on-snowmelt peak day for the 2-year, 5-year, 10-year, 25-year, 50-year, and 100-year storms, with no reductions applied to non-peak days. For the Timmins and Timmins with Climate Change storms, an ARF of 0.79 was used, based values established by the MRNF.

The ARFs were applied for calculating peak flows throughout the majority of the watershed. However, in order to avoid underestimating flows along the East Creemore Drain (reaches R-05 to R-09), the model was re-run without an ARF for determining flows along this tributary.

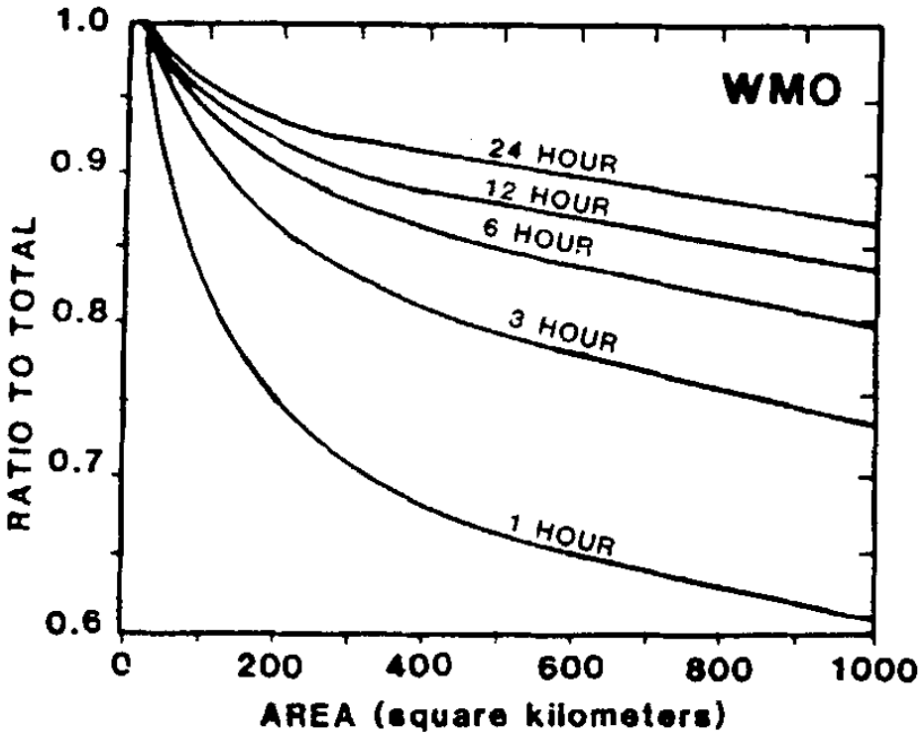

Figure 2-9: WMO Areal Reduction Factors

2.14 Model Results

The hydrologic model was run for the 2-year, 5-year, 10-year, 25-year, 50-year, 100-year, Timmins, and Timmins with Climate Change events. Results are presented at key junctions in **Table 2-8** below. Peak flows for all junctions are recorded in **Appendix C**. The Timmins storm event under the effects of climate change was found to produce

substantially higher flows than under historic climate conditions. Based on this analysis, it is anticipated that regulatory peak flows at the watershed outlet (Jun-01) would increase from 227.45 m^3/s to 311.58 m^3/s due to climate change, which represents a 37.0% increase.

Table 2-8: Peak Flows at Key Locations within the Upper Mad River Flood Study Area

Junction ID	Description	2-yr	5-yr	10-yr	25-yr	50-yr	100-yr	Timmins	Timmins with Climate Change
Jun-06	Main Branch at County Road 9	44.06	67.31	83.07	102.91	117.71	132.42	161.75	220.47
Jun-05	Main Branch Upstream of Creemore	46.98	71.87	88.73	109.94	125.78	141.57	171.84	234.40
Jun-03	Main Branch at the WSC Avening Gauge	50.66	77.66	95.88	118.79	136.06	153.17	187.20	255.94
Jun-02-1	Outflow from the East Creemore Drain (Flowing to the North of Creemore)	5.39	8.35	10.42	13.06	15.04	17.02	31.32	42.68
Jun-02	Confluence of the Main Branch with the East Creemore Drain	59.14	90.62	112.01	137.29	156.81	176.36	226.43	310.07
Jun-01	Outflow of the Upper Mad River Watershed	59.28	90.86	112.23	137.35	156.95	176.57	227.45	311.58

2.15 Site Frequency Analysis

As a point of comparison, a site frequency analysis was completed for the WSC flow gauge located along the Upper Mad River at Avening (ID #02ED015). Annual peak flow records were available between 1989 and 2022, though some records were missing. In total, there were 26 available records, which are listed in **Appendix D**. All recorded annual peak flows occurred between November and early June, aside from the 2013 peak flow, which occurred in July. This indicates that most flood events result from snowmelt, wet conditions during the spring freshet, and/or frozen ground conditions.

The site frequency analysis was undertaken using HEC-SSP (ver. 2.3) statistical analysis software. A goodness of fit test was first performed to compare various probability models (e.g., Generalized Extreme Value, Ln-normal, Log-Pearson Type III, etc.) using the Kolmogorov-Smirnov Test and Chi-Square Test, as well as a visual inspection of fit. Based on this comparison, the Ln-Normal distribution was found to have the best fit. The fitted curve and 90% confidence limits for the fitted distribution are shown in **Figure 2-10**.

A comparison between site frequency estimates and model results for rain-on-snow design storms under AMC III is provided in **Table 2-9**. All modelled peak flows were within the 90% confidence limits of the corresponding frequency analysis estimates.

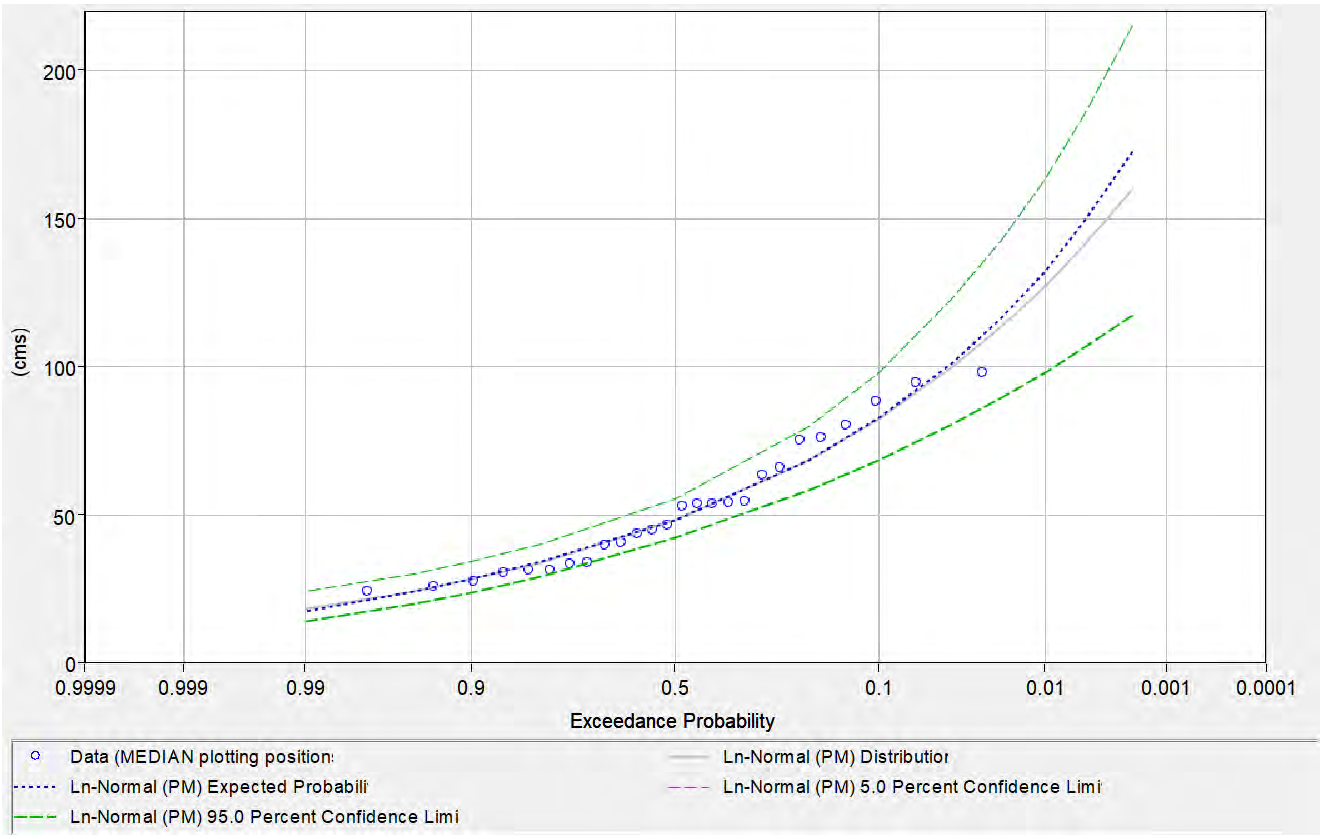

Figure 2-10: Best Fit Ln-Normal Distribution Curve with 90% Confidence Limits

Table 2-9: Comparison of Modelled Rain-on-Snowmelt Peak Flows at the Avening Gauge with Fitted Ln-Normal Distribution Flows and Confidence Limits

Percent Chance Exceedance	Ln-Normal Median Curve (m^3/s)	0.95 Confidence Limit (m^3/s)	0.05 Confidence Limit (m^3/s)	Modelled Peak Flows (m^3/s)
2-year	48.37	55.29	42.27	50.66
5-year	68.60	80.12	58.55	77.66
10-year	82.35	98.33	68.53	95.88
25-year	100.07	123.58	80.65	118.79
50-year	113.49	143.33	89.44	136.06
100-year	127.09	164.00	97.81	153.17

3 REFERENCES

Brater, E.F., Sangal, S., & Sherrill, J.D. (1974). Seasonal effects in flood synthesis. *Water Resources Research, 10*(3), 441-445. https://doi.org/10.1029/WR010i003p00441

Chow, V.T., Maidment, D.R., & Mays, L.W. (1988). *Applied Hydrology*. McGraw-Hill Company, NJ.

Ministry of Transportation Ontario (1997). *MTO Drainage Management Manual*.

Oak Ridges Moraine Groundwater Program (2023). *Rainfall-runoff modelling of the Mad River*.

TRCA, CVC, CLOCA, GRCA, GC, & NVCA (2017). *Technical guidelines for flood hazard mapping*. Downsview, ON: Toronto and Region Conservation Authority.

United States Army Corps of Engineers (2000). *Hydrological modeling system HEC-HMS: Technical reference manual*.

United States Army Corps of Engineers (2022). *Hydrological modeling system: HEC-HMS user's manual* (Ver. 4.10).

Upper Thames River Conservation Authority (2004). *Reference manual for the use of precipitation design events in the Upper Thames River watershed*.

APPENDIX A – HYDROLOGIC MODEL PARAMETERS

Table A.1: Calibrated Subbasin Parameters

Subbasin ID	Drainage Area (ha)	TOC (hrs)	Storage Coefficient (hrs)	CN – AMC II	CN – AMC III	I_a (mm)	Imperious Fraction (%)
Sub-01	96.4	1.568	1.761	44.9	61.6	5.04	2.49
Sub-02	1051.5	3.18	1.908	54.7	73.1	4.45	1.41
Sub-03	684.2	1.726	1.035	52.0	70.2	5.20	1.35
Sub-04	199.5	2.246	1.348	49.2	66.4	4.25	13.79
Sub-05	658.2	1.503	0.902	52.1	70.3	5.49	1.42
Sub-06	243.4	2.217	1.391	45.1	64.8	3.97	0.70
Sub-07	556.8	3.938	2.363	40.4	60.1	4.21	1.88
Sub-08	93.5	1.536	0.922	39.4	59.4	4.18	2.19
Sub-09	72.1	1.319	0.791	39.8	59.4	3.64	11.58
Sub-10	185.3	1.755	1.053	53.4	72.0	4.71	2.82
Sub-11	959.4	1.702	1.655	48.2	66.8	6.08	1.34
Sub-12	1258.0	1.822	6.54	52.3	70.6	5.31	1.18
Sub-13	501.1	1.277	0.952	51.7	70.6	5.60	1.05
Sub-14	608.9	1.281	0.768	46.0	64.8	5.79	1.36
Sub-15	1274.3	3.204	23.417	60.0	75.8	5.38	1.25
Sub-16	818.3	2.526	11.748	51.7	68.5	4.87	1.62
Sub-17	737.6	3.211	10.298	60.0	76.5	4.63	1.08
Sub-18	709.9	2.335	10.508	56.9	73.5	4.86	1.15
Sub-19	975.7	4.042	17.652	62.2	77.7	4.81	1.24
Sub-20	1708.5	4.015	49.666	65.7	79.3	5.27	1.58
Sub-21	403.0	1.375	0.825	52.3	70.3	5.38	0.97
Sub-22	766.4	1.927	2.094	54.7	72.9	5.24	0.77
Sub-23	1035.5	1.591	18.007	60.3	76.2	5.43	1.41
Sub-24	1137.4	1.907	2.624	53.6	71.6	4.62	0.81
Sub-25	1869.8	3.238	22.918	57.5	74.0	5.53	1.94
Sub-26	1119.6	3.637	51.067	71.9	83.1	6.05	0.68
Sub-27	964.4	3.957	37.302	68.7	81.1	6.01	1.17
Sub-28	1549.0	3.929	33.151	60.8	76.1	4.94	1.05
Sub-29	953.7	4.188	47.766	75.3	85.5	6.05	0.74
Sub-30	1185.0	4.787	25.77	62.7	78.0	4.86	1.24
Sub-31	720.1	5.321	45.233	81.5	89.4	6.30	0.84
Sub-32	90.9	2.298	1.379	54.1	72.8	3.99	0.48
Sub-33	938.7	6.046	75.83	88.6	93.5	6.94	0.40

Subbasin ID	Drainage Area (ha)	TOC (hrs)	Storage Coefficient (hrs)	CN – AMC II	CN – AMC III	I_a (mm)	Imperious Fraction (%)
Sub-34	843.4	6.877	44.49	74.3	84.5	6.06	0.91

Table A.2: Reach Parameters

Reach	Routing Method	Length (m)	Slope (m/m)	Channel Manning's n	Shape	Width (m)	Side Slope (H:V)	Left Overbank Manning's n	Right Overbank Manning's n
R-01	Muskingum-Cunge	1725.17	0.00216	0.035	Eight Point			0.08	0.08
R-02	Muskingum-Cunge	6256.34	0.00259	0.035	Eight Point			0.055	0.055
R-03	Muskingum-Cunge	2918.04	0.00581	0.035	Eight Point			0.08	0.08
R-04	Muskingum-Cunge	2267.54	0.00590	0.035	Eight Point			0.045	0.055
R-05	Muskingum-Cunge	2695.16	0.00659	0.035	Eight Point			0.08	0.08
R-06	Muskingum-Cunge	2230.58	0.00453	0.03	Trapezoid	0.9	6.3		
R-07	Muskingum-Cunge	3798.78	0.00385	0.03	Triangle		14.52		
R-08	Muskingum-Cunge	1221.71	0.00487	0.03	Rectangle	40			
R-09	Muskingum-Cunge	1158.62	0.00556	0.03	Trapezoid	0.5	3.45		
R-10	Muskingum-Cunge	3737.85	0.01023	0.035	Eight Point			0.08	0.08
R-11	Muskingum-Cunge	1647.87	0.01212	0.035	Eight Point			0.08	0.08
R-12	Muskingum-Cunge	1309.93	0.01335	0.035	Eight Point			0.08	0.08
R-13	Muskingum-Cunge	1064.46	0.02917	0.035	Eight Point			0.08	0.08
R-13-DS-1	Muskingum-Cunge	3592.83	0.01908	0.035	Eight Point			0.08	0.08
R-14	Muskingum-Cunge	826.69	0.00032	0.035	Rectangle	100			
R-14-DS-1	Muskingum-Cunge	1269.27	0.01419	0.035	Eight Point			0.08	0.08
R-15	Muskingum-Cunge	1701.61	0.00074	0.035	Rectangle	100			
R-16	Muskingum-Cunge	2320.70	0.00709	0.035	Eight Point			0.08	0.08
R-17	Muskingum-Cunge	188.57	0.00697	0.035	Eight Point			0.08	0.08
R-18	Muskingum-Cunge	7208.35	0.01648	0.035	Eight Point			0.08	0.08
R-19	Muskingum-Cunge	1357.57	0.00024	0.035	Eight Point			0.045	0.04
R-19-DS-1	Muskingum-Cunge	9711.27	0.01981	0.035	Eight Point			0.08	0.08
R-20	Muskingum-Cunge	2600.57	0.00024	0.035	Eight Point			0.08	0.08
R-21	Muskingum-Cunge	4026.33	0.00039	0.035	Eight Point			0.04	0.04
R-21-DS-1	Muskingum-Cunge	1892.67	0.00432	0.035	Eight Point			0.08	0.08
R-21-DS-2	Muskingum-Cunge	1175.04	0.00024	0.035	Eight Point			0.08	0.08
R-22	Muskingum-Cunge	3682.37	0.00017	0.035	Rectangle	100			
R-23	Muskingum-Cunge	3545.54	0.00235	0.035	Triangle		6.84		
R-23-DS-1	Muskingum-Cunge	2477.66	0.00015	0.035	Rectangle	100			
R-24	Muskingum-Cunge	1290.07	0.00135	0.035	Trapezoid	1.6	10.6		

APPENDIX B – RAIN-ON-SNOWMELT DESIGN STORM DATA

Table B.1: Daily Distribution and Ranking of Precipitation Amounts for the 10-day Rain-on-Snowmelt with a 100-year Return Period

Storm Duration (days)	Total Depth (mm)	Incremental Depth (mm)	Rank
1	52.67	52.67	1
2	80.1	27.43	2
3	96.06	15.96	10
4	116	19.94	3
5	133.17	17.17	7
6	152.99	19.82	4
7	171.24	18.25	5
8	189.15	17.91	6
9	205.14	15.99	9
10	221.4	16.26	8

Table B.2: Ranking of Precipitation Amounts Received on Each Day of the 10-day Rain-on-Snowmelt Event

Day	Rank
1	10
2	8
3	6
4	5
5	4
6	3
7	2
8	1
9	7
10	9

Table B.3: Rain-on-Snowmelt Peak Day Distribution in 2-hr Increments

Time Interval (hrs)	Fraction of Daily Precipitation (%)
0 - 2	2
2- 4	2
4 - 6	3
6 - 8	4
8 - 10	7
10 - 12	16
12 - 14	39
14 - 16	13
16 - 18	6
18 - 20	4
20 - 22	2
22 - 24	2

Table B.4: Daily Snowmelt Distribution Derived from the Modified Sinusoidal Curve for Non-Peak Days in 2-hr Increments

Time Interval (hrs)	Integral of Modified Sine Function	Fraction of Daily Precipitation (%)
0 - 2	0.0236	0.38
2- 4	0.1576	2.51
4 - 6	0.3896	6.20
6 - 8	0.6576	10.47
8 - 10	0.8896	14.16
10 - 12	1.0236	16.29
12 - 14	1.0236	16.29
14 - 16	0.8896	14.16
16 - 18	0.6576	10.47
18 - 20	0.3896	6.20
20 - 22	0.1576	2.51
22 - 24	0.0236	0.38

Table B.5: 10-Day Rain-on-Snowmelt Design Storm Precipitation for the 2-yr, 5-yr, 10-yr, 25-yr, 50-yr, and 100-yr Events with an Areal Reduction Factor of 0.919 Applied to the Peak Day

Time (hrs)	Rainfall Depth (mm)					
	2-year	5-year	10-year	25-year	50-year	100-year
2	0.0191	0.0303	0.0377	0.0472	0.0539	0.0599
4	0.1276	0.2024	0.2520	0.3150	0.3596	0.4003
6	0.3156	0.5004	0.6232	0.7789	0.8892	0.9897
8	0.5327	0.8446	1.0518	1.3145	1.5008	1.6703
10	0.7207	1.1426	1.4230	1.7783	2.0304	2.2597
12	0.8292	1.3147	1.6373	2.0462	2.3361	2.6001
14	0.8292	1.3147	1.6373	2.0462	2.3361	2.6001
16	0.7207	1.1426	1.4230	1.7783	2.0304	2.2597
18	0.5327	0.8446	1.0518	1.3145	1.5008	1.6703
20	0.3156	0.5004	0.6232	0.7789	0.8892	0.9897
22	0.1276	0.2024	0.2520	0.3150	0.3596	0.4003
24	0.0191	0.0303	0.0377	0.0472	0.0539	0.0599
26	0.0210	0.0326	0.0410	0.0488	0.0544	0.0611
28	0.1402	0.2179	0.2739	0.3258	0.3634	0.4078
30	0.3466	0.5389	0.6772	0.8055	0.8985	1.0083
32	0.5850	0.9095	1.1428	1.3595	1.5165	1.7017
34	0.7915	1.2304	1.5461	1.8392	2.0516	2.3022
36	0.9107	1.4157	1.7790	2.1162	2.3606	2.6489
38	0.9107	1.4157	1.7790	2.1162	2.3606	2.6489
40	0.7915	1.2304	1.5461	1.8392	2.0516	2.3022
42	0.5850	0.9095	1.1428	1.3595	1.5165	1.7017
44	0.3466	0.5389	0.6772	0.8055	0.8985	1.0083
46	0.1402	0.2179	0.2739	0.3258	0.3634	0.4078
48	0.0210	0.0326	0.0410	0.0488	0.0544	0.0611
50	0.0225	0.0342	0.0415	0.0516	0.0595	0.0673
52	0.1500	0.2282	0.2771	0.3446	0.3970	0.4492
54	0.3708	0.5643	0.6852	0.8520	0.9816	1.1106
56	0.6258	0.9524	1.1564	1.4380	1.6567	1.8744
58	0.8467	1.2885	1.5645	1.9454	2.2413	2.5358
60	0.9742	1.4825	1.8002	2.2384	2.5789	2.9177
62	0.9742	1.4825	1.8002	2.2384	2.5789	2.9177
64	0.8467	1.2885	1.5645	1.9454	2.2413	2.5358
66	0.6258	0.9524	1.1564	1.4380	1.6567	1.8744
68	0.3708	0.5643	0.6852	0.8520	0.9816	1.1106
70	0.1500	0.2282	0.2771	0.3446	0.3970	0.4492
72	0.0225	0.0342	0.0415	0.0516	0.0595	0.0673
74	0.0231	0.0352	0.0422	0.0528	0.0607	0.0685
76	0.1542	0.2352	0.2816	0.3526	0.4055	0.4577

Time (hrs)	Rainfall Depth (mm)					
	2-year	5-year	10-year	25-year	50-year	100-year
78	0.3814	0.5817	0.6964	0.8719	1.0027	1.1317
80	0.6436	0.9817	1.1753	1.4715	1.6923	1.9100
82	0.8708	1.3281	1.5900	1.9907	2.2895	2.5840
84	1.0019	1.5281	1.8295	2.2905	2.6343	2.9731
86	1.0019	1.5281	1.8295	2.2905	2.6343	2.9731
88	0.8708	1.3281	1.5900	1.9907	2.2895	2.5840
90	0.6436	0.9817	1.1753	1.4715	1.6923	1.9100
92	0.3814	0.5817	0.6964	0.8719	1.0027	1.1317
94	0.1542	0.2352	0.2816	0.3526	0.4055	0.4577
96	0.0231	0.0352	0.0422	0.0528	0.0607	0.0685
98	0.0257	0.0353	0.0448	0.0568	0.0657	0.0744
100	0.1713	0.2357	0.2992	0.3789	0.4384	0.4971
102	0.4235	0.5829	0.7398	0.9370	1.0839	1.2291
104	0.7148	0.9838	1.2485	1.5814	1.8294	2.0743
106	0.9670	1.3309	1.6891	2.1394	2.4750	2.8063
108	1.1127	1.5314	1.9435	2.4616	2.8477	3.2289
110	1.1127	1.5314	1.9435	2.4616	2.8477	3.2289
112	0.9670	1.3309	1.6891	2.1394	2.4750	2.8063
114	0.7148	0.9838	1.2485	1.5814	1.8294	2.0743
116	0.4235	0.5829	0.7398	0.9370	1.0839	1.2291
118	0.1713	0.2357	0.2992	0.3789	0.4384	0.4971
120	0.0257	0.0353	0.0448	0.0568	0.0657	0.0744
122	0.0262	0.0388	0.0476	0.0586	0.0668	0.0749
124	0.1748	0.2593	0.3177	0.3912	0.4459	0.5001
126	0.4322	0.6412	0.7857	0.9674	1.1025	1.2365
128	0.7295	1.0821	1.3260	1.6326	1.8608	2.0868
130	0.9869	1.4640	1.7939	2.2088	2.5174	2.8233
132	1.1355	1.6845	2.0641	2.5414	2.8966	3.2484
134	1.1355	1.6845	2.0641	2.5414	2.8966	3.2484
136	0.9869	1.4640	1.7939	2.2088	2.5174	2.8233
138	0.7295	1.0821	1.3260	1.6326	1.8608	2.0868
140	0.4322	0.6412	0.7857	0.9674	1.1025	1.2365
142	0.1748	0.2593	0.3177	0.3912	0.4459	0.5001
144	0.0262	0.0388	0.0476	0.0586	0.0668	0.0749
146	0.0433	0.0593	0.0699	0.0833	0.0931	0.1030
148	0.2894	0.3960	0.4667	0.5560	0.6219	0.6879
150	0.7156	0.9791	1.1540	1.3748	1.5379	1.7010
152	1.2077	1.6525	1.9476	2.3202	2.5955	2.8707
154	1.6339	2.2357	2.6350	3.1390	3.5114	3.8838
156	1.8800	2.5724	3.0318	3.6117	4.0402	4.4686

Time (hrs)	Rainfall Depth (mm)					
	2-year	5-year	10-year	25-year	50-year	100-year
158	1.8800	2.5724	3.0318	3.6117	4.0402	4.4686
160	1.6339	2.2357	2.6350	3.1390	3.5114	3.8838
162	1.2077	1.6525	1.9476	2.3202	2.5955	2.8707
164	0.7156	0.9791	1.1540	1.3748	1.5379	1.7010
166	0.2894	0.3960	0.4667	0.5560	0.6219	0.6879
168	0.0433	0.0593	0.0699	0.0833	0.0931	0.1030
170	0.4731	0.6056	0.6933	0.8041	0.8865	0.9681
172	0.4731	0.6056	0.6933	0.8041	0.8865	0.9681
174	0.7097	0.9084	1.0399	1.2062	1.3297	1.4521
176	0.9462	1.2112	1.3866	1.6083	1.7729	1.9361
178	1.6559	2.1197	2.4265	2.8144	3.1026	3.3883
180	3.7848	4.8450	5.5463	6.4330	7.0917	7.7446
182	9.2255	11.8096	13.5192	15.6804	17.2861	18.8775
184	3.0752	3.9365	4.5064	5.2268	5.7620	6.2925
186	1.4193	1.8169	2.0799	2.4124	2.6594	2.9042
188	0.9462	1.2112	1.3866	1.6083	1.7729	1.9361
190	0.4731	0.6056	0.6933	0.8041	0.8865	0.9681
192	0.4731	0.6056	0.6933	0.8041	0.8865	0.9681
194	0.0210	0.0338	0.0412	0.0508	0.0576	0.0645
196	0.1404	0.2255	0.2751	0.3391	0.3847	0.4306
198	0.3473	0.5575	0.6803	0.8384	0.9512	1.0647
200	0.5861	0.9409	1.1481	1.4149	1.6054	1.7969
202	0.7929	1.2729	1.5532	1.9143	2.1720	2.4311
204	0.9123	1.4646	1.7871	2.2026	2.4991	2.7972
206	0.9123	1.4646	1.7871	2.2026	2.4991	2.7972
208	0.7929	1.2729	1.5532	1.9143	2.1720	2.4311
210	0.5861	0.9409	1.1481	1.4149	1.6054	1.7969
212	0.3473	0.5575	0.6803	0.8384	0.9512	1.0647
214	0.1404	0.2255	0.2751	0.3391	0.3847	0.4306
216	0.0210	0.0338	0.0412	0.0508	0.0576	0.0645
218	0.0200	0.0326	0.0392	0.0476	0.0542	0.0601
220	0.1337	0.2174	0.2618	0.3180	0.3616	0.4010
222	0.3305	0.5376	0.6474	0.7863	0.8942	0.9915
224	0.5578	0.9074	1.0926	1.3270	1.5091	1.6735
226	0.7547	1.2276	1.4782	1.7953	2.0417	2.2640
228	0.8683	1.4124	1.7008	2.0657	2.3492	2.6049
230	0.8683	1.4124	1.7008	2.0657	2.3492	2.6049
232	0.7547	1.2276	1.4782	1.7953	2.0417	2.2640
234	0.5578	0.9074	1.0926	1.3270	1.5091	1.6735
236	0.3305	0.5376	0.6474	0.7863	0.8942	0.9915

Time (hrs)	Rainfall Depth (mm)					
	2-year	5-year	10-year	25-year	50-year	100-year
238	0.1337	0.2174	0.2618	0.3180	0.3616	0.4010
240	0.0200	0.0326	0.0392	0.0476	0.0542	0.0601

APPENDIX C – HYDROLOGIC MODEL RESULTS

Table C.1: Peak Flows under the 2-year, 5-year, 10-year, 25-year, 50-year, and 100-year Rain-on-Snowmelt Events and under the Timmins Storms with/without Climate Change

Junction ID	2-yr	5-yr	10-yr	25-yr	50-yr	100-yr	Timmins	Timmins with Climate Change
Jun-01	59.28	90.86	112.23	137.35	156.95	176.57	227.45	311.58
Jun-02	59.14	90.62	112.01	137.29	156.81	176.36	226.43	310.07
Jun-02-1	5.39	8.35	10.42	13.06	15.04	17.02	31.32	42.68
Jun-02-2	54.67	83.85	103.49	127.27	145.45	163.57	207.71	284.24
Jun-03	50.66	77.66	95.88	118.79	136.06	153.17	187.20	255.94
Jun-04	48.03	73.42	90.62	112.25	128.37	144.41	175.56	239.34
Jun-05	46.98	71.87	88.73	109.94	125.78	141.57	171.84	234.40
Jun-06	44.06	67.31	83.07	102.91	117.71	132.42	161.75	220.47
Jun-07	4.38	6.72	8.34	10.42	11.97	13.50	24.47	33.25
Jun-08	2.26	3.43	4.24	5.27	6.04	6.80	12.45	16.97
Jun-09	1.78	2.67	3.27	4.03	4.60	5.16	9.78	13.25
Jun-10	1.34	1.99	2.43	2.99	3.40	3.80	7.36	9.96
Jun-11	17.25	26.49	32.78	40.61	46.48	52.34	74.82	102.16
Jun-12	13.64	21.04	26.10	32.36	37.07	41.78	57.51	78.58
Jun-13	12.17	18.14	22.24	27.33	31.13	34.88	50.85	69.54
Jun-13-Bk1	9.31	13.84	16.91	20.78	23.63	26.46	39.24	53.00
Jun-14	9.32	13.85	16.91	20.78	23.64	26.46	39.24	53.01
Jun-14-Bk1	7.68	11.34	13.81	16.92	19.20	21.47	31.67	42.62
Jun-15	7.70	11.38	13.86	16.97	19.27	21.54	31.83	42.83
Jun-16	4.16	6.12	7.45	9.13	10.36	11.58	15.43	20.59
Jun-17	20.54	31.05	38.28	47.40	54.15	60.84	65.92	89.27
Jun-18	15.37	23.16	28.57	35.43	40.50	45.54	47.40	63.25
Jun-18-Bk1	11.10	16.20	19.67	24.02	27.26	30.43	35.49	46.88
Jun-19	2.08	3.08	3.74	4.57	5.19	5.79	8.82	11.86
Jun-20	11.12	16.22	19.70	24.06	27.30	30.48	35.56	46.98
Jun-21	9.90	14.46	17.58	21.48	24.37	27.20	32.50	42.91
Jun-21-Brk1	6.82	9.83	11.86	14.40	16.27	18.12	22.65	29.71
Jun-21-Brk2	6.82	9.83	11.85	14.40	16.27	18.12	22.64	29.70
Jun-22	6.83	9.86	11.89	14.44	16.33	18.19	22.89	30.15
Jun-23	5.62	8.08	9.73	11.81	13.35	14.87	19.14	25.19
Jun-23-Brk1	3.78	5.33	6.37	7.67	8.63	9.58	12.36	15.93
Jun-24	3.78	5.33	6.37	7.67	8.63	9.58	12.36	15.93

Junction ID	2-yr	5-yr	10-yr	25-yr	50-yr	100-yr	Timmins	Timmins with Climate Change
Jun-25	2.50	3.54	4.23	5.09	5.73	6.37	8.10	10.43

APPENDIX D – SITE FREQUENCY ANALYSIS STREAMFLOW DATA

Table D.1: Annual Peak Flows from the WSC Gauge at Avening (02ED015) used in the Site Frequency Analysis

Date	Peak Flow (m^3/s)
Mar 28, 1989	53.9
Apr 09, 1991	63.4
Nov 13, 1992	54.7
Apr 10, 1993	45
May 26, 1994	27.5
Nov 11, 1995	31.3
Mar 27, 1998	80.3
Jun 02, 1999	33.9
May 13, 2000	46.5
Apr 08, 2001	76.2
Mar 09, 2002	30.7
Mar 05, 2004	52.9
Mar 31, 2005	39.9
Mar 13, 2006	65.8
Apr 01, 2008	98.1
Mar 15, 2010	31.3
Mar 18, 2011	54.1
Mar 08, 2012	53.9
Jul 08, 2013	88.3
Apr 14, 2014	75.4
Apr 10, 2015	25.9
Mar 28, 2016	94.6
May 05, 2017	40.6
Jan 11, 2020	33.7
Mar 11, 2021	43.5
Mar 31, 2022	24.3
Mar 28, 1989	53.9
Apr 09, 1991	63.4
Nov 13, 1992	54.7
Apr 10, 1993	45
May 26, 1994	27.5
Nov 11, 1995	31.3

Mar 27, 1998	80.3
Jun 02, 1999	33.9
May 13, 2000	46.5
Apr 08, 2001	76.2
Mar 09, 2002	30.7
Mar 05, 2004	52.9
Mar 31, 2005	39.9
Mar 13, 2006	65.8
Apr 01, 2008	98.1
Mar 15, 2010	31.3
Mar 18, 2011	54.1
Mar 08, 2012	53.9
Jul 08, 2013	88.3
Apr 14, 2014	75.4
Apr 10, 2015	25.9
Mar 28, 2016	94.6
May 05, 2017	40.6
Jan 11, 2020	33.7
Mar 11, 2021	43.5
Mar 31, 2022	24.3

APPENDIX E – PREVIOUS ORMGP HYDROLOGIC MODELLING REPORT

Rainfall-Runoff Modelling of the Mad River

An event-based HEC-HMS model of the Upper Mad River watershed. Prepared for the NVCA

Oak Ridges Moraine Groundwater Program

19 December, 2023

Introduction

Upper Mad River

The Nottawasaga Valley Conservation Authority (NVCA) and The Oak Ridges Moraine Groundwater Program (ORMGP) have partnered to explore the applicability of the **ORMGP's historical climate data service** (https://owrc.github.io/interpolants/modelling/waterbudget/data.html) in supporting event-based HEC-HMS models built in Southern Ontario to investigate the rainfall-runoff response to extreme summer rainfall events. As a proof of concept, the ~246km² Upper Mad River watershed was identified as a good first candidate.

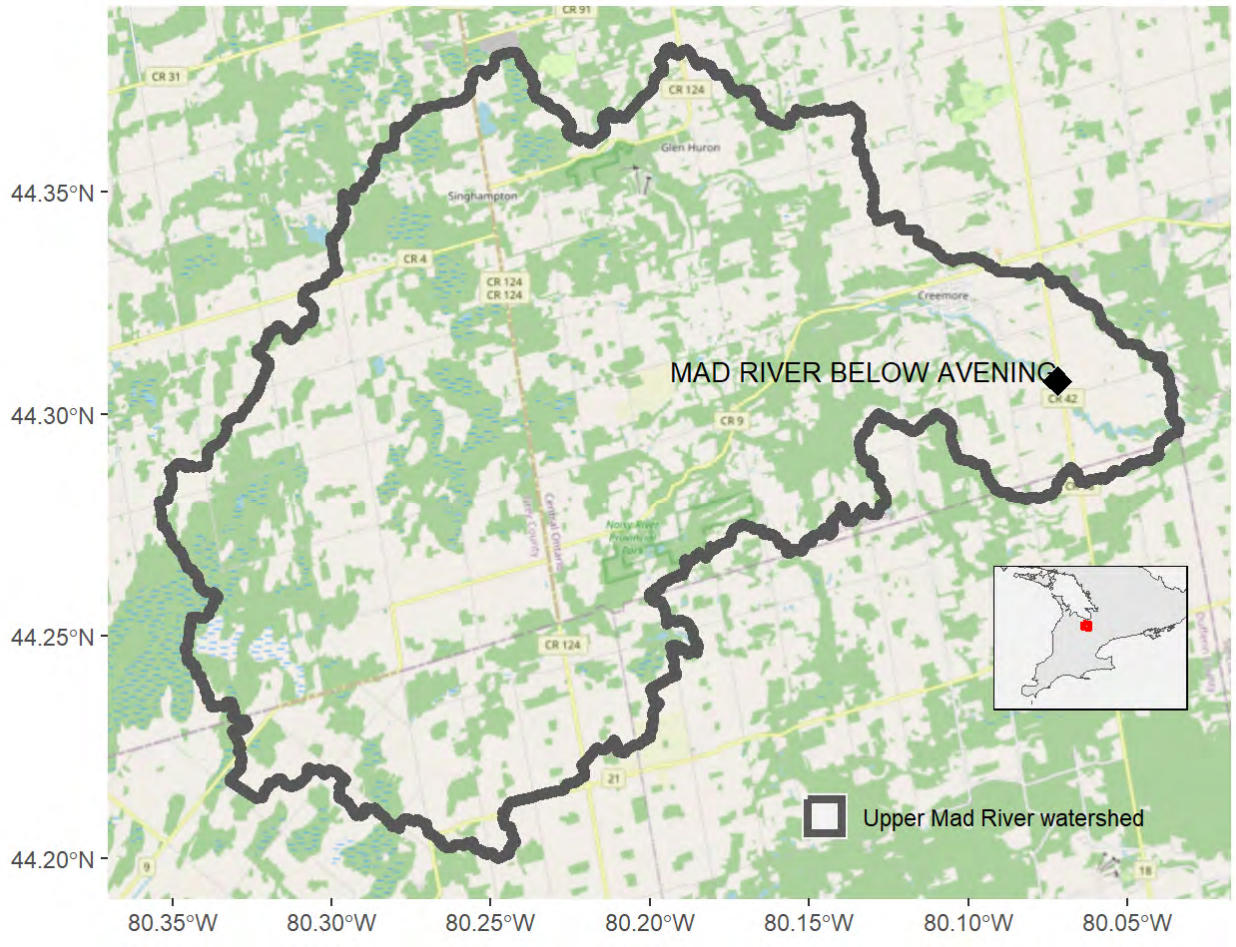

Upper Mad River watershed and the Water Survey of Canada (WSC) gauge targeted for HEC-HMS calibration

HEC-HMS

The HEC-HMS model development proceeded in a manner such that planned future long-term continuous simulations could be readily accommodated. As such, the NVCA requested a “Deficit and Constant” method suitable for long term continuous modelling be included with the delivered model. The HEC-HMS model code offered by the US Army Corps of Engineers Hydrologic Engineering Center (https://www.hec.usace.army.mil/software/hec-hms/) includes such functionality. Many other model codes investigated for this study (including PRMS (https://www.usgs.gov/software/precipitation-runoff-modeling-system-prms), Raven (http://raven.uwaterloo.ca/), MikeSHE (https://www.mikepoweredbydhi.com/products/mike-she), HydroGeoSphere (https://www.aquanty.com/hydrogeosphere), etc.), also incorporate this functionality, yet HEC-HMS was ultimately chosen due to the code:

1. being free of cost;
2. having an integrated Graphical User Interface (GUI);
3. having both event and continuous/deficit and constant modelling capabilities;
4. has powerful capabilities such as the 2D shallow water flow module included in HEC-RAS (https://www.hec.usace.army.mil/confluence/rasdocs/r2dum/latest/introduction/hec-ras-2d-modeling-advantages-capabilities).

5. being widely used both professionally and academically, thus making HEC-HMS the right application to be adopted institutionally due to its transferability.

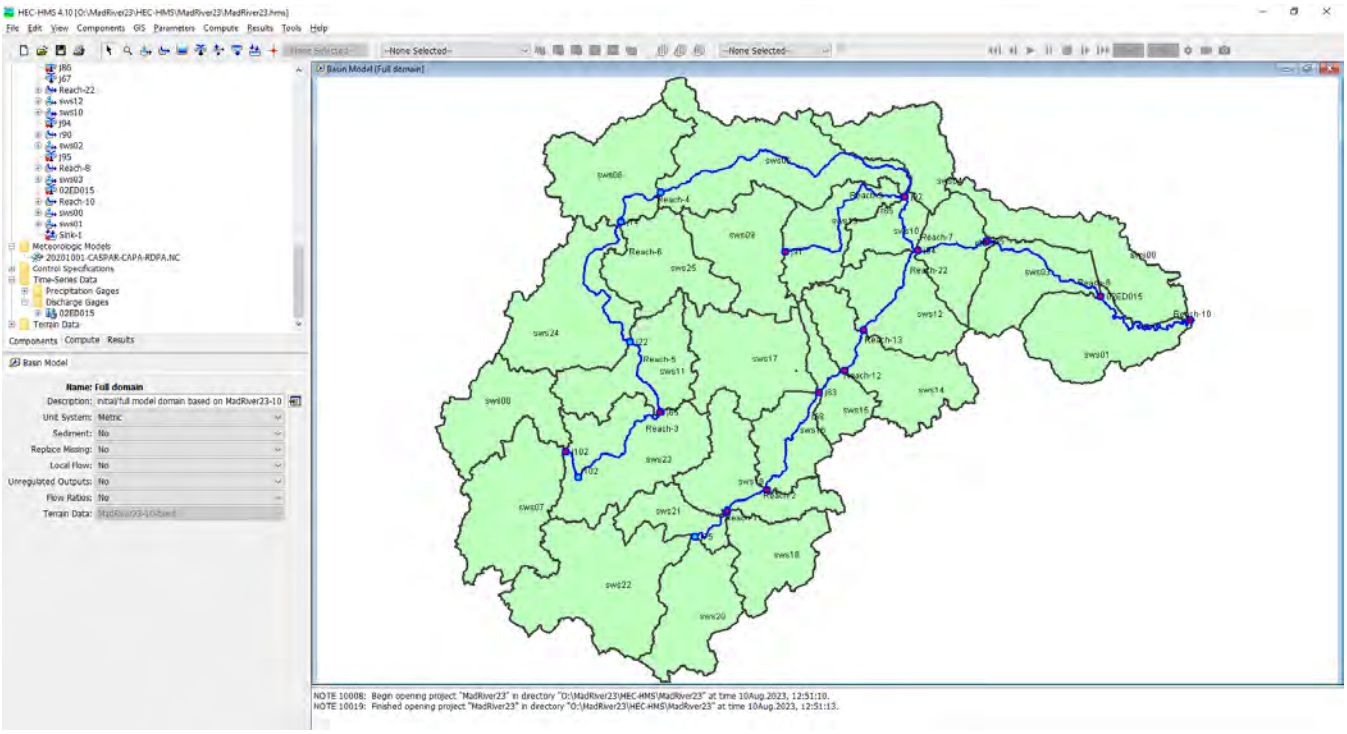

Snapshot of the Mad River HEC-HMS project.

Design Criteria

The model construction phase proceeded with certain constraints such that the model can readily simulate continuous processes. For instance, the model was built with:

1. smaller (~10km²) subbasins commensurate with sub-watershed boundaries managed by the NVCA that also coincide with the ORMGP climate data service distribution. In total there are 27 HEC-HMS subbasins (see Figure @ref(fig:leaflet)).
2. subbasins and reaches using HEC-HMS's "GIS" functionality based on a 10m DEM.
3. applied map-based hydrologic processes (i.e., SCS curve method) that is best suited for simulating future land use change.

It's important to note that in practice, models are developed to be either event-based (e.g., individual extreme rainfall events) or continuous (e.g., long-term/seasonal hydrology, climate change, etc.) but rarely both. The ORMGP maintains a near-real-time daily data set complete since 1901, that was built to support long term continuous modelling needed for groundwater resource management. However, the ORMGP also maintains a 6-hour, near-real-time climate data set since 2002. Both of these products are complete and are spatially distributed to thousands of ~10km² sub-watersheds covering the ORMGP jurisdiction (https://owrc.github.io/interpolants/modelling/waterbudget/data.html).

This has been prepared to satisfy the agreement between NVCA and ORMGP with respect to the Mad River Modelling study. Specifically, it satisfies Task 1.4 (assist the NVCA with preparation of HEC-HMS Technical Memo). To meet this task, this document includes the methods used to i) compile the necessary data (Task

1.1); ii) build the model (Task 1.2); and iii) calibrate/verify the model and conduct a sensitivity analysis (Task 1.3).

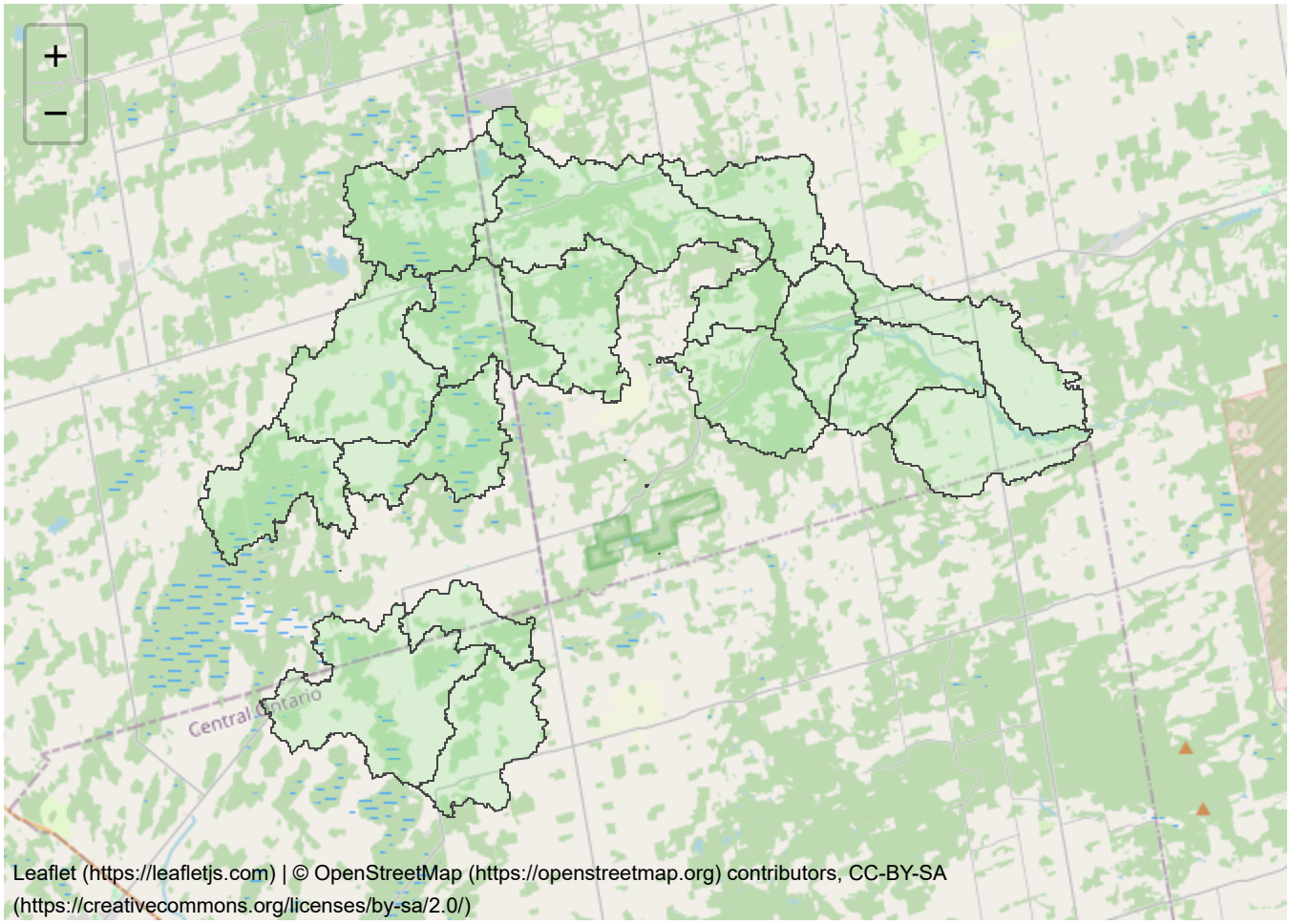

Mad River HEC-HMS subbasins (click on basins to see properties)

** interactive maps are only when viewed as a webpage (https://owrc.github.io/projects/2023/MadRiver23/).*

Data Collection

The Data Collection piece (Task 1.1) relied upon the incorperation of the ORMGP climate data service. Each of the HEC-HMS subbasins mapped well to the ORMGP's sub-watershed delineation. Rainfall accumulations was nonetheless derived from the ~10km² CaPA-RDPA (https://weather.gc.ca/grib/grib2_RDPA_ps10km_e.html) grid shown below. Compared with meteorological stations, the CaPA-RDPA product offers a finer spatial distribution of precipitation amounts. Given that southern Ontario extreme summer events are typically of the convective type (Klaassen, 2014), many of these storms are small in scale and are susceptible of being unobserved by southern Ontario's relatively coarse meteorological station network.

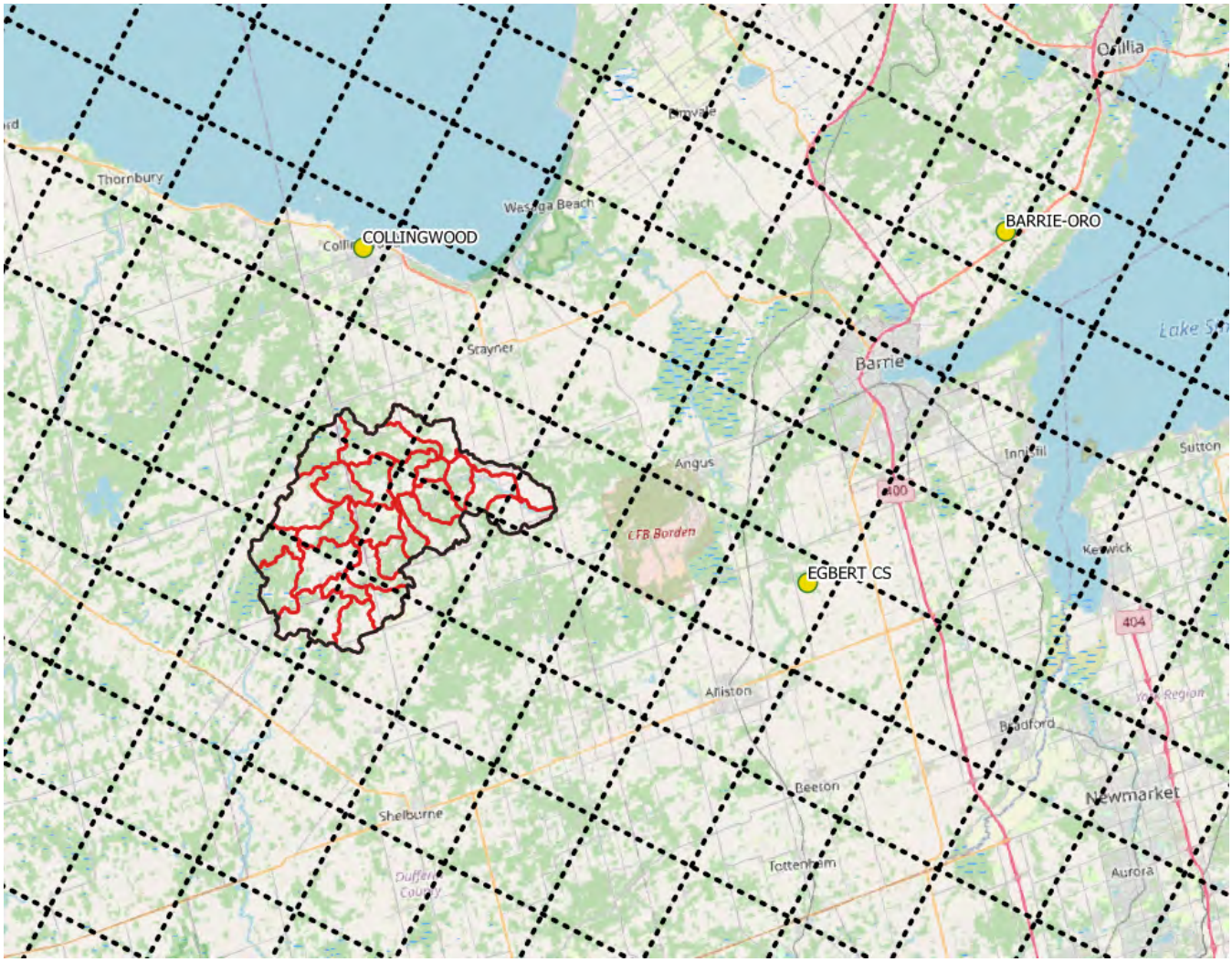

HEC-HMS subbasins vs. CaPA-RDPA resolution vs Nearest Active hourly climate stations.

Meteorological Data

For the study, meteorological data (i.e., precipitation, snow, temperature, radiation) from three local active meteorological stations having hourly precipitation data (click on a station below to view ORMGP's *sHydrology* data analysis suite) are analyzed. Note that these stations only date back to approximately 2000, so longer term trends (greater than about 25 years) cannot be evaluated using these local stations.

1. **6111792: COLLINGWOOD** (https://owrc.shinyapps.io/sHyMet/?sID=148613)
2. **6117700: BARRIE-ORO** (https://owrc.shinyapps.io/sHyMet/?sID=697655275)
3. **611E001: EGBERT CS** (https://owrc.shinyapps.io/sHyMet/?sID=360000028)

There is no general trend to annual precipitation in the region. For instance, Collingwood shows a increasing trend of annual precipitation volumes over the since 1997 (Figure @ref(fig:6111792-annual-precip-trend)), whereas a decreasing trend is found at Egbert CS and no trend is identified at Barrie-Oro (graphs for Egbert and Barrie-Oro not shown here but are readily available by clicking on above links). Trends are assessed both visually and quantitatively using the Mann-Kendall test for trend ($p<0.05$) using annual precipitation accumulations in years that have complete data.

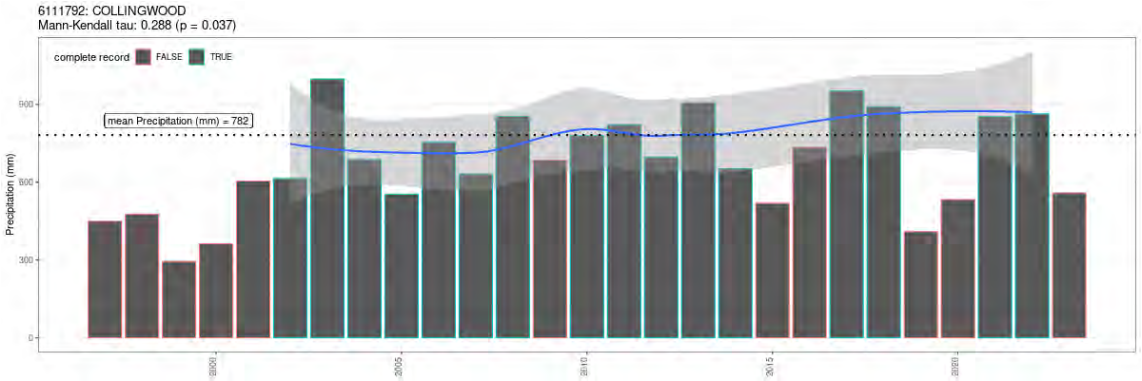

Annual precipitation. Red outlines signify years that do not pass the WMO 3/5 rule (https://climate.weather.gc.ca/glossary_e.html#wmo_standards).

From 2000, mean annual snowpack depths, as shown at Egbert CS (Figure @ref(fig:6111792-annual-snowpack-trend)), appear to be on the decline. (Note: Mann-Kendall test for trend was not applied as snowpacks do not persist year-round.)

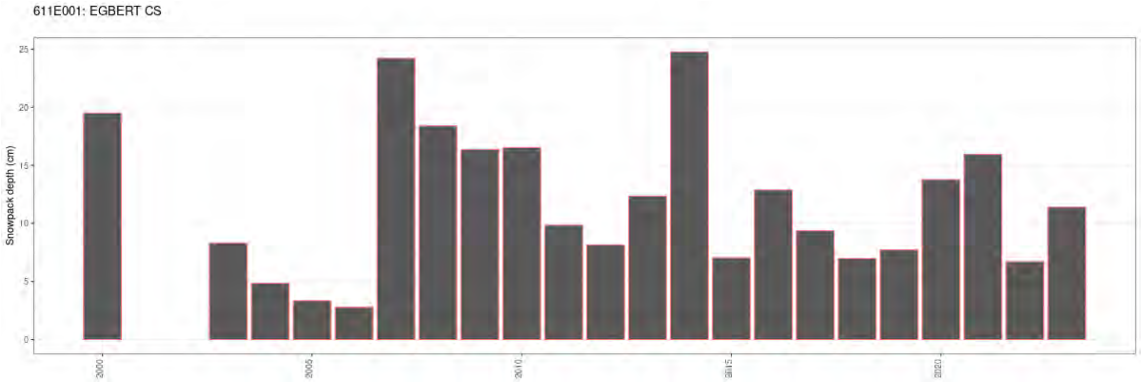

Mean annual snowpack depth (cm). (Snow depth is not monitored at Collingwood).

Lastly, air temperatures over the past 25 years at all location stations do not appear to show any trend (Figure @ref(fig:6111792-annual-meantemp-trend)).

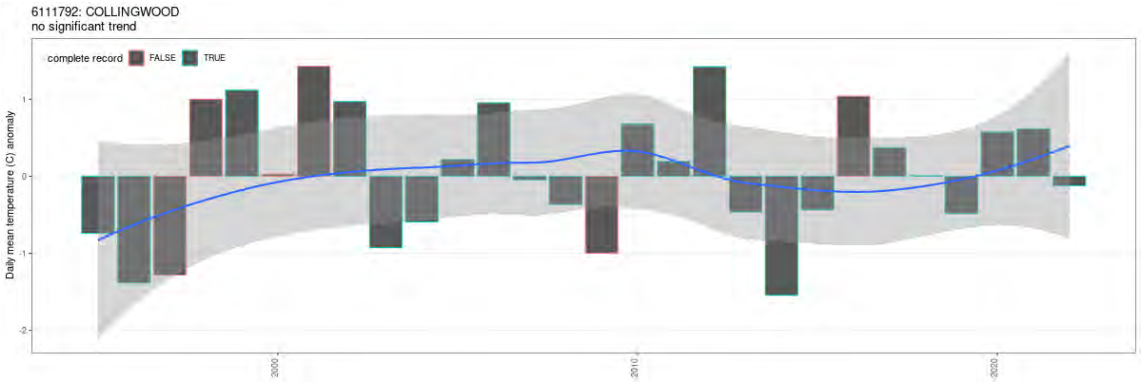

Departure from mean daily temperature (8°C) at Collingwood.

24-hour Precipitation Returns

Below shows the frequency analysis performed on the 24-hour accumulations observed at Collingwood (also available form the links above). From 22 years of data (1995-2023), the extrapolated 100-year return 24-hour accumulation looks to be close to range between 110-130 mm, depending on the frequency model applied. Below the Log-Pearson III is shown bounded by the 90% confidence interval.

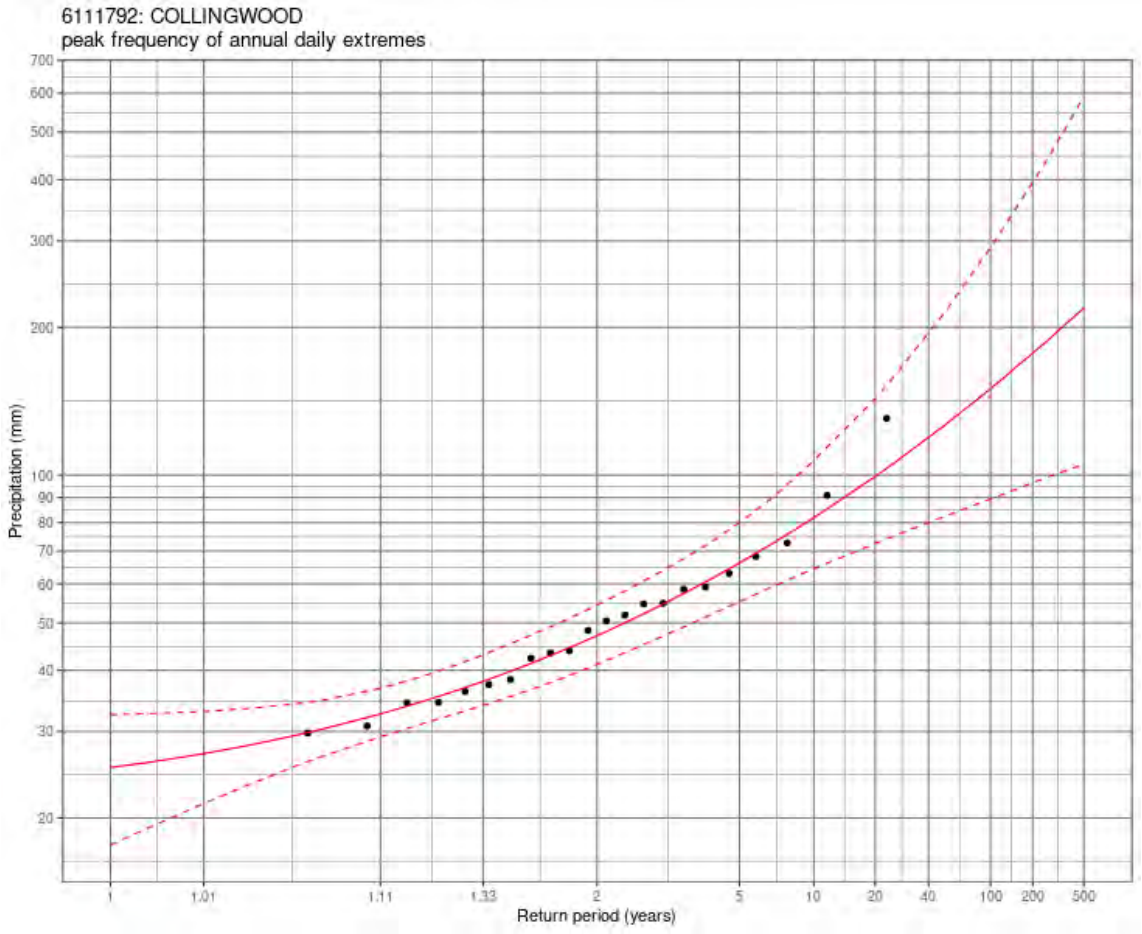

Projected 24-hour accumulated precipitation frequency plot for Collingwood.

Streamflow Data

Next, streamflow data are analyzed to characterize large events based on hydrograph, baseflow, and statistical analyses. Instantaneous (5-minute) streamflow records have been acquired since 2011 at 02ED015: MAD RIVER BELOW AVENING (https://wateroffice.ec.gc.ca/report/real_time_e.html?stn=02ED015). This station is the sole hydrometric station available for model calibration.

Flow Regime

From the daily historic records at 02EC015 (hosted here) (https://owrc.shinyapps.io/sHyStreamflow/?sID=149142), it is apparent that there was a change in flow regime that occurred sometime in 2005, where annual runoff yields show a definite increase relative to the pre-2005 period. This can be shown using cumulative discharge plots of both total flow and baseflow (Figure @ref(fig:02ED015-cumulative)).

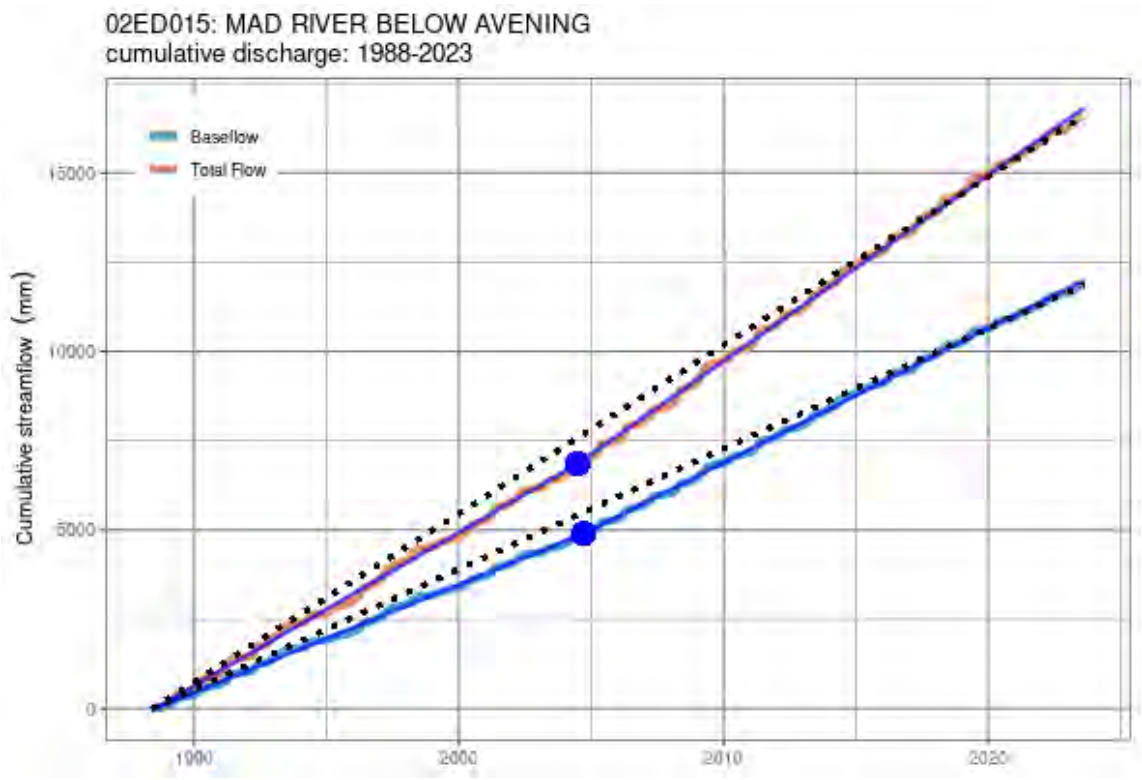

cumulative discharge of both total flow and separated baseflow.

Baseflow was determined as the median of 14 automated hydrograph separation methodologies (https://owrc.github.io/info/hydrographseparation/). The hydrograph in Figure @ref(fig:02ED015-baseflow) (also available here) (https://owrc.shinyapps.io/sHyStreamflow/?sID=149142) illustrates the wide range in baseflow estimates (the green ribbon) as well as the median value (blue).

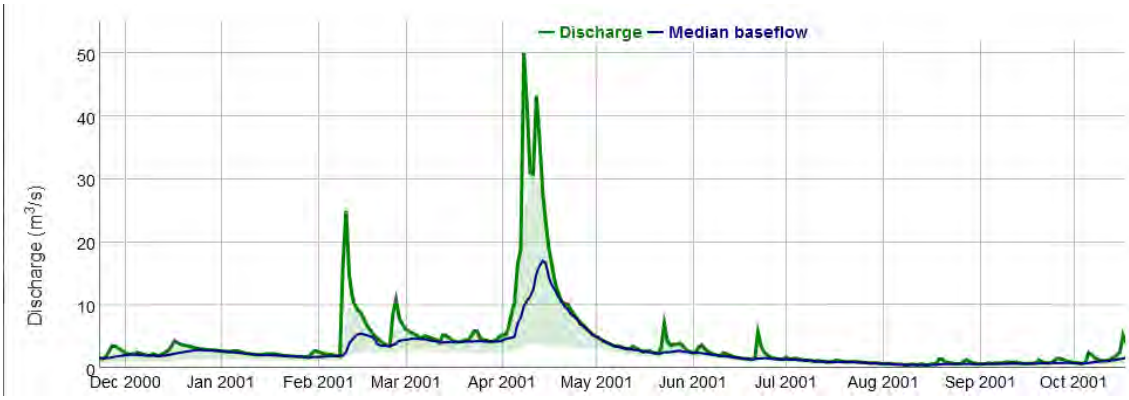

A sample of baseflow separation performed on the Mad River (02ED015) hydrograph.

Aggregating baseflow approximations during each calendar month shows significant seasonality in the baseflow regime that is clearly dominated by the spring freshet (Figure @ref(fig:02ED015-monthly-baseflow)). Consequently, annual extreme discharge tends to occur during the spring months (Figure @ref(fig:02ED015-extremes-dist)) when water tables are high and snow is melting. This makes for wet antecedent conditions at this time of the year.

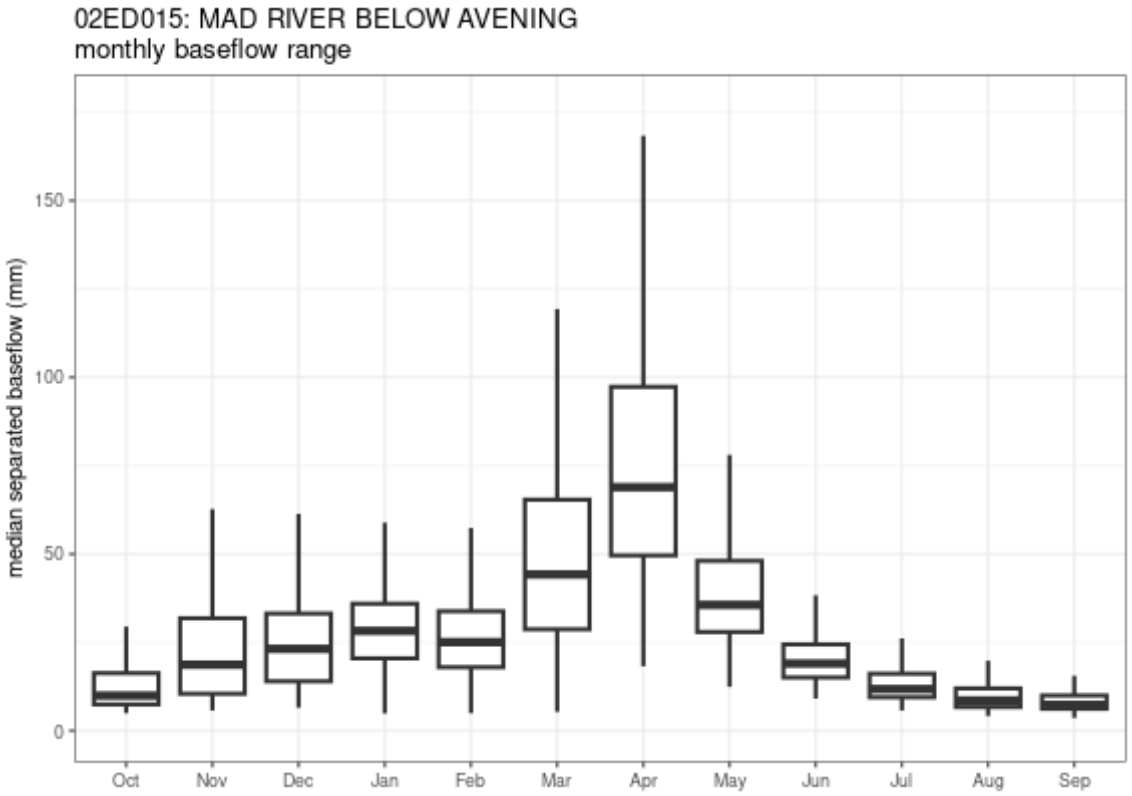

Distributions of monthly baseflow discharge. Notice how March-April-May have significantly greater yields than the rest of the year.

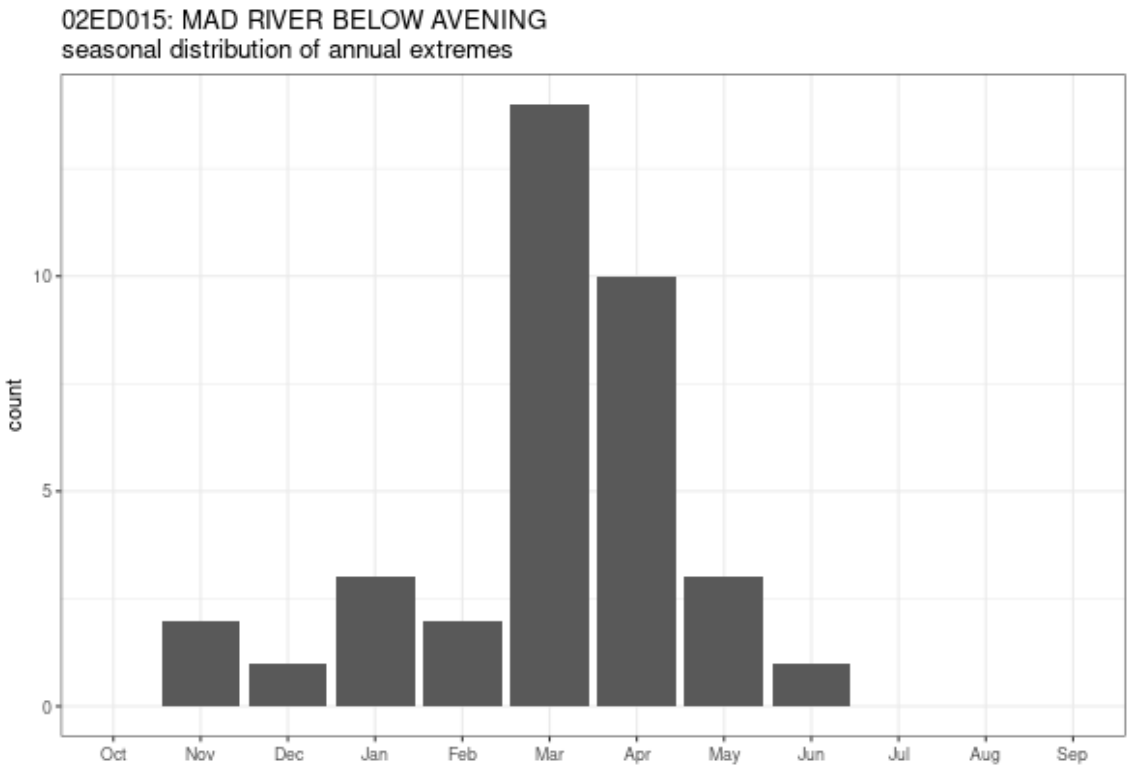

Distribution of annual extremes shows prevalence for spring occurrence.

Peak Flow Events

For model calibration, efforts were made to isolate events that are not caused by snowmelt nor those that occurred during seasonally wet/freshet conditions. This way, the rainfall-runoff relationship can be assessed without any additional influence of wet conditions. Only events occurring from June through September are considered (Figure @ref(fig:extr-freq), Table @ref(tab:evnt-table)).

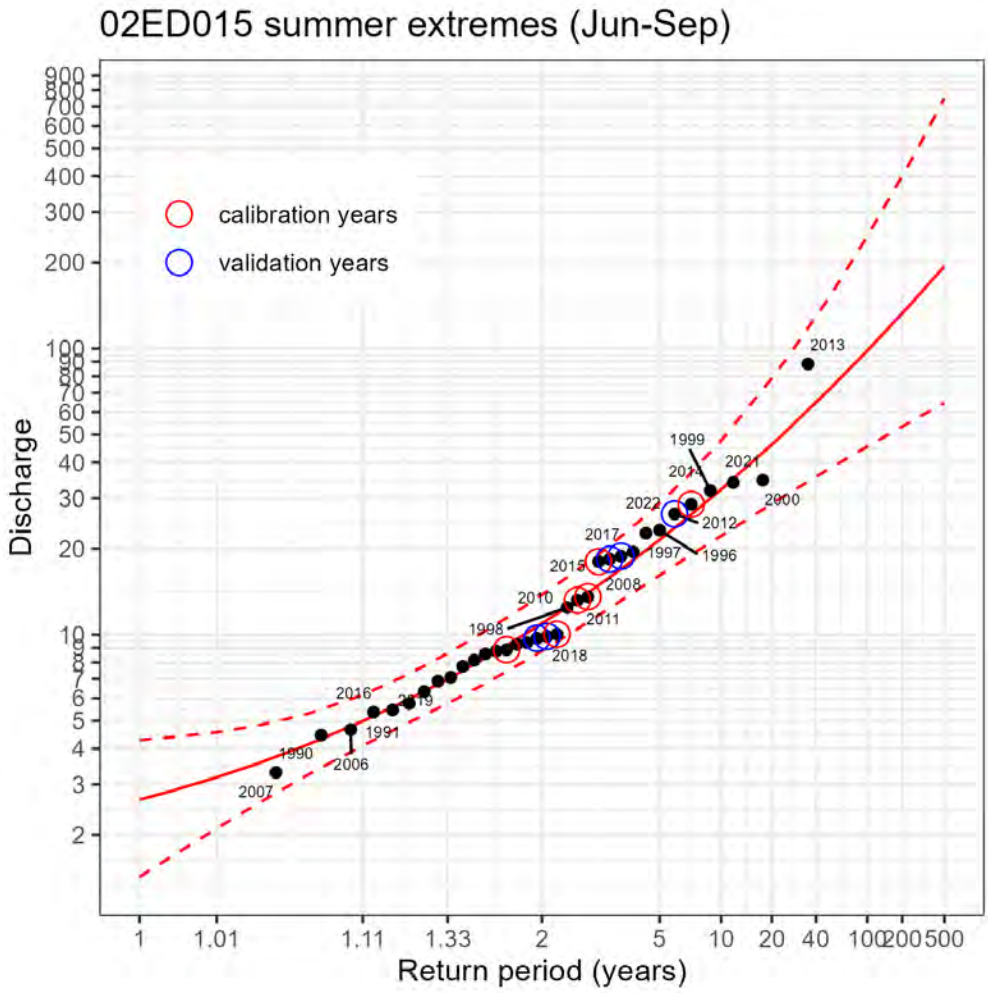

Peak flow frequency of summer (Jun-Sep) events only. Calibration and validation events are encircled.

The cumulative discharge plotting had identified a clear break in flow regime just before 2005. All calibration storms occur after 2005. It is important for the calibration to remain within this regime as it remains relatively stationary up to present.

Timescale

A comparison of timescales was performed to identify the model time step (Figure @ref(fig:compare1)). Discharge is available at the 5-minute time step, which is considered close to instantaneous. Below, the instantaneous data are aggregated four ways: 15-minute rolling average, 6-hour rolling average, 24-hour rolling average and the daily mean step function. Discrepancies tend to appear the coarser the time step: daily mean peak discharge tends to be half that of the instantaneous peak discharge during summer events.

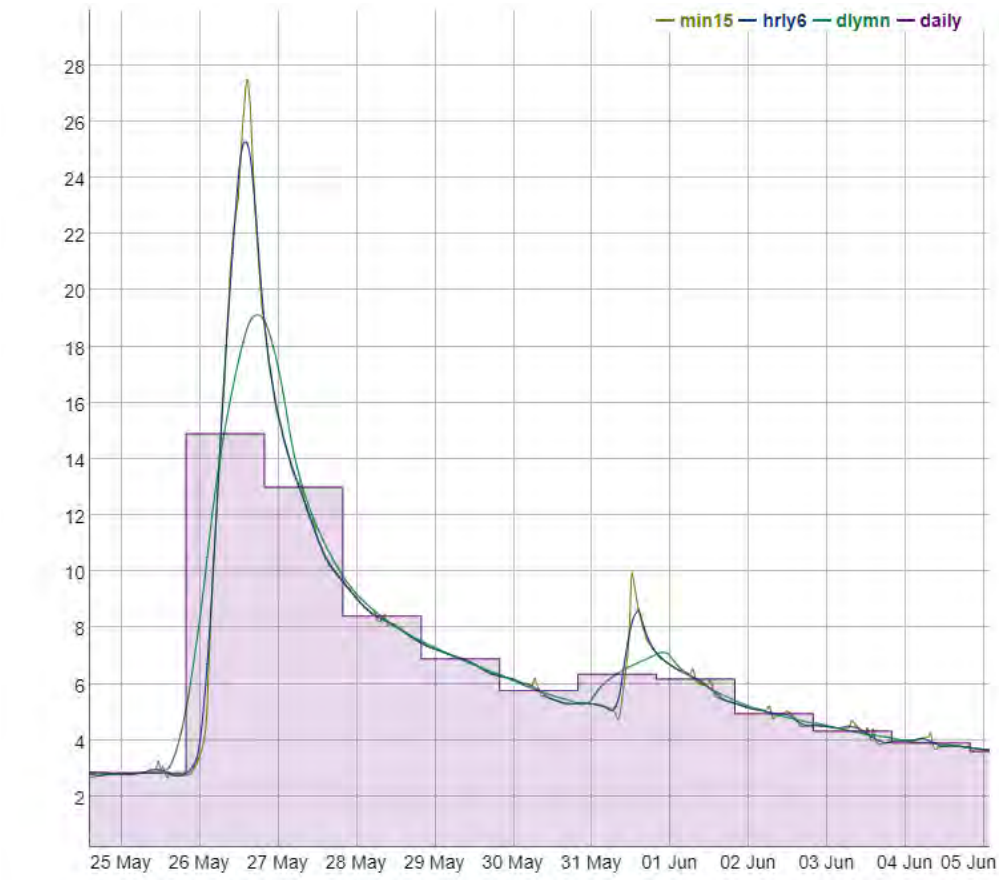

Comparison of streamflow (m³/s) at different averaging intervals at 02ED015.

When plotted, the discrepancy between the instantaneous to the 15-minute time step is barely distinguishable. From this, the model time step is set to 15 minutes as it represents the minimum possible scale at which a model could possibly resolve discharge observed at the outlet.

Most importantly, the 6-hourly hydrograph exhibits minor difference from the instantaneous hydrograph for 2 to 10 year events, which is promising as the input climate data set used in this exercise is aggregated to this 6-hourly scale.

Recession Coefficient

One necessary HEC-HMS model input parameter is the baseflow coefficient: an exponential law of streamflow recession. The web application hosted by the ORMGP contains an automated recession coefficient calculator, determined by plotting discharge versus the discharge the following day, if and only if the succeeding day's discharge is the lesser of the two. The slope of the plotting a line enveloping the base of this scatter plot defines the recession coefficient (Figure @ref(fig:recession-coef)).

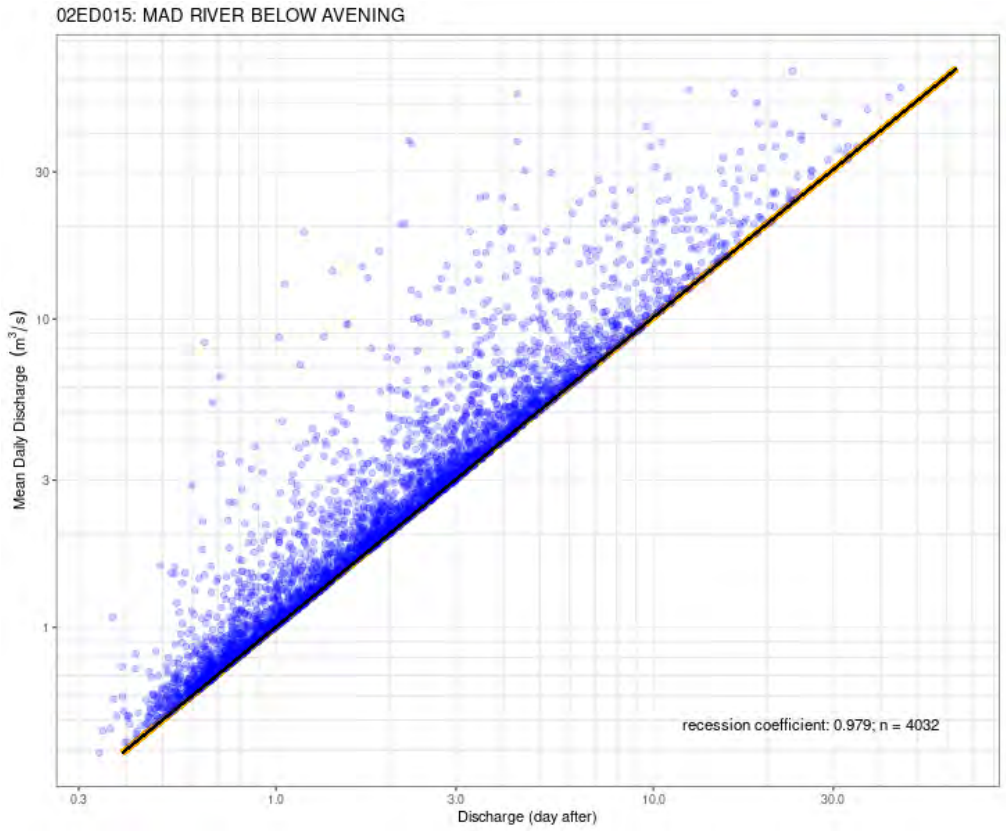

Automated recession coefficient estimate (ORMGP, 2023).

Recession coefficient k is defined as:

$$Q_t = kQ_{t-1}$$

for the Mad River below Avening (02ED015):

$$k = 0.979$$

Geospatial Data

The HEC-HMS model design is dependent on several digital geospatial data sets including, but not limited to, soils and land use mapping that defines the function of “hydrologic response units” (HRUs). Topography needed delineate appropriate catchment areas, also defines flow lengths and catchment slopes.

DEM

The digital elevation model (DEM) defines the physical constraints of the HEC-HMS model. It was derived from the Ontario Digital Elevation Model (https://geohub.lio.gov.on.ca/maps/mnrf::ontario-digital-elevation-model-imagery-derived/about) (OMRF, 2019b), specifically:

1. SWOOP 2015, package B, and
2. SCOOP 2013, package A.

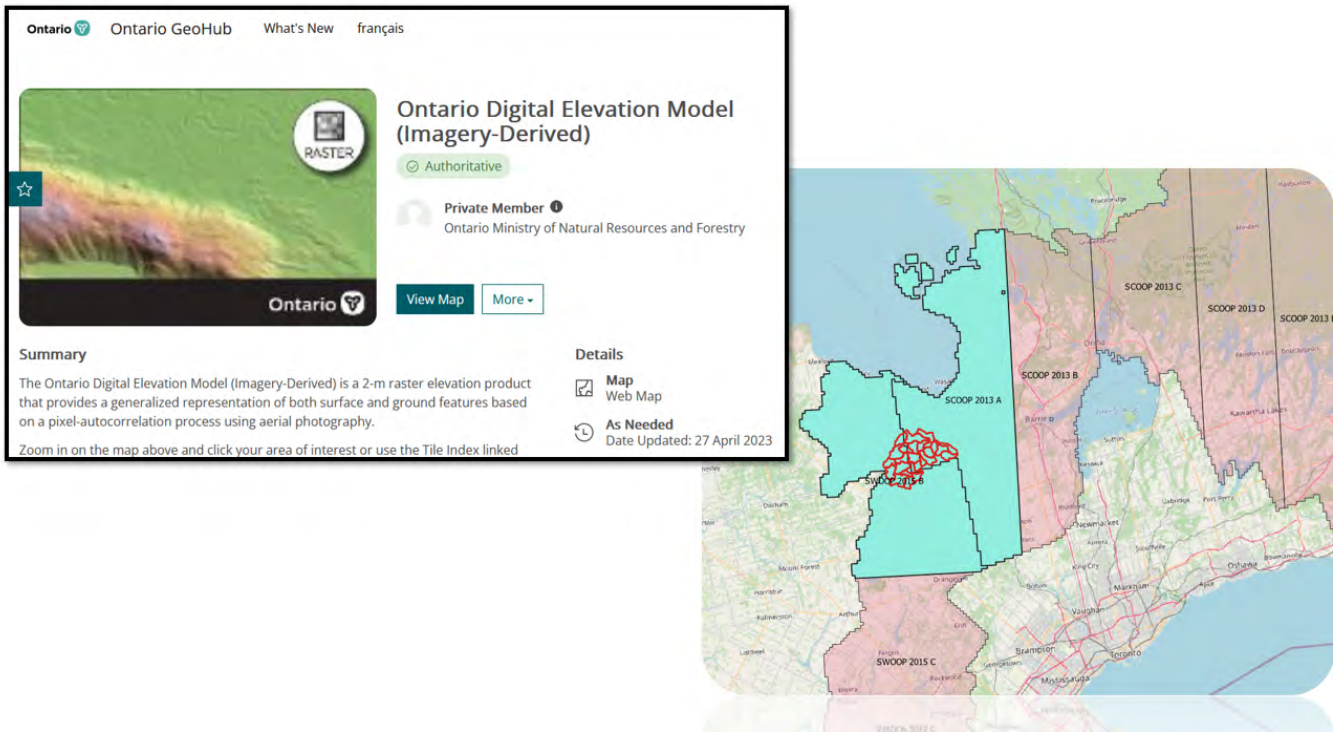

Screen capture of the Provincial DEM source.

The 2m provincial DEM is upscaled to a 10m (horizontal resolution) DEM raster with:

- a EPSG: 3161 NAD83 Ontario MNR Lambert projection;
- an upper-left coordinate E:1,300,400; N:11,986,700; and,
- 2120 rows by 2600 columns (5,512,000 cells)
- UTM Zone 17N
- Height reference system: CGVD28

Using HEC-HMS's native "GIS" package (https://www.hec.usace.army.mil/confluence/hmsdocs/hmsguides/gis-tutorials-and-guides), the DEM was used to define subbasins. Some manual alterations were applied to align the subbasins with existing catchment areas employed by the NVCA.

Land Use and Surficial Geology

Land Use Lookup

The Southern Ontario Land Resource Information System (SOLRIS v3.0 (https://geohub.lio.gov.on.ca/documents/0279f65b82314121b5b5ec93d76bc6ba/about)—OMNR, 2019a) provides a set of land use identifiers. From these, a look-up table is used to assign data-based model parameters such as percent imperviousness and initial abstractions.

The overall makeup of the Mad River watershed is:

SOLRIS (OMNR, 2019a)	Percent coverage
Undifferentiated	40%

SOLRIS (OMNR, 2019a)	Percent coverage
Tilled	22%
Treed Swamp	16%
Deciduous Forest	8%
Mixed Forest	5%
Other	9%

Percent Imperviousness

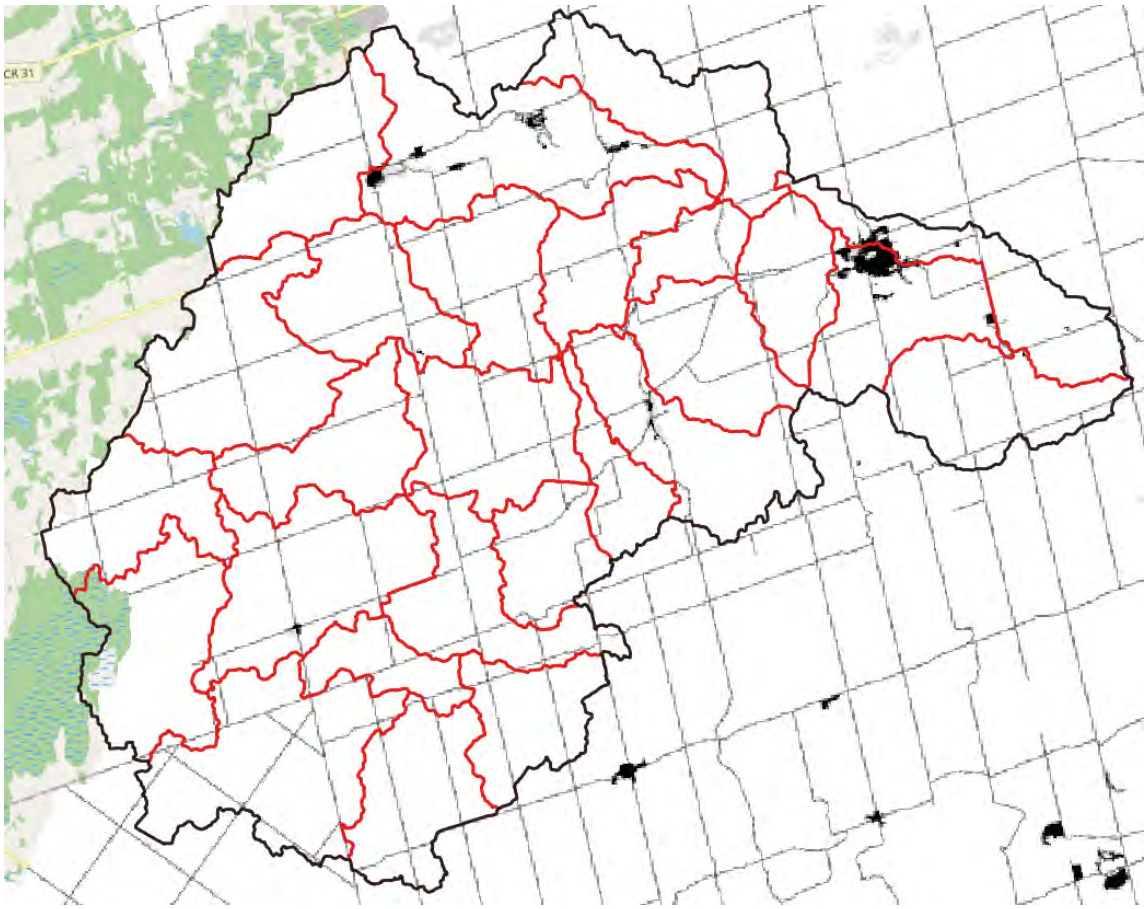

Percent imperviousness based on SOLRIS mapping.

Initial Abstraction

With SOLRIS land use mapping, canopy cover density is distributed to provide first estimates of initial abstraction capacities:

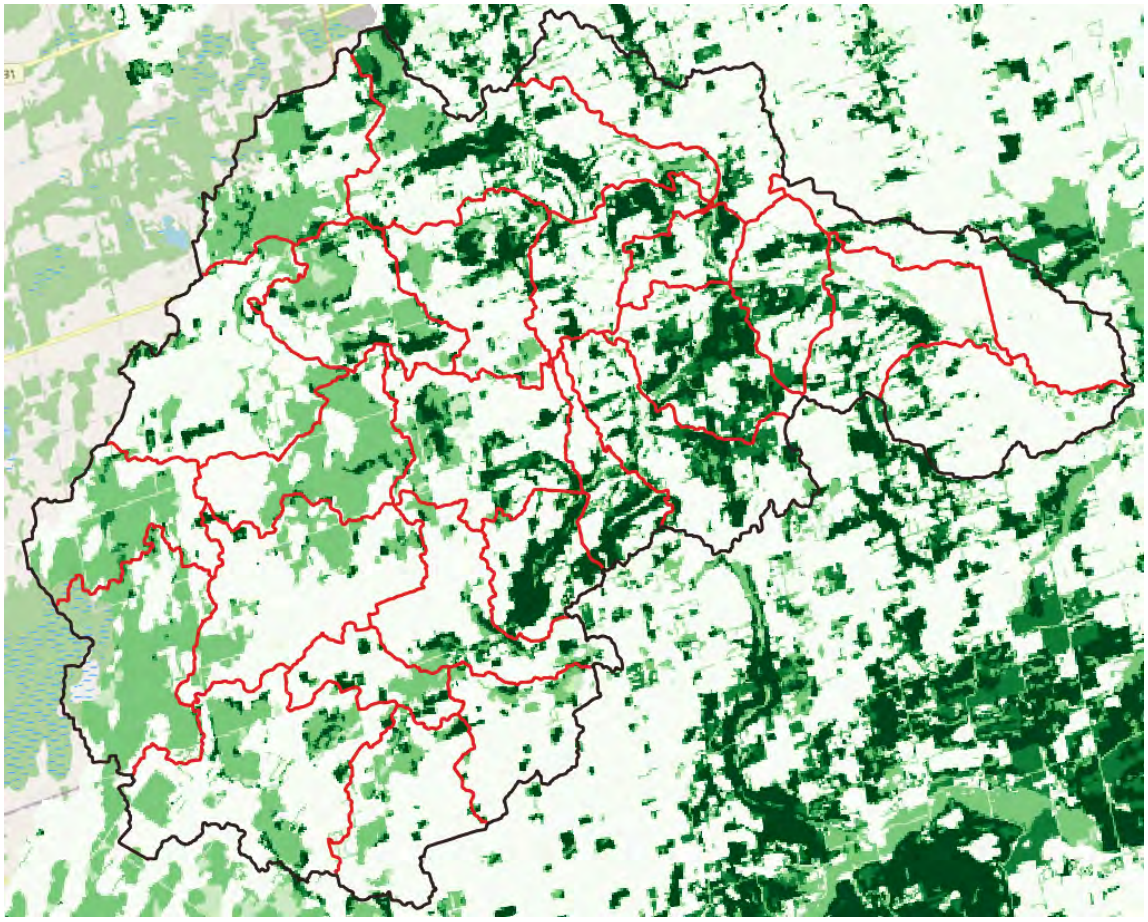

Relative vegetation cover based on SOLRIS mapping. Darker greens reflect greater cover density.

Soil Characteristics

Surficial Geology mapping (OGS, 2010) was used to define soil characteristics. The OGS layer is attributed with a set of “relative permeabilities” There are used to map so-called “Hydrologic Soil Groups” (https://directives.sc.egov.usda.gov/OpenNonWebContent.aspx?content=17757.wba). Using the *“PERMEABILI”* attribute of the OGS (2010) layer, soil groups (A, B, C, D) are mapped to (High, Medium, Low-medium, Low) permeabilities. This was needed to estimate infiltration loss parameters for the Upper Mad River Watershed:

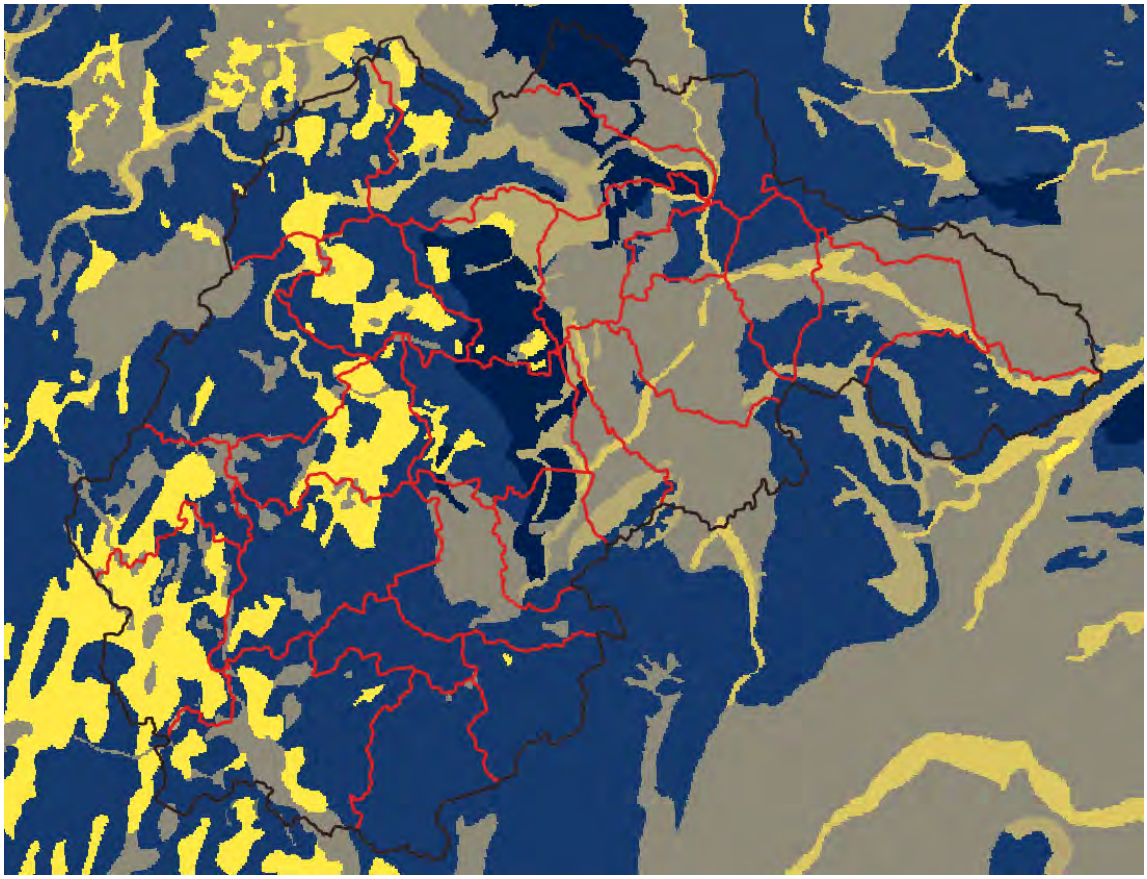

Relative infiltration rates based on OGS (2010). The darker the blue, the less permeable the soil; yellows are the most permeable.

Relative permeability class	hydrologic soil group	Percent coverage
Low permeability	A	7%
Medium-Low	B	48%
High	D	26%
Variable	C	6%
Alluvial	C	3%
Organics	C	11%

Composite Layers

SOLRIS land use (OMNR, 2019a) and OGS surficial geology (2010) are combined to determine SCS Curve Numbers (CN) using standard SCS lookup tables (https://www.hec.usace.army.mil/confluence/hmsdocs/hmstrm/cn-tables).

Curve Number

The SCS Curve Number (CN) is dependent on the land use type and the hydrologic soil group. From standard SCS lookup tables, CNs can be mapped (Figure @ref(fig:basin-cn)).

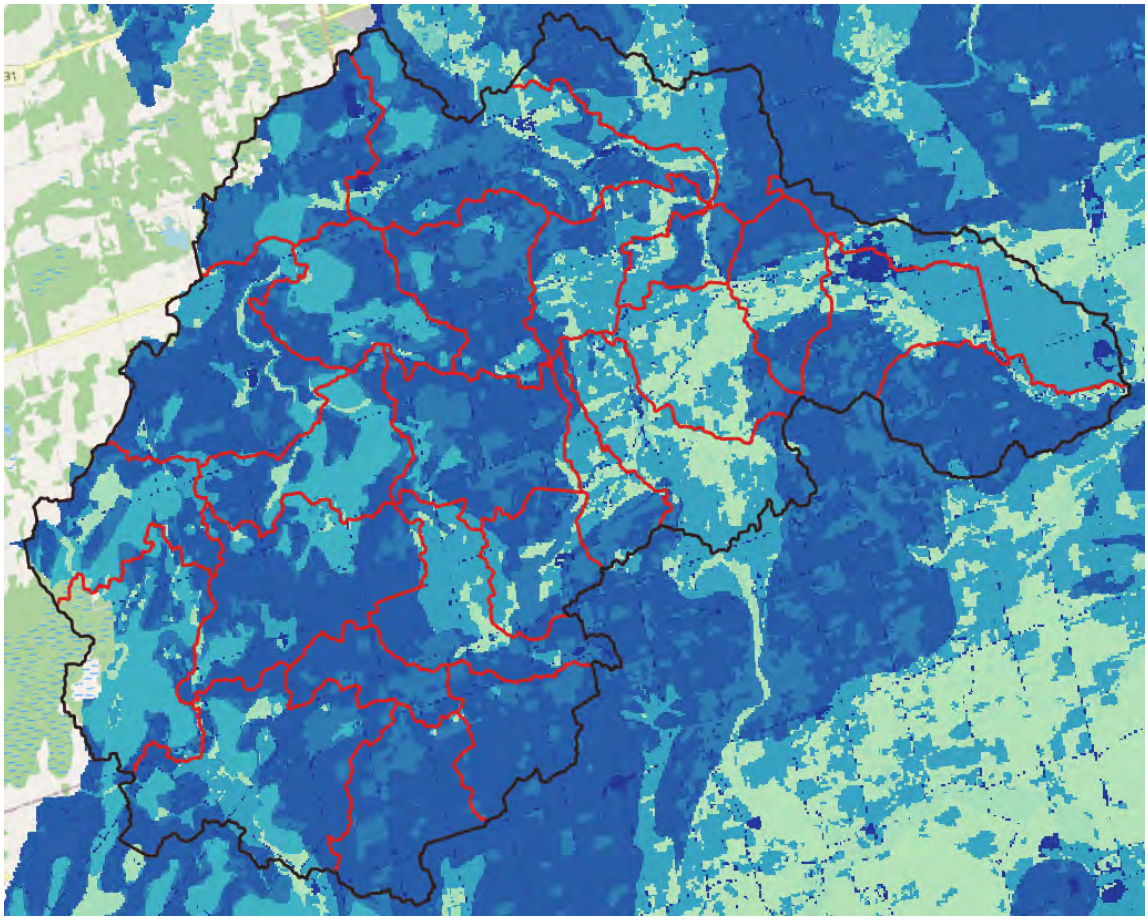

SCS Curve Numbers based on a geospatial overlay of SOLRIS and OGS surficial geology. Darker blue: higher CN.

HEC-HMS Modelling

The Upper Mad River Hydrologic Model is built using HEC-HMS (https://www.hec.usace.army.mil/software/hec-hms/) (Task 1.2). The HEC-HMS model consists of 27 subbasins, 25 of which drain to the sole hydrometric station at Avening. The HEC-HMS model was designed for event-based analysis. Model design included (USACE, 2000):

- the SCS-CN methodology for runoff generation,
- th Syder unit hydrograph for basin transfer
- a simple lag function for reach transfer, and
- a simple recession coefficient baseflow simulator that is activated by a ratio to simulated peak.

Climate Zones and Subbasins

Climate zones/subbasins were delineated based on the DEM and were built internally using HEC-HMS's GIS package. Meteorological and streamflow data processing for the Upper Mad River watershed are confined within these bounds (Figure @ref(fig:basin-compare)).

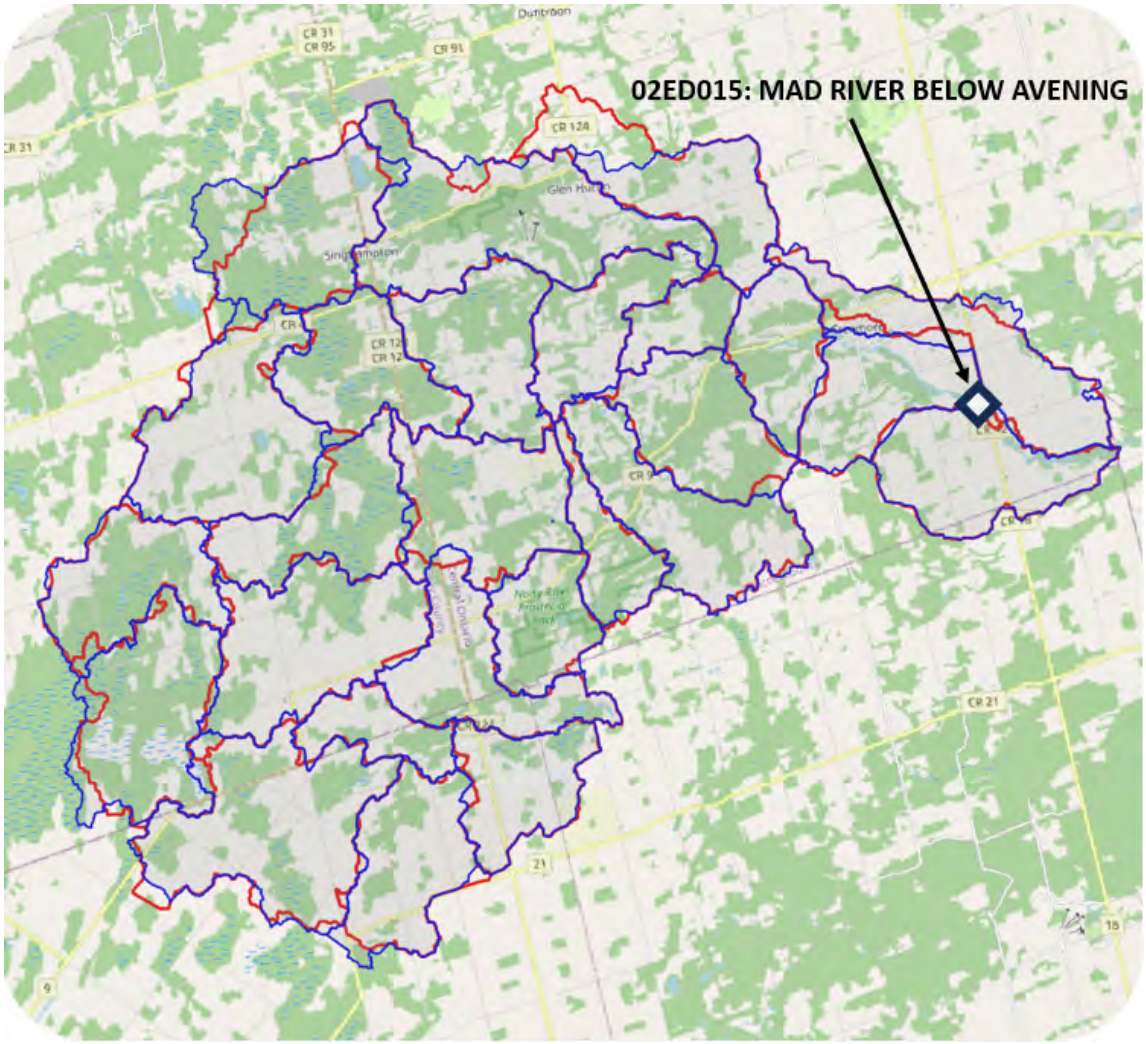

Map of HEC-HMS-derived subbasins (blue) compared to the basins provided by the NVCA (red).

Model Structure

The (sub-)models used in the HEC-HMS design include:

- Loss method: Soil Conservation Service (SCS) curve number;
- Transform method: Snyder unit hydrograph;
- Routing method: simple lag; and
- Baseflow method: simple recession.

Model Parameters

Some *"free"* parameters are applied uniformly (i.e., globally) across the model. Differences in the water budgeting at each subbasin are then attributed to:

1. land use mapping
2. surficial geology mapping
3. topography (DEM), defining:
    - subbasin form;

- channel length; and
- channel slope.

> Subbasin parameter assignment can be inspected in the interactive Figure @ref(fig:leaflet)

Calibration parameters include:

1. SCS Curve Number (CN) method for runoff generation (generated by mapping discussed above)
2. Initial abstraction for rainfall retention (generated by mapping discussed above)
3. Subbasin area and topology (based on DEM topography)
4. c_t Snyder unit hydrograph basin coefficient (global)
5. c_p Snyder unit hydrograph peaking coefficient (global)
6. k baseflow (simple) recession coefficient (global), calculated above
7. r_p ratio to peak flow needed to specify the baseflow regime (global)
8. lag Simple lag for reaches (dependent on reach length)
9. Q_0 is the initial discharge, set to the observed discharge at the beginning of the model run
10. f_{ia} a multiplicative factor applied globally to initial abstraction
11. f_{CN} a multiplicative factor applied globally to CN

Antecedent conditions

With the intention of preparing a model for future long-term continuous simulations in addition to the scope of work presented herein, pre-conditioning every model run according to antecedent conditions is avoided. Rather, once the model moves to a long-term continuous simulation application, the model will rely on so-called “deficit and constant” mechanisms to establish antecedent states, where antecedent moisture conditions are effectively computed. Here, setting initial discharge (Q_0) prior to the model run serves as the sole means of establishing an initial state.

Event Selection

A total of 11 annual extreme events are selected (Table @ref(tab:evnt-table)), 6 are used for calibration, 5 for validation. All selected events exceed bankfull discharge (defined here as events exceeding the 1.5 year return flow). Events are encircled in Figure @ref(fig:extr-freq).

Selection of the calibration and validation events were made randomly from the initial 11 events. A twelfth event, occurring in 2013 looks to be a choice event, but for reasons discussed below, this event unfortunately had to be excluded.

Model Calibration and Verification

The HEC-HMS hydrologic model was calibrated and verified using available streamflow gauge data (Task 1.3). A range of annual extreme events exceeding the 1.5-yr return period are used to simulate the flood flow regime.

The events selected span a wide range of peak discharges for both the calibration and validation exercises. Given that there is a decade’s worth of events, it is unlikely that extreme discharges (say greater than a 20-year return) have not been observed and will thus not constrain the model.

Objective Function

Calibration and validation were optimized both by visual fit and objective function minimization. The objective function targeted is the peak-weighted root mean square error described in USACE (1998):

$$Z = \sqrt{\frac{1}{n}\sum^{n}\left[(q_s - q_o)^2 \quad \left(\frac{q_o - \overline{q_o}}{\overline{q_o}}\right)\right]}$$

where q_s, q_o and $\overline{q_o}$ are the simulated, observed and mean-observed discharge respectively.

Calibration

The model fairs well at matching peak discharge for a wide range of events up to the 10-year return. There are 2 characteristically different hydrographs observed among the calibration set: the 2014, 2018 and 2020 events exhibit a short-duration flashy response, while the 2010, 2011 and 2015 events demonstrate events that appear to have greater storage and lag. This lag may be a sign of wetter antecedent conditions as the initial discharge Q_0 tends to be higher compared to the flashy events.

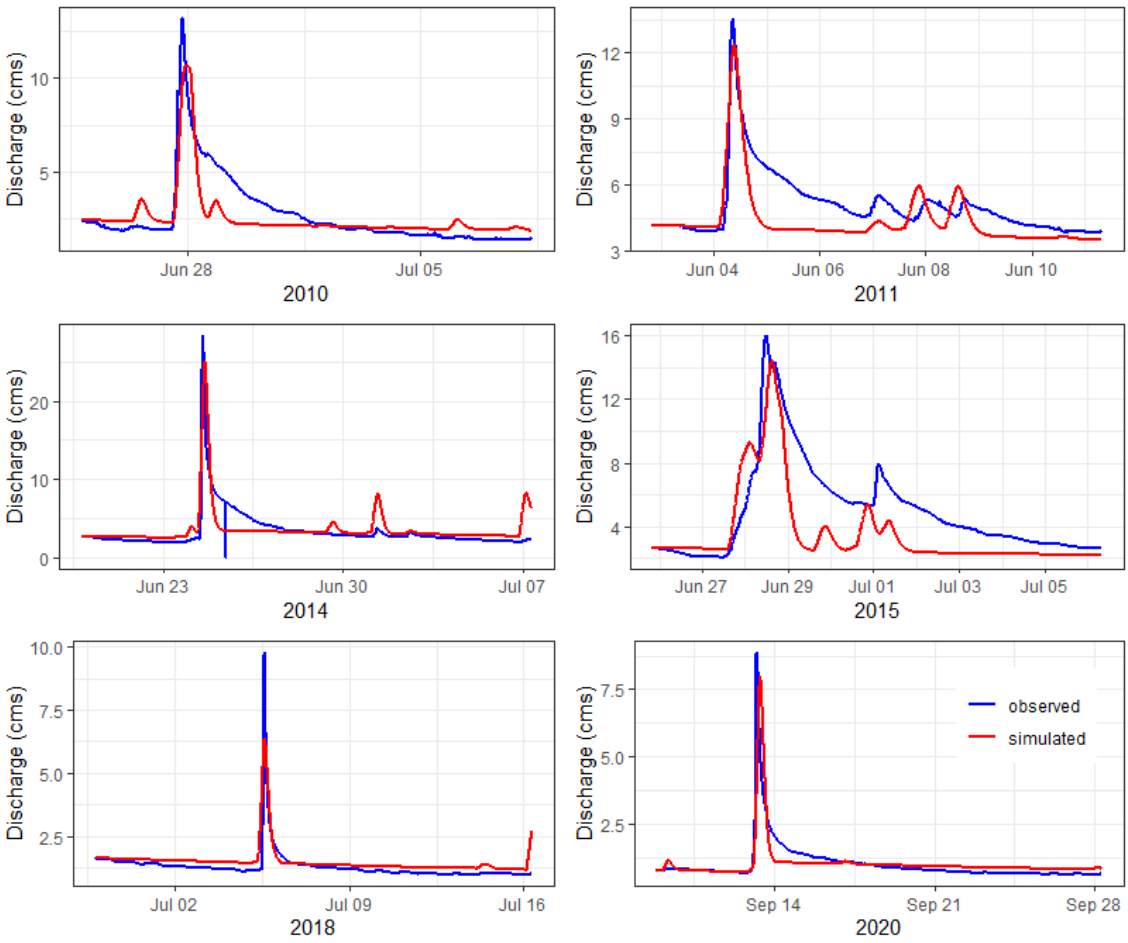

Calibration performed to 6 annual extreme events.

Verification

The verification events as expected do not perform as well as the calibration set. Overall, 3 of the 5 events (2002, 2008 and 2012) performed well. During the iterative process of calibration and validation, the 2009 and 2017 events were notoriously difficult to simulate, without sacrificing the performance of the calibration set. They are nonetheless included here for the sake of transparency.

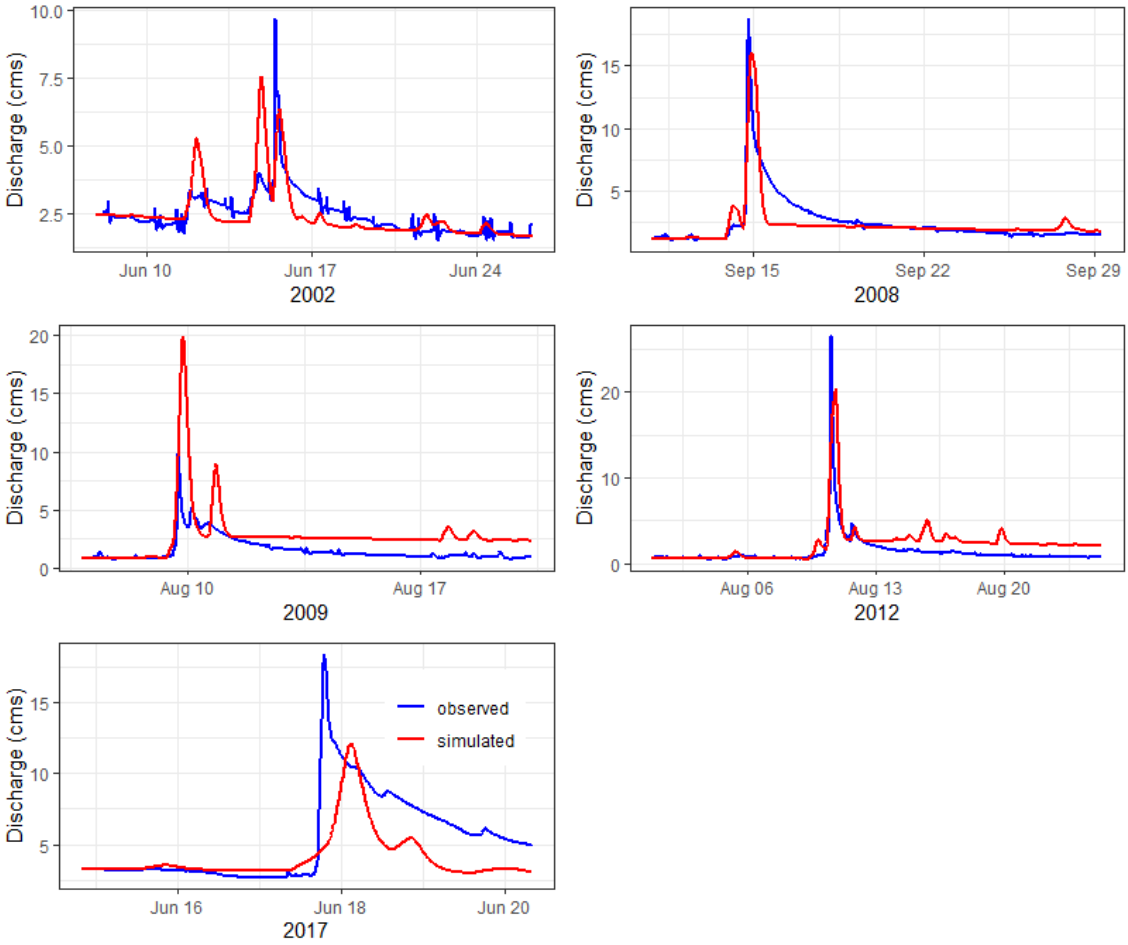

Model varification performed to 5 annual extreme events.

Sensitivity Analysis

Five parameters (c_t, r_p, lag, f_{ia}, and f_{CN}) were fed into a Shuffled Complex Evolution (SCE - Duan et.al., 1993) optimization scheme. Subbasin lag coefficient performed best when minimized ($t_p = 0$) , indicating that the modelled upper Mad River watershed is quite flashy. (The recession coefficient k was determined from flow records and the Snyder UH peaking coefficient was kept at a constant value $c_p = 0.4$.) A global calibration is performed on subsets of 6 The 11 events. Choosing 6 of 11 events yields ${}_{11}C_6 = 462$ SCE trials that are optimized and compared in order to assess two crucial issues with numerical model calibration, namely:

1. Parameter inter-dependence: Can the selection of a parameter value be confidently estimated by another parameter, if so, then the dimensionality of the inverse problem is reducible, and
2. Parameter identifiability: Are there optimized parameters that appear to seek a particular/unique value?

Below the results are presented in the form of a correlation matrix. This figure will highlight cross-correlation either visually (lower-left scatter plots) and statistically (upper-right listed coefficient of determinations). Identifiability can be determined visually from the density plots along the diagonal: plots that show greater peakedness (less spread) are deemed most sensitive to change.

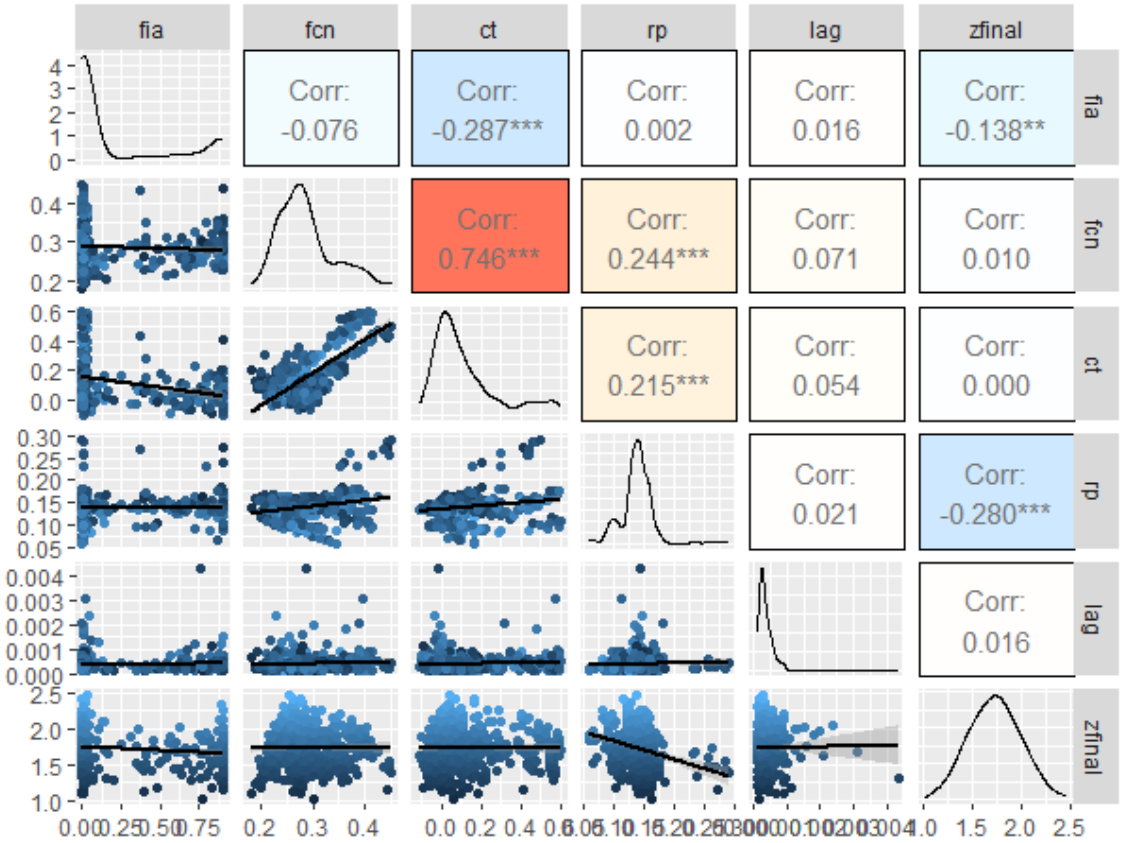

Model parameter correlation matrix built for sensitivity analysis. `zfinal` is the average peak-weighted RMSE minimized by the SCE scheme.

Key takeaways from Figure @ref(fig:corr-matrix-final):

1. initial abstraction (i_a) and reach lag appear to perform best when minimized—resulting from the flashiness of the selected events;
2. ratio to peak (r_p) appears to be the most identifiable, meaning that its calibrated value has the greatest confidence and that the model is most sensitive to change in r_p; and
3. CN values appear to correlate well with the Snyder UH basin coefficient (c_t)—meaning that changes to one parameter can be compensated by the other, and thus the model's sensitivity to these parameters would have been overstated should a global sensitivity analysis (as done here) had not been performed.

Event Modelling

With the calibrated parameters and the model set, the model is then run through a set of scenarios. Two designed storms, the SCS type II method and the Timmins storm are applied as per NVCA guidelines. In addition, a projected storm under a changing climate is applied.

Design Storms

Three forms of synthetic hyetographs are developed to test design events now and under the changing climate. The Timmins Storm is pre-defined while the SCS type II design storms and the climate change projections are constructed using the “alternating block” synthetic hyetographs (NRC-PCS, 2018).

Application of these storms are multiplied by areal reduction factors (as a function of the study area’s “circular drainage area”—EWRG, 2017). Here, the Mad River model has an approximate 415 km² circular drainage area.

Timmins Storm

A 193 mm, 12-hour storm was recorded in Timmins, Ontario on August 31, 1961 (https://www.canada.ca/en/environment-climate-change/services/water-overview/quantity/floods/events-ontario.html#Section3). With a 415 km² circular drainage area, the Timmins areal reduction factor would be 76%. It’s hourly hyetograph is given as (EVA, 2017):

hour	Acc. Precip. (mm)	Reduced (mm)
1	15	11.4
2	20	15.2
3	10	7.6
4	3	2.28
5	5	3.8
6	20	15.2
7	43	32.68
8	20	15.2
9	23	17.48
10	13	9.88
11	13	9.88
12	8	6.08

SCS type II

The 2-, 5-, 10-, 25-, 50-, and 100-year SCS type II 24-hour design storms were re-casted as synthetic hyetographs using the alternate block method. 24-hour rainfall return periods were taken (conservatively) as the maximum posted 24-hour return intensities (mm) of four local meteorological stations with IDF curves:

T (years)	Collingwood	Barrie*	Egbert	Barrie Oro	max
2	46.7	47.4	40.5	43.4	47.4
5	60.6	63.8	55.2	52.2	63.8

T (years)	Collingwood	Barrie*	Egbert	Barrie Oro	max
10	69.8	76.2	67.9	58.1	76.2
25	81.6	94.0	88.2	65.6	94.0
50	90.3	108.8	107.3	71.2	108.8
100	99.0	125.1	130.4	76.8	130.4

** Barrie is no longer an active station, however an IDF curve is available.*

This produces the hyetographs in Figure @ref(fig:scsii-rainfall).

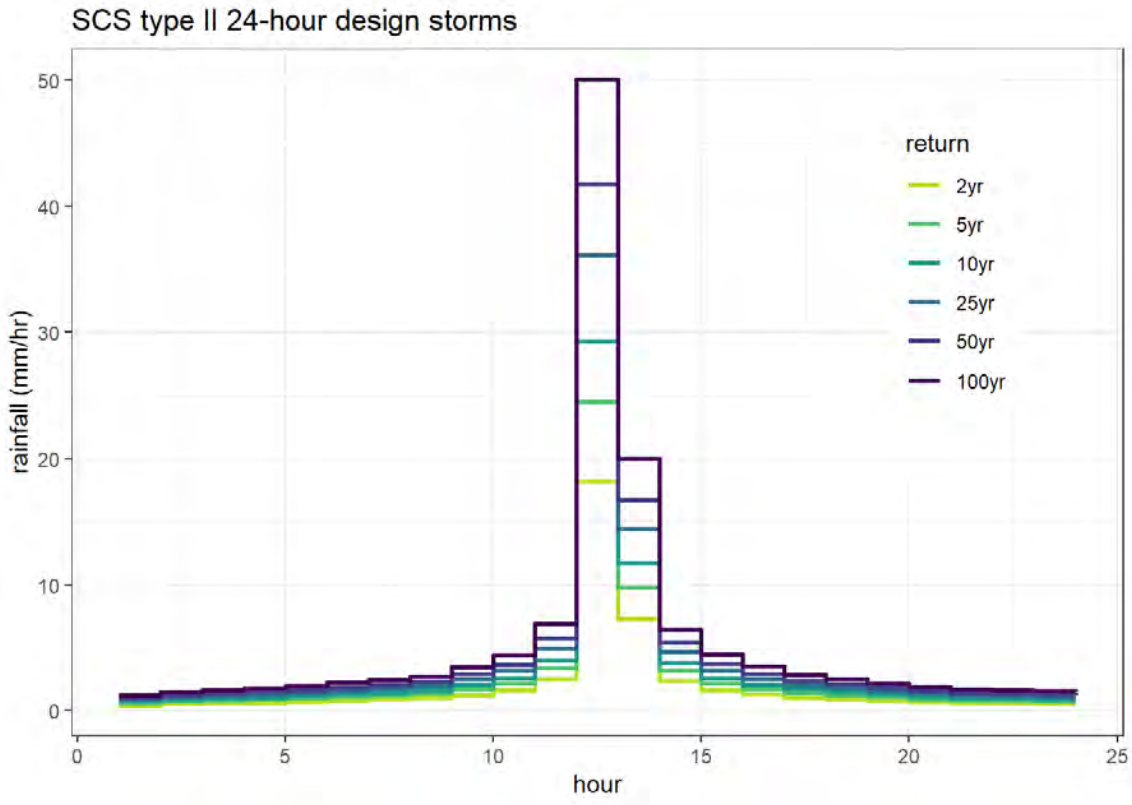

SCS type II 24-hour design storm hyetographs.

Results

The Design storms of Timmins and SCS type II 100-year return storms exceed flows ever measured at the Avening gauge (Figures @ref(fig:timmins-result) and @ref(fig:scsii-result)).

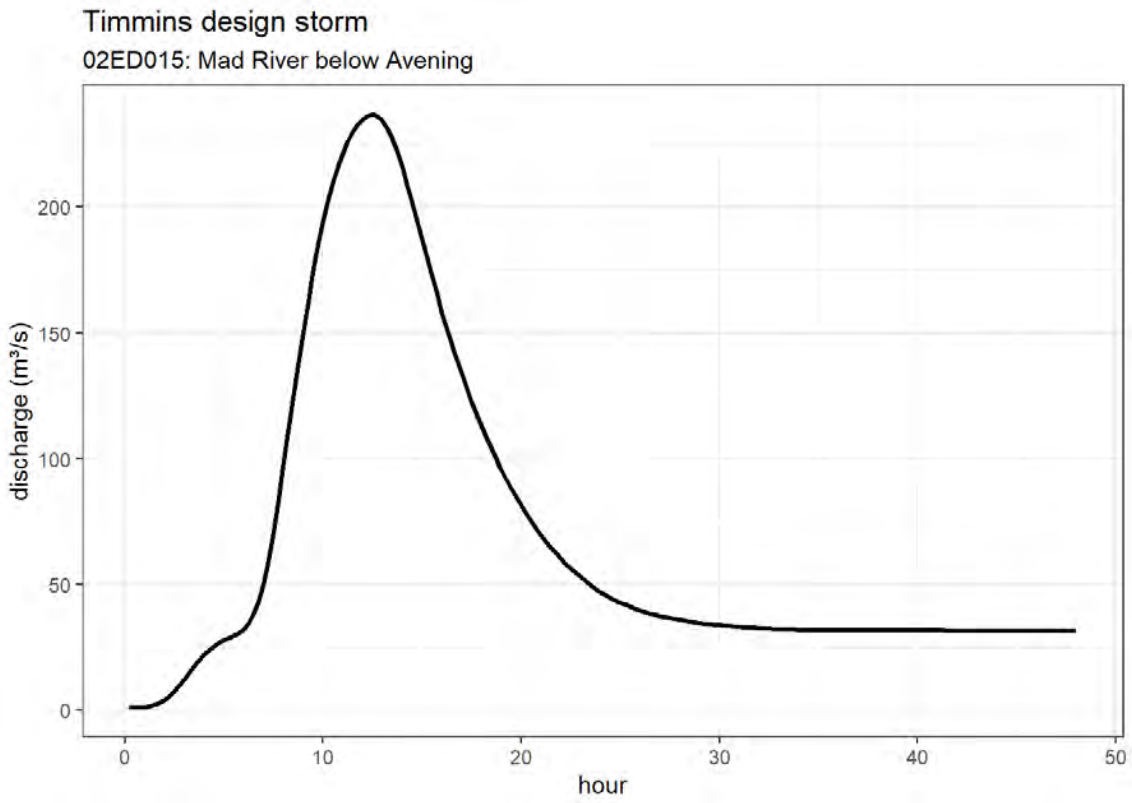

Modelled dicharge under the Timmins design storm.

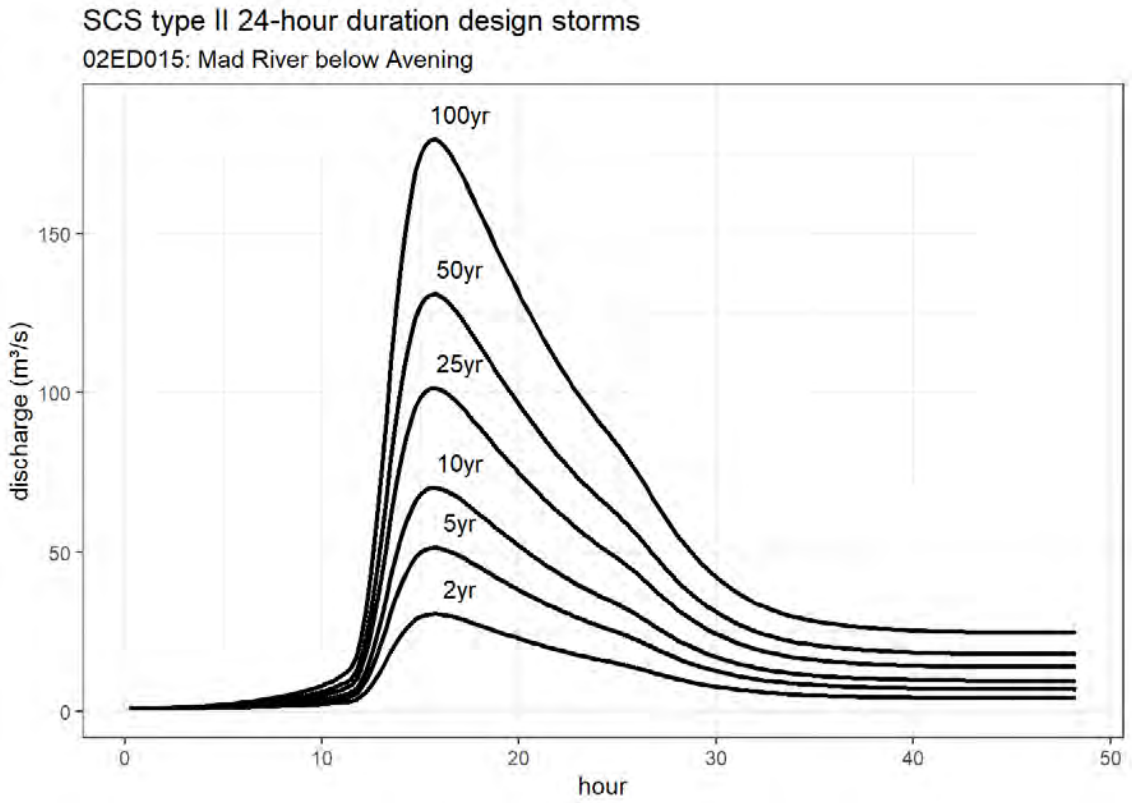

Modelled dicharges under the SCS type II design storms.

Climate Change

Climate change scenarios are built using projected IDF curves offered by the IDF-CC (https://www.idf-cc-uwo.ca/) tool (Simonovic et.al., 2015). Like the SCS method, the alternating block approach is used to convert the IDF curve into a design hyetograph. The IDF-CC design storm is processed as follows:

1. The IDF-CC (https://www.idf-cc-uwo.ca/) design support tool was used to acquire current and projected Intensity-Duration-Frequency (IDF) curves. From this tool, the CMIP6 (https://esgf-node.llnl.gov/projects/cmip6/) ensemble, downscaled and biased corrected as per PCIC (https://www.pacificclimate.org/data/statistically-downscaled-climate-scenarios), are packaged into future projected IDF curves.
2. 3 climate change scenarios (SSP1-2.4, SSP2-4.5 and SSP5-8.5) are considered.
3. IDFs produced for the time horizons 2015-2045 and 2045-2100 are compared with current IDF curves, i.e., 3 IDFs per scenario.
4. The 100-year return precipitation events are created using the alternating block approach following the Natural Resources Canada document: *Case studies on climate change in floodplain mapping* (NRC, 2018).

IDF

IDFs are defined by (Simonovic et.al., 2015):

$$i = A \quad (t + t_0)^B$$

where i is rainfall rate (mm/hr), t duration of precipitation event (hr), A, B and t_0 are coefficients provided by the IDF-CC tool. According to Simonovic et.al. (2015) the IDF parameters for the study area are:

T (years)	Coefficient A	Coefficient B	Coefficient t_0	24-hour event (mm)
2	22.1	-0.755	0.070	48.0
5	30.1	-0.771	0.091	62.1
10	35.6	-0.780	0.103	71.4
20	40.9	-0.788	0.112	79.9
25	42.6	-0.790	0.115	82.7
50	47.8	-0.796	0.123	91.0
100	53.0	-0.802	0.129	99.0

Results

Climate change projections see a general increase to return floods: slightly for the near-term (Figure @ref(fig:cc2015-result)), more pronounced in the long-term (Figure @ref(fig:cc2045-result)).

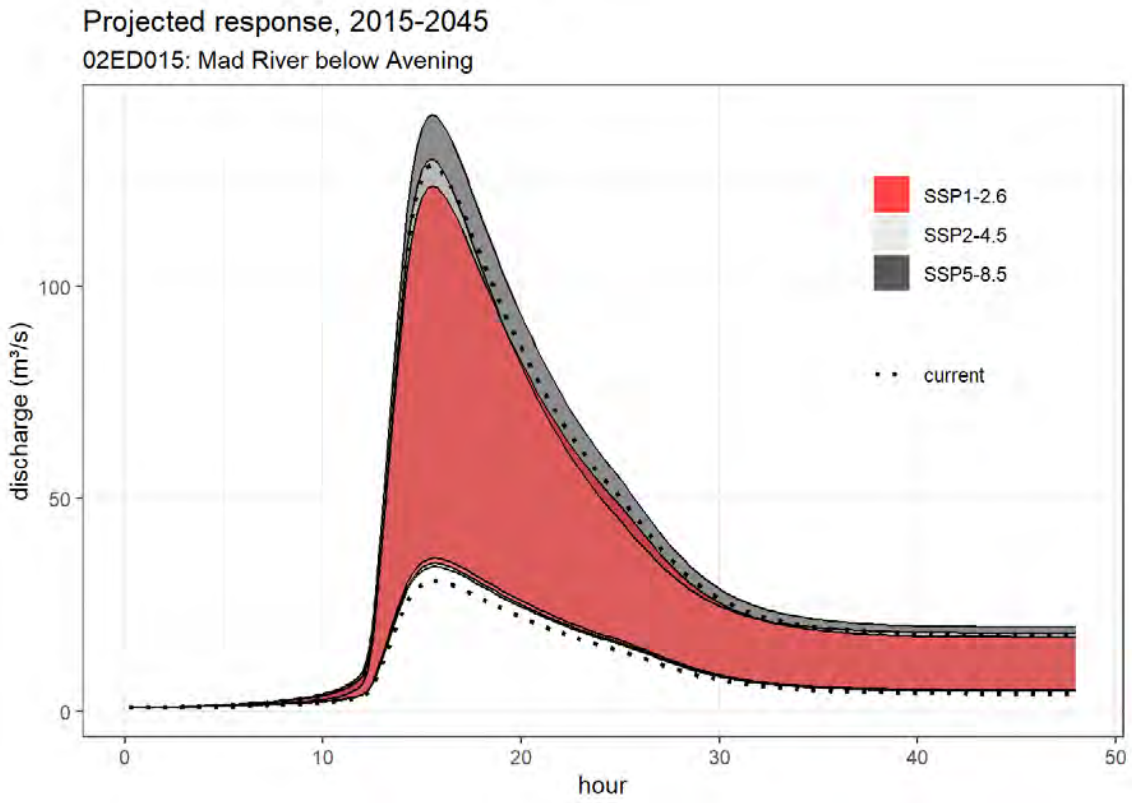

Projected change in runoff ranging from a 2- to 100-year rainfall events, 2015-2045.

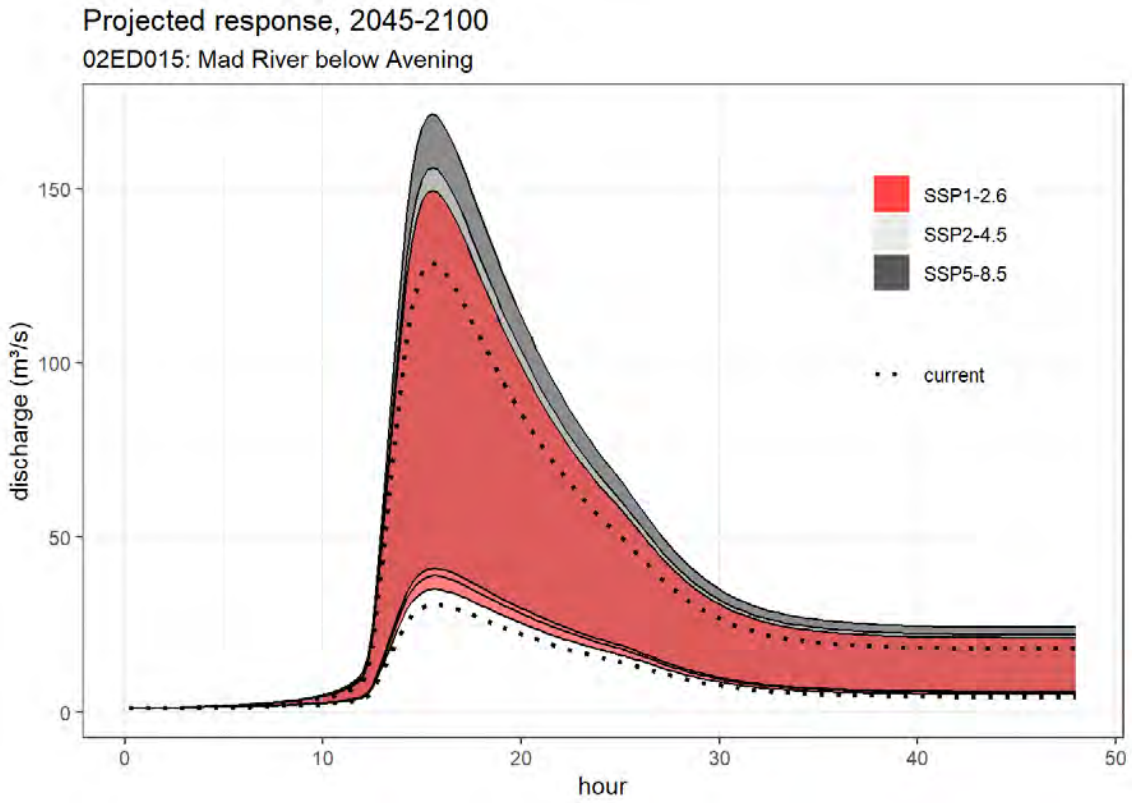

Projected change in runoff from ranging from a 2- to 100-year rainfall events, 2045-2100.

Discussion of Model Limitations

Omission of the 2013 Storm

The July 8, 2013 storm was a notable event, causing mass power outages and leaving stranded cars and even trains in the GTA. It was also a particularly distinct event observed at the 02ED015 Avening stream flow gauge and would be an obvious target for modelling extreme events. For reasons best described by the plot below, there was a mismatch in data availability preventing model calibration to this event.

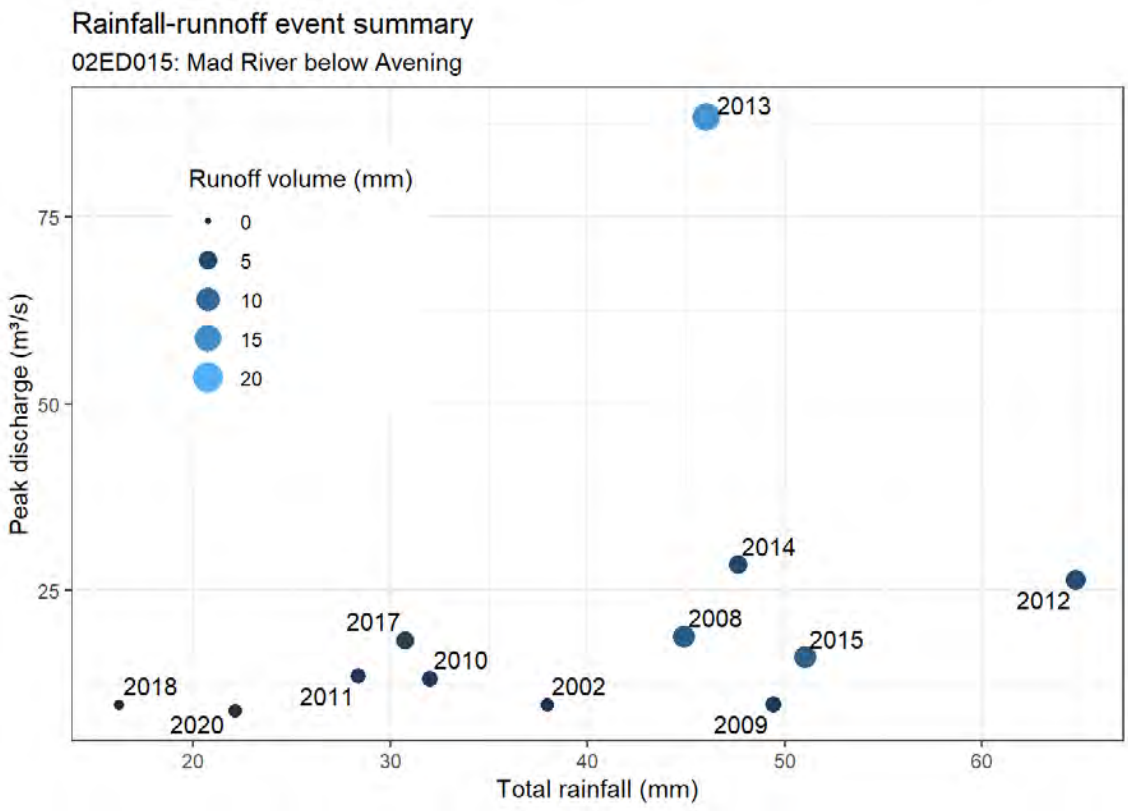

Rainfall-runoff magnitudes of 12 recent flood events.

There is a clear discrepancy between the accumulative rainfall observed and both the peak and cumulative discharge measured at the Mad River gauge. The 2013 storm appears to be highly localized that failed to be registered by either the CaPA-RDPA system or the Environment Canada meteorological station network. Including the storm into the calibration required sacrifice that was too costly to the global calibration; thus the 2013 storm was omitted.

Before doing so, an *hourly* hyetograph obtained from the Mount Forest (AUT)—6145504 (https://climate.weather.gc.ca/climate_data/hourly_data_e.html?StationID=7844&txtStationName=mount+forest) meteorological station was substituted for the *6-hourly* CaPA-RDPA to check whether rainfall intensity factored in the calibration mismatch. This was *not* the case.

NOTE: The Mount Forest (AUT) dataset is included with the model file delivery.

Flashy System

As evidenced by the tendency for model (calibration) performance to increase with decreased lag times, the modelling exercise suggests that the upper Mad River is a flashy system. Lag times had to be reduced to match the speed of rising limbs.

It is recommended that future modelling of extreme events be performed with monitoring data at or below a 15-minute temporal resolution.

Initial Abstractions

Along with lag times, sensitivity analysis showed that model calibration could be accomplished quite well assuming initial abstractions can be neglected $(f_{ia} \rightarrow 0)$. This is a consequence of calibrating to flashy systems. However, given that the intent of this study was ta also develop a model with continuous modelling applicability, neglecting i_a is untenable.

Therefore, cover density (Figure @ref(fig:basin-cov)) was multiplied by a summertime standard leaf-area index $\mathrm{LAI} = 5$ to determine i_a for each subbasin. Initial abstraction (i_a) was kept constant and calibration proceeded by adjusting the remaining parameters.

Baseflow Dependence

There is some indication that the early summer hydrograph form is affected by the state in groundwater levels. The Flashiest of storms tended to occur near the end of the summer season and when initial discharge (Q_0) was relatively low. It appears that the groundwater and hydrological systems should *not* be de-coupled in this system, especially when modelling the spring freshet seasons.

Conclusions

A HEC-HMS model of the Mad River has been built to project the runoff response to extreme summer rainfall events occurring upstream of Creemore, Ontario. The model was calibrated using 6 events and verified using 5 additional events to the sole streamflow monitoring gauge: Mad River below Avening (Water Survey of Canada gauge 02ED015).

Input data sources

In addition to only one monitoring location, input data access was also limited: the nearest active climate station is over 20km away. In southern Ontario, extreme summer events are historically convective in nature (Klaassen, 2014) the kind of storm that typically extend less than 10km. Consequently, any modelling of rainfall events in the study area using station data must rely on spatial extrapolation methods that do nothing but overestimate the likely extent of the rainfall events being modelled.

After demonstrating the distributed climate data service hosted by the ORMGP, the NVCA sought to have a rainfall-runoff model built that relied on the distributed rainfall re-analysis product (i.e., CaPA-RDPA) offered by Environment and Climate Change Canada that is resolved at the scale that best resembles southern Ontario convective storms. The disadvantage of CaPA-RDPA is that it is currently offered at a time step of 6-hour accumulations—too coarse for many rainfall-response modelling applications.

In part, this modelling exercise was a test of whether model uncertainty can be reduced by improving rainfall distribution at the expense of lowered rainfall intensities. Given the lack of station data for the study area, we were unable to conclude one way or the other; however, the model did succeed at matching peak flows and it was evident that by increasing curve numbers peak flow could easily be overestimated, suggesting that rainfall intensity may not be as critical to modelling upper Mad River events.

The Role of Groundwater

The flow regime of the upper Mad River is highly seasonal having the highest discharge rates occurring during the spring freshet season. In fact, only one of the events modelled (2013) represented that year's the annual extreme; in all other cases, spring discharge rates exceeded the observed response of the selected storms. This suggests that from a flood risk perspective, it may be ill-advised to rely solely on summer extreme rainfall events while neglecting the spring freshet flow conditions.

Spring events are not necessarily driven by rainfall intensities experienced in the summertime rather a combination of high water tables present (i.e., wet antecedent conditions) during snowpack melt events. Modelling this phenomenon not only requires the continuous modelling of snowpack formation and ablation, but also requires the explicit representation of the shallow groundwater system's interaction with the ground surface. From this, one may conclude that HEC-HMS, or for that matter any other rainfall-runoff model typically used in this application, is insufficient for the upper Mad River. Rather a physics-based integrated groundwater-surface water model is warranted for spring flows.

The need for an integrated model may be bolstered further by the fact that there exists Karstic features in the northern portions of the model domain. Karst is notorious for having quick response to rainfall events independent of surface drainage pathways.

In closing

The HEC-HMS model built here for the Mad River upstream of Creemore has exhausted all available data and has been shown to adequately simulate peak-flow response to storms up to the 10-year return. Limitations implied in this statement is not a function of model capability, but one of data availability. Improvements to this model would be gained by added long-term monitoring.

References

Duan, Q.Y., V.K. Gupta, and S. Sorooshian, 1993. Shuffled Complex Evolution Approach for Effective and Efficient Global Minimization. Journal of Optimization Theory and Applications 76(3) pp.501-521.

Environmental Water Resources Group, 2017. Technical Guidelines for Flood Hazard Mapping (March, 2017). 137pp.

Klaassen, J., 2014. Ontario Rainfall Climatology. Internal Environment Canada (Meteorological Service of Canada) publication. Prepared in support of the Toronto 2015 Pan Am and Parapan Am Games. Toronto, Ontario.

Natural Resources Canada, Public Safety Canada. 2018. Case studies on climate change in floodplain mapping v.1 ANNEX C: FLOOD MAPPING AND CLIMATE CHANGE: WATERFORD RIVER CASE STUDY ANALYSIS.

Oak Ridges Moraine Groundwater Program (2023). sHydrology stream flow analysis tool [Online image]. https://www.oakridgeswater.ca/ (https://www.oakridgeswater.ca/)

Ontario Geological Survey 2010. Surficial geology of southern Ontario; Ontario Geological Survey, Miscellaneous Release— Data 128 – Revised.

Ontario Ministry of Natural Resources and Forestry, 2019a. Southern Ontario Land Resource Information System (SOLRIS) Version 3.0: Data Specifications. Science and Research Branch, April 2019

Ontario Ministry of Natural Resources and Forestry, 2019b. Ontario Digital Elevation Model (Imagery-Derived).

Simonovic, S.P., A. Schardong, R. Srivastav, and D. Sandink (2015), IDF_CC Web-based Tool for Updating Intensity-Duration-Frequency Curves to Changing Climate – ver 6.5, Western University Facility for Intelligent Decision Support and Institute for Catastrophic Loss Reduction, open access https://www.idf-cc-uwo.ca (https://www.idf-cc-uwo.ca).

US Army Corps of Engineers, USACE (1998). HEC-1 flood hydrograph package user’s manual. Hydrologic Engineering Center, Davis, CA.

US Army Corps of Engineers, USACE (2000). Hydrologic Modeling System HEC-HMS Technical Reference Manual. Hydrologic Engineering Center, Davis, CA.